TÉCNICO LISBOA

Convex relaxation methods for opportunistic localization of a communications satellite

Renato Manuel Lourenço Dias

Thesis to obtain the Master of Science Degree in

Electrical and Computer Engineering

Supervisor(s): Prof. João Pedro Castilho Pereira Santos Gomes

Examination Committee

Chairperson: Prof. João Fernando Cardoso Silva Sequeira
Supervisor: Prof. João Pedro Castilho Pereira Santos Gomes
Member of the Committee: Prof. António Pedro Rodrigues Aguiar

October 2021

Declaration

I declare that this document is an original work of my own authorship and that it fulfills all the requirements of the Code of Conduct and Good Practices of the Universidade de Lisboa.

”If you only do what you can do, you will never be more than who you are”

Master Shifu

Acknowledgments

I would like to express my gratitude to my supervisor, Professor João Pedro Gomes, for the technical guidance but also for the motivational support by believing in my work when I did not believe.
As this project closes a chapter of my life, I want to thank all people that have took part in it, in particular: to my long-time friends and to the new ones, for the long nights and days we shared struggling to solve lab assignments but specially for the priceless coffee-break discussions; to my girlfriend, for her patience by having my time stolen and for her immense support and motivation; to my brother, for the constant companionship and for sacrificing his time to save mine.
Finally I want to thank to my parents and great-uncles, for the education that defined my values and for their immeasurable support, availability and love that made me who I am today.

Resumo

Os CubeSats são uma solução atrativa devido à sua flexibilidade e baixo custo de desenvolvimento, lançamento e operação. Contudo, esta redução do custo reflete-se na quantidade e qualidade do equipamento instalado no aparelho.

Um dos sensores que tem a sua operacionalidade mais limitada é o recetor GPS que pode eventualmente nem ser incorporado a bordo, sendo necessários métodos alternativos para localização.

Nesta tese estudou-se o uso de informação de oportunidade para obter estimativas moderadamente aceitáveis da posição do satélite recorrendo a métodos de otimização convexa.

Desenvolveram-se várias relaxações convexas alternativas relativas à função de custo que incorpora informação do desvio de Doppler para incluir este termo num problema de otimização que utiliza relaxações já conhecidas para posição e ângulo.

Um estudo preliminar do limite inferior de Cramér-Rao indicou que as aproximações utilizadas devem contribuir com informação adicional. No entanto, este estudo não é suficiente para concluir acerca da qualidade das relaxações desenvolvidas que podem degradar a performance do estimador.

Esta suspeita foi confirmada em simulação dado que nenhuma das relaxações melhorou significativamente a solução obtida na formulação em que não foi incluída informação sobre o desvio de Doppler.

Apesar deste inconveniente, foram propostas relaxações para funções de custo baseadas nas leis do movimento de um satélite para regularizar a sua posição em cada instante. A combinação destes termos de regularização com as relaxações previamente estudadas constitui uma boa alternativa para a geração de estimativas que podem ser usadas como inicialização de métodos de estimação sequencial para refinar o resultado.

Palavras-chave: Otimização convexa, Relaxação convexa, Desvio de Doppler, CRLB, CubeSats

Abstract

CubeSats are an attractive solution due to their numerous applications and low-cost development, deployment and operation.

However, this reduction in cost impacts the quantity and quality of the equipment aboard the satellite. One of the sensors whose operation is more limited is the GPS receiver, which in some cases may not even be included with the satellite, which requires some alternative methods to obtain position information.

In this work, a study was made on the usage of information of opportunity to obtain a coarse position of a satellite using convex optimization methods. Several convex relaxations for the Doppler-shift cost function were developed to include this information in a formulation that utilizes already known convex relaxations for cost functions based on distance and angular information.

A preliminary theoretical study of the Cramér-Rao Lower Bound strongly suggests that the use of approximate functions for the Doppler-Shift cost function introduces additional information to the estimation problem. However, this study is not sufficient to conclude about the tightness of the developed relaxations which may degrade the estimator performance. This insight was confirmed in the simulations, where no relaxation method could outperform the formulation where no Doppler-shift information is used.

Nonetheless, additional relaxations were proposed to use cost functions based on the known movement laws of satellites. The combination of these regularization terms with the previously studied relaxations constitute good candidates to generate position estimates which may be used to initialize sequential algorithms which can provide refined estimates.

Keywords: Convex optimization, Convex relaxation, Doppler-shift, CRLB, CubeSats

Contents

List of Tables

List of Figures

Nomenclature

Roman symbols

$CRLB$ Cramér-Rao Lower Bound

$CWLS$ Constrained Weighted Least Squares

FIM Fisher Matrix Infomrmation

LS Least Squares

ML Maximum Likelihood

SDP Semidefinite Program

$SOCP$ Second Order Cone Program

SVD Singular Value Decomposition

$TDOA$ Time Difference Of Arrival

VMF von Mises-Fisher

WLS Weighted Least Squares

$\boldsymbol{r}$ Satellite's position vector.

$\boldsymbol{r}_{gs}$ Station's position vector.

$\boldsymbol{v}$ Satellite's velocity vector.

$\boldsymbol{v}_{gs}$ Station's velocity vector.

$F(\boldsymbol{r})$ Regularizer cost function from dynamics.

f_r^k Station's receiving frequency.

f_t^k Satellite's transmitting frequency.

Superscripts

T Transpose.

Chapter 1

Introduction

1.1 Motivation

In the last two decades, GPS became a very useful tool for precise orbit determination of satellites in Low Earth Orbit (LEO) [1]. The usage of GPS measurements in combination with models of the forces (perturbations) acting on the satellite enable the trajectory to be estimated to an accuracy at the centimeter-level [2].

However these tools may not always be available as we are witnessing with the advent of CubeSats, small satellites with dimensions of $10\,\text{cm} \times 10\,\text{cm} \times 10\,\text{cm}$ which are used as a super low-cost alternative to conventional satellites but targeted for very specific tasks.

In fact, one of the sensors with limited operation is the GPS receiver. In some rare cases, these tiny satellites are even sent without a GPS sensor or, if it is present, it remains turned off to save energy, which reduces the quantity of available information relative to localization. Moreover, to reduce the deployment cost, it is foreseen that these satellites will eventually be collectively launched in swarms of dozens or hundreds. Due to their similarities and lack of precise localization data, locating each one individually configures a real challenge with reported cases where a satellite remains unidentified even one week after launch [3].

This new reality requires the study of alternative localization methods which can provide sufficient accuracy for the mission requirement of the satellite.

One source of information which is readily available and does not pose any energetic or computational overhead is the metadata that is inherent to the satellite's operation, such as the time-stamps present on exchanged messages, the pointing direction where the ground antennas find the greatest signal strength, and the received frequency. This free information is called: information of opportunity.

With these measurements, one should be able to acceptably perform orbit determination for unclassified satellites and track known ones if GPS is not an option or if it becomes unavailable.

1.2 Topic Overview

In recent years, several studies were dedicated to the problem of orbit determination using information of opportunity. Some of these works recover some techniques used in the early days of the spatial era when Sputnik I was launched in 1957, and which inspired the creation of the first navigation system (TRANSIT) [4]. These first methods used range measurements from powerful radars and angle information based on radio interferometers. With this information, some crude estimates of a satellite's position could be obtained and the orbit parameters calculated using previously developed analytical and geometrical methods (ex: Gibbs, Gauss, Laplace, Double-r) which were originally intended to study the orbits of planets. This process is known as preliminary orbit determination [5].

Besides distance and angular measurements, there exists another valuable source of information that may be used to help in obtaining correct orbital parameters: the Doppler-shift. This corresponds to the frequency drift of a sent, and subsequently received, signal which is a manifestation of the relative velocity between the emitter and the receiver. This valuable source of information is very cheap due to the modest hardware requirements for receiving the signals.

Once an initial estimate for orbital parameters is available, the common choice to improve the estimation accuracy is to utilize a batch estimator such as Least-Squares or a sequential estimator such as the Extended Kalman filter [6]. Both techniques allow the inclusion of more information sources and are prepared to cope with the measurement and modeling errors to refine the initial estimate in a process which is known as orbit estimation. This produces very good results for moderate measurement uncertainty but may have convergence problems for large noise magnitude. Old studies and application cases may be found in [7], [8], [9], and [10]. Similarly, recent works such as [11], apply a sequential correction algorithm that uses Doppler to refine the position estimates of a CubeSat with previously determined orbital elements.

Some other recently published works explore non-conventional methods for orbit determination. In [12], the author proposes the exploitation of a global network of small ground stations to estimate and correct orbital parameters by means of a supervised learning algorithm, for a satellite from which only the frequency is known. The idea of using machine learning algorithms is also explored in [13], where the author proposes a solution using a genetic algorithm to search for the best orbital parameters that explain the angular measurements taken by an in-orbit observer.

Although not directly related to orbit determination, [14] follows a conceptually similar strategy to develop a localization algorithm (to estimate the crash site location of the plane involved in a very well-known accident of Malaysian Airlines, Flight MH370) using only range and Doppler-shift information, since there were no angular measurements available on that case. However, the way that Doppler-shift information was included differs from the one that is envisaged here, since it uses a particle filter requiring a heavy computational effort adding to the lack of convergence guarantees.

Based on the problems of the previously cited works, this thesis searches for an alternative approach to include Doppler-shift information in target localization. This study follows a line of work on convex algo-

rithms for cooperative localization which have shown very good results in scenarios of sensor networks [15] although they solely used angular and distance information. Since the Doppler-shift effect has a clear manifestation in satellite communications, this constitutes a good candidate scenario to test the extension of the previously developed algorithms to include this additional source of information.
However, the results of this work are not intended to outperform the state-of-the-art algorithms in performance but may be useful when there is large uncertainty about the initial satellite's position, providing better estimates for initialization.
This is an innovative work on this field since to the best of our knowledge there is no published literature that uses convex optimization tools to perform preliminary orbit determination or orbit estimation.
The investigation on this thesis emerges as contribution to project INFANTE, in which IST collaborates. This project aims to develop a satellite constellation to contribute to Earth Observation tasks related to maritime surveillance, environmental monitoring, and extreme event detection focusing in the Atlantic area.
The launch date of first satellite belonging to INFANTE's constellation was not scheduled yet, but when launched, it will orbit Earth in LEO (Low Earth Orbit).

1.3 Objectives

The goal of this thesis is to formulate a fast and robust method for initial orbit determination and orbit estimation using information of opportunity associated with a satellite telecommunication link.
The problem scenario is composed of two agents: the satellite, in particular a CubeSat, and a ground station that observes it. It is assumed that the observer has few resources (which is close to the reality in an academic context) and so the measurements may present moderate to large error.
The estimation follows the classical Maximum Likelihood framework but adopts convex relaxation and optimization techniques rather than EKF-based tracking or local search algorithms as a way of attaining improved robustness to model uncertainties which may cause the algorithm to diverge. This builds on previous work [15] which developed an efficient convex relaxation approach for collaborative localization of autonomous vehicles combining range and angular information. The novelty introduced in this thesis is the incorporation of Doppler-shift information that is present in a satellite communication context, as well as the integration of motion models into the problem that are more pertinent for satellite orbits than the generic ones adopted in [15].
Extending the approach to a collaborative context with more than one target and one observer is envisaged as a future development.

1.4 Thesis Outline

In Chapter 2 some background concepts are introduced relative to the satellite's dynamics, classical description of the orbits and the observation models of interest.

Next, some mathematical background is given on statistical estimation, with a particular focus on the Maximum-Likelihood framework for the optimization problem formulation, the Cramér-Rao Lower Bound for benchmark, and the Convex Optimization framework for actual problem-solving. This is followed by a survey of known cost function relaxations and a discussion about their validity when applied to the current problem.

Chapter 3 is devoted to the actual development of convex relaxations to accommodate Doppler-shift measurements and later to create convex cost functions based on the satellite's dynamics constraints.

The description of the simulations and their results are presented in Chapter 4, where a comparison is made between the performances of the proposed relaxations and some preliminary conclusions are taken.

Finally, Chapter 5 contains a summary of the work done and the major conclusions obtained from comparing the simulation results and the theoretical analysis. It also discusses some possible research directions that could be pursued to improve the results.

Chapter 2

Background

2.1 Coordinate Systems

Before discussing the movement of any body in space, it is necessary to specify the reference frame where the motion is described.

The motion of Earth-orbiting satellites is usually described in an Earth-Centered Inertial (ECI) frame. However, the majority of observations are made at ground sites and the output of sensors are relative to the *Local Tangent* (LT) coordinate system or *Topocentric Horizon* (TH) coordinate system.

In order to convert an observation taken at the LT frame to the ECI frame, an intermediary frame must be used to account for Earth's rotation. This coordinate system is called *Earth-Centered Earth Fixed* (ECEF) frame. This frame rotates along with Earth such that a point at Earth's surface always has the same coordinates. A comparison is given in Fig. 2.1.

2.1.1 Earth-Centered Inertial frame (ECI)

Since this frame has no rotation or acceleration, it is adequate to describe the motion of a satellite using Newton's laws [16].

The origin is placed at Earth's center and the equator defines the $X - Y$ plane. The direction of $+X$ is defined by a vector with the same orientation and direction as the Vernal Equinox, (Υ). This another celestial reference is a vector collinear with the intersection of the Earth's equatorial plane with the plane described by Earth's translations around the Sun (the ecliptic plane) on the March Equinox and has the direction form Earth to Sun at that time. The Vernal Equinox is a fixed reference over time (neglecting Precession and Nutation effects for relatively short periods of time). The $+Y$ axis is 90° to the east in the equatorial plane and the $+Z$ direction is aligned with the North Pole, completing the right-handed coordinate system, as described in Fig. 2.1 [5].

2.1.2 Earth-Centered Earth Fixed frame (ECEF)

Similar to ECI, the ECEF coordinate system has its origin at the center of the Earth but unlike the former, its axes rotate synchronously with the Earth, such that the coordinates of a point at its surface (or at any depth) remain constant over time. In this case, the $+X$ axis is along $0°$ latitude and $0°$ longitude, the intersection between the Greenwich meridian and the Equator. On the other hand, the $+Z$ axis is aligned with the true North, coinciding with Earth's rotational axis. Finally, the $+Y$ axis completes the right-handed coordinate system.

An intuitive way to relate the ECEF with the ECI is to note that the ECEF corresponds to the rotation of the ECI frame about the $+Z$ axis by an angle (Θ) that is equal to the one measured between the Vernal Equinox and the Greenwich meridian, as shown in Fig. 2.1.

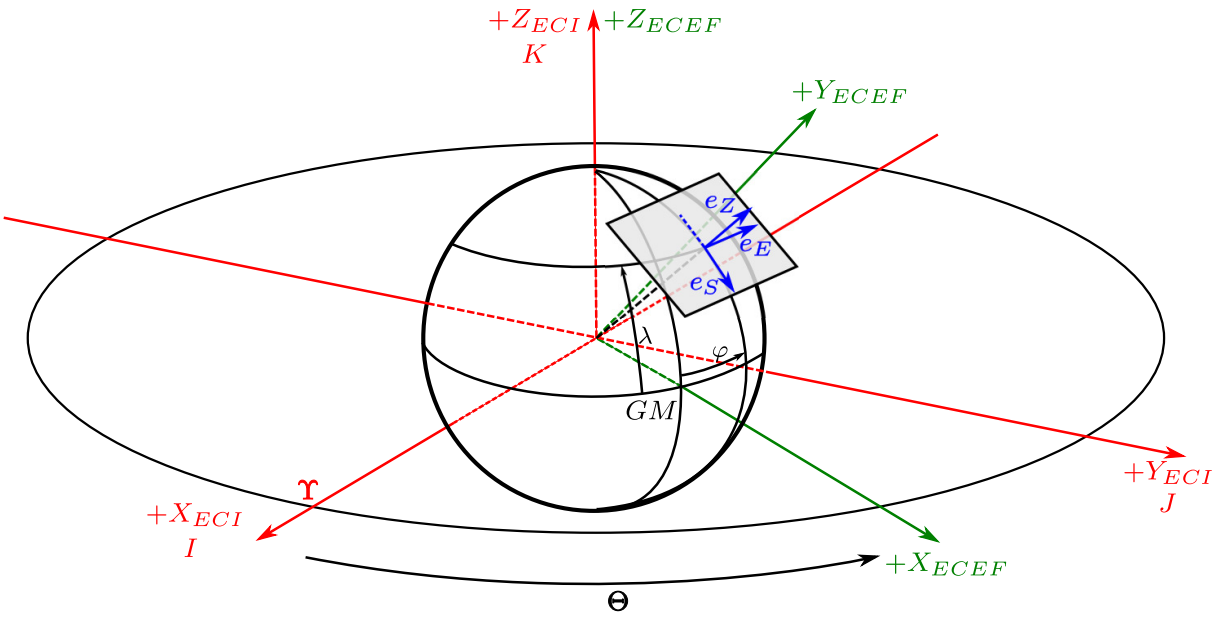

Figure 2.1: Representation of ECI frame (Red), ECEF frame (Green), *Local Tangent* frame (Blue). Θ is the Greenwich Apparent Siderial Time, a time-varying angle between the Vernal Equinox (Υ) and the Greenwich meridian (GM) that increases by $360°$ every $24\,\mathrm{h}$. Ground station's latitude and longitude are represented by λ and φ respectively. (Figure based on [6])

2.1.3 Local Tangent Plane Frame

This system is more adequate to describe an observation than the ECEF frame since its origin is fixed at the station's location and its fundamental plane is tangent to Earth's surface.
The fundamental plane is described by two unitary vectors: $\mathbf{e}_E$ pointing East and aligned with a parallel; $\mathbf{e}_S$, pointing South and aligned with a meridian. To complete the right handed coordinate frame, the third vector $\mathbf{e}_Z$ points to the Zenith, away from the center of the Earth [6] as described in Fig. 2.1.

To locate a satellite in the sky, only two angles are needed: Azimuth and Elevation. A visual representation is depicted in Fig. 2.2.

These angles can be readily calculated using the satellite's position expressed in *Local Tangent*

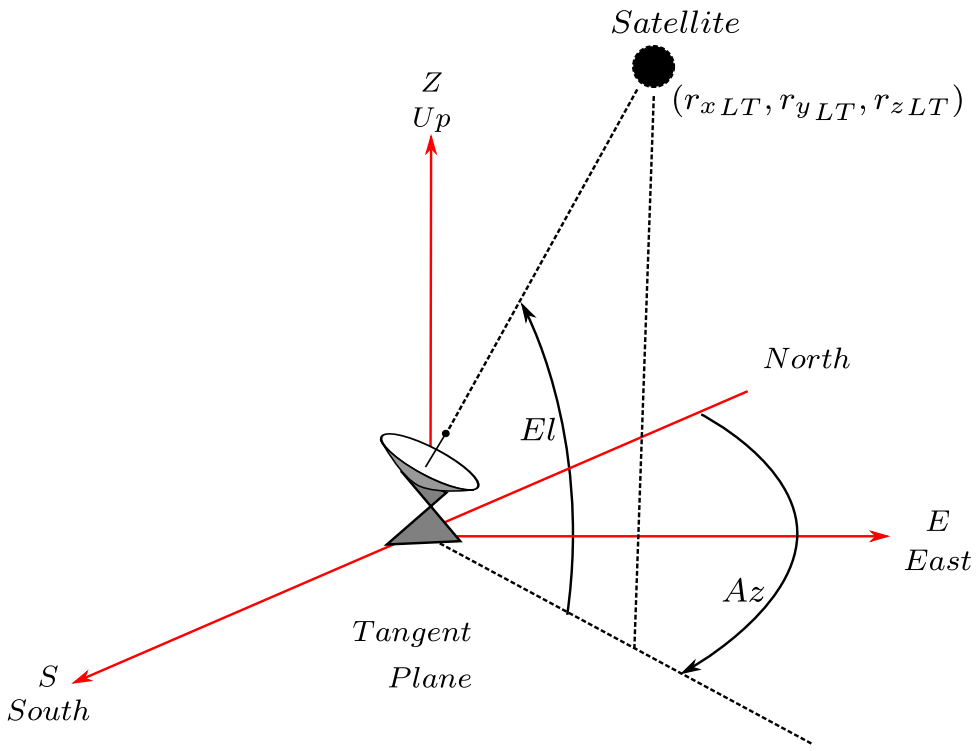

Figure 2.2: Representation of Azimuth (Az) and Elevation (El) angles in *Local Tangent* Coordinates. (Figure based on [16])

.

coordinate system

$$El = \arctan\left(\frac{\boldsymbol{r}_{z\,LT}}{\sqrt{\boldsymbol{r}_{x\,LT}^2 + \boldsymbol{r}_{y\,LT}^2}}\right)$$
$$Az = \pi - \arctan\left(\frac{\boldsymbol{r}_{y\,LT}^2}{\boldsymbol{r}_{x\,LT}^2}\right). \tag{2.1}$$

The full transformation that relates a position vector in ECI and LT frames is given by

$$\begin{bmatrix}\boldsymbol{r}_x\\ \boldsymbol{r}_y\\ \boldsymbol{r}_z\end{bmatrix}_{LT} + \begin{bmatrix}0\\0\\R_{E+h}\end{bmatrix} = \begin{bmatrix}\cos(\frac{\pi}{2}-\lambda) & 0 & -\sin(\frac{\pi}{2}-\lambda)\\ 0 & 1 & 0\\ \sin(\frac{\pi}{2}-\lambda) & 0 & \cos(\frac{\pi}{2}-\lambda)\end{bmatrix} \cdot \begin{bmatrix}\cos(\varphi) & 0 & -\sin(\varphi)\\ 0 & 1 & 0\\ \sin(\varphi) & 0 & \cos(\varphi)\end{bmatrix} \cdot$$
$$\cdot \begin{bmatrix}\cos(\Theta) & \sin(\Theta) & 0\\ -\sin(\Theta) & \cos(\Theta) & 0\\ 0 & 0 & 1\end{bmatrix} \begin{bmatrix}\boldsymbol{r}_x\\ \boldsymbol{r}_y\\ \boldsymbol{r}_z\end{bmatrix}_{ECI} \tag{2.2}$$

where λ and φ represent the station's latitude and longitude respectively, Θ the Greenwich Apparent Sidereal Time and R_{E+h} is the Earth's radius added to the ground station's altitude. Equations (2.2) and (2.1) will be useful later in Appendix D.

2.2 Celestial Mechanics

Newton's second law and his universal law of gravitation are the starting point for virtually any study of orbital motion, especially when combined with Kepler's Laws [5].

In order to study the relations between some observations and the true position of a satellite, its dynamics must be addressed in the first place.

2.2.1 Two Body Problem

The gravitational interaction between two spherically symmetric bodies with reference to an inertial frame is described by Newton's law of universal gravitation. Denoting the mass of each body by M and m, the displacement vector between the two by $\boldsymbol{r}$, the norm of $\boldsymbol{r}$ by r and the universal constant of gravitation by G, the force vector acting on each body (assuming no other forces than gravity) is given by the *inverse-square* law

$$\boldsymbol{F_{grav}} = \frac{GMm}{r^2}\frac{\boldsymbol{r}}{r}. \tag{2.3}$$

Since $\boldsymbol{F_{grav}}$ is a vector quantity which is collinear with $\boldsymbol{r}$, its direction is captured by the unitary vector $\frac{\boldsymbol{r}}{r}$.

A particularization of the study corresponding to the interaction between the Earth and a satellite is depicted in Fig. 2.3 [1].

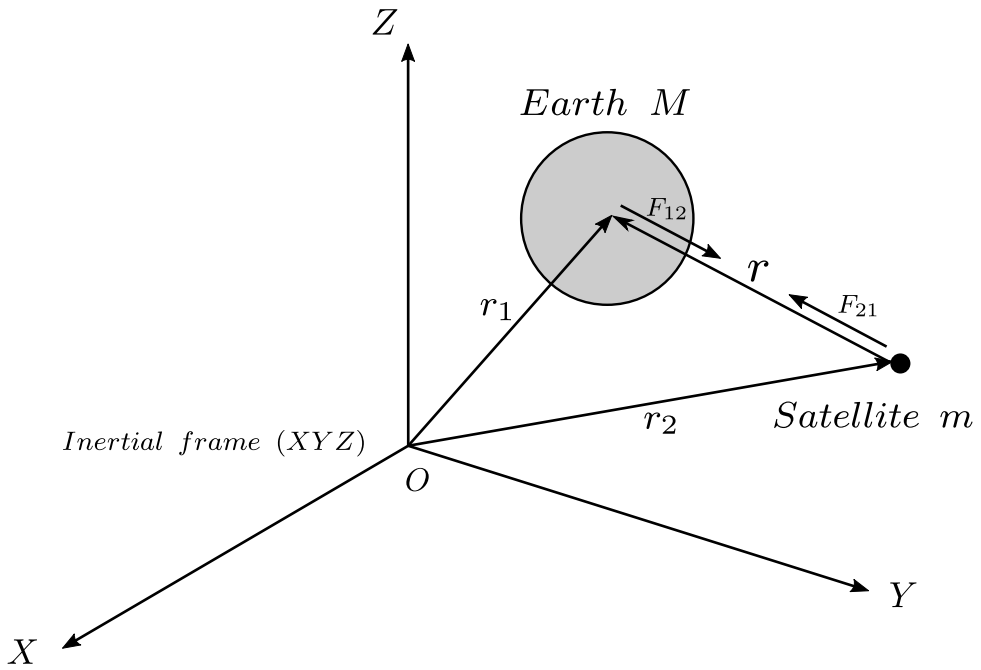

Figure 2.3: Representation of the satellite and Earth described in an inertial reference frame.

The position of the satellite relative to Earth is represented by $\boldsymbol{r}$ and may be obtained from Earth and satellite position vectors $\boldsymbol{r_1}$ and $\boldsymbol{r_2}$, respectively, according to the expression

[1] Note, however, that this is an approximation since this equation is only valid for spherical and uniformly dense bodies, which is not the case neither for the Earth nor for the satellite.

$$\boldsymbol{r} = \boldsymbol{r_2} - \boldsymbol{r_1}. \tag{2.4}$$

Although an expression for $\boldsymbol{r}$ cannot be readily obtained, one for $\ddot{\boldsymbol{r}} = \ddot{\boldsymbol{r}}_2 - \ddot{\boldsymbol{r}}_1$ certainly can, using the *inverse-square* gravity law

$$\begin{cases} \boldsymbol{F_{12}} = M\ddot{\boldsymbol{r}}_1 = \frac{GMm}{\|\boldsymbol{r}\|^2}\left(\frac{\boldsymbol{r}}{r}\right) \\ \boldsymbol{F_{21}} = m\ddot{\boldsymbol{r}}_2 = \frac{GMm}{\|\boldsymbol{r}\|^2}\left(\frac{-\boldsymbol{r}}{r}\right) \end{cases} \tag{2.5}$$

resulting in

$$\ddot{\boldsymbol{r}} = \frac{GM}{r^2}\left(\frac{-\boldsymbol{r}}{r}\right) - \frac{Gm}{r^2}\left(\frac{\boldsymbol{r}}{r}\right) = -\frac{G(M+m)}{r^3}\boldsymbol{r}. \tag{2.6}$$

Finally, the last expression may even be simplified due to the difference of nearly 22 orders of magnitude between the mass of the bodies, so the term m may be neglected leading to

$$\ddot{\boldsymbol{r}} \approx -\frac{\mu}{\|\boldsymbol{r}\|^3}\boldsymbol{r} \tag{2.7}$$

where $\mu = GM$ is the *gravitational parameter*. Physically, this means that Earth's center is approximately coincident with the center of the inertial frame, and so, $\boldsymbol{r}$ becomes the position vector of the satellite with $\boldsymbol{r} = [r_x \; r_y \; r_z]$.

From the second-order non-linear differential equation (2.7) and given initial conditions for position and velocity, it is possible to obtain the satellite's position at any instant using a numerical solver. The plot in Fig. 2.4 shows the result of a simple experiment to sketch the position of a satellite during one orbital period using MATLAB® integration routine `ode45`.

The fact that the orbit is contained on a plane is not a particularity of the chosen initial conditions but rather is intrinsic to the gravitational law.

The cross product between the position and acceleration vectors corresponds to

$$\boldsymbol{r} \times \ddot{\boldsymbol{r}} = \boldsymbol{r} \times \frac{-\mu}{r^3}\boldsymbol{r} = 0 \tag{2.8}$$

which is zero since the cross product of two collinear vectors is zero.

On the other hand, taking the time derivative of the cross product between position and velocity vectors, one obtains

$$\frac{d}{dt}(\boldsymbol{r} \times \boldsymbol{v}) = \boldsymbol{v} \times \boldsymbol{v} + \boldsymbol{r} \times \ddot{\boldsymbol{r}} = 0 + 0 \tag{2.9}$$

meaning that $\boldsymbol{r} \times \boldsymbol{v} =$ constant.

Since this constant vector quantity is normal to $\boldsymbol{r}$ and $\boldsymbol{v}$ (from the definition of cross product), it results that position and velocity are contained on a plane that does not change over time since its normal vector is constant over time. This normal vector, usually designated by $\boldsymbol{h} = \boldsymbol{r} \times \boldsymbol{v}$, is called *angular momentum per unit mass*.

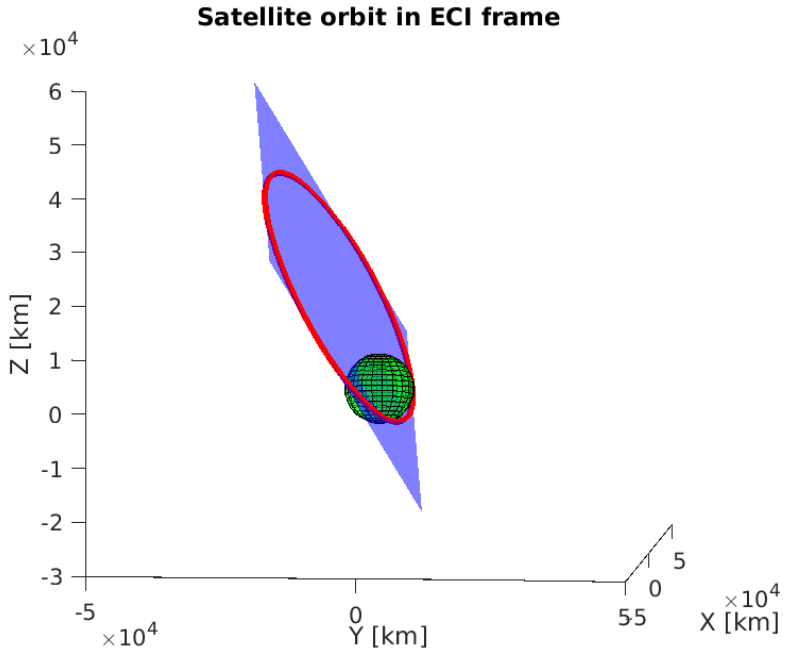

Figure 2.4: Numerical integration of satellite's dynamics equation, (2.7), with initial conditions $\boldsymbol{r}_0 = [9031.5 - 5316.9 - 1647.2]^T[km]$, $\boldsymbol{v}_0 = [-2.8640; 5.1112; -5.0805]^T[km/s]$.

Another physical variable that remains constant over time is the *specific energy*, which is given by

$$\xi = \frac{v^2}{2} - \frac{\mu}{r} = \text{constant} \tag{2.10}$$

For a satellite in a closed orbit (elliptical path) this quantity is negative, whereas for an open trajectory (parabolic or hyperbolic path) the satellite's *specific energy* is positive. The two constant quantities will become handy later on to formulate constraints for satellite positions.

2.2.2 Keplerian Elements

Although equation (2.7), along with a set of initial conditions, completely characterizes the orbital motion of a satellite, it does not provide an intuitive feel for its orbit [16].
There is an alternative description of a body's movement in the conditions verified by the two-body problem, developed by Johannes Kepler at the beginning of the 17th century. According to Kepler's formulation, an orbit may be described with a set of 6 parameters, 5 of which define the shape and orientation of the orbit in space and the last one accounts for the satellite's position along the trajectory. These are known as *orbital elements*.

The representation of each parameter is illustrated in Fig. 2.5 and their meaning is explained below.

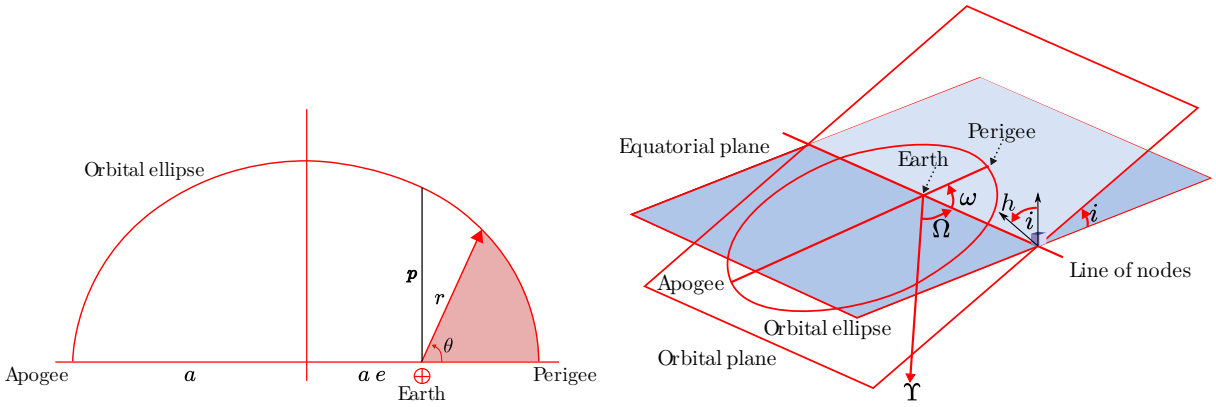

(a) Perifocal plane

(b) Perifocal plane spatial orientation

Figure 2.5: Kepler orbital elements illustration.

.

Eccentricity (e) - Measures the orbit shape deviation from a circle (which corresponds to $e = 0$). The range $0 < e < 1$ leads to an ellipse, while $e = 1$ corresponds to a parabola and $e > 1$ to an hyperbola.

Semi-major axis (a) - Represents the mean distance between *Perigee* (orbit point closest to origin) and *Apogee* (orbit point further from origin).

Semi-latus rectum (p) (optional parameter) - This corresponds to the chord perpendicular to the *semi-major axis* and it is defined from one focus to the boundary of the ellipse. The parameter is related with a and e by $p = a(1 - e^2)$.

Inclination (i) - Represents the inclination between the orbital plane and the equatorial plane.

Right Ascension of the Ascending Node (RRAN) (Ω) - Represents the angle between the *Vernal Equinox* and the *Ascending Node* (point of intersection of the satellite's orbit with the equatorial plane when the satellite is moving from South to North). It is measured positively from the *Vernal Equinox* to the *Ascending Node* in the anti-clockwise direction.

Argument of periapsis (ω) - Corresponds to the angle between the direction of *Ascending Node* and the direction of *Perigee*. It is measured from the *Line of Nodes* to the direction of *Perigee*.

True anomaly (θ) - Represents the position of the satellite at epoch t_0. It is the angle between satellite position and the *Perigee* measured in the anti-clockwise direction.

Given a set of values for the orbital parameters at some epoch t_1, Kepler's equations provide a convenient way to determine the orbital elements at some future time t_2. In order to do this, the following steps should be followed:

1. Compute *Eccentric Anomaly* (E_1) from *True Anomaly* (θ_1) at instant t_1.
2. Compute Mean Anomaly (M_1) from Eccentric Anomaly (E_1) at instant t_1.
3. Calculate Mean Anomaly (M_2) at instant t_2 from Mean Anomaly (M_1) at instant t_1.

4. Solve Kepler's transcendental equation to compute Eccentric Anomaly (E_2) at time t_2 from Mean Anomaly (M_2) at time t_2.

5. Compute True Anomaly (θ_2) from the propagated Eccentric Anomaly (E_2)

A summary of calculations is given in Appendix A. A more detailed and comprehensive explanation is provided in [16].

The result which is obtained by propagating the orbit with Kepler's equations is in accordance with the study of the motion using Newton's second law: the satellite positions are contained in a plane whose orientation does not change over time.

The novelty that Kepler's description adds is that the shape of the orbit remains constant, too. In fact, the position update described above only affects the True Anomaly (θ), and the other 5 parameters remain constant, which provides a convenient representation of the trajectory. This reduced and intuitive description makes this format ideal for exchanging updated satellite orbits through what is known as *Two-line Element Set* (TLE). As the name indicates, TLEs are composed of two lines in which the first contains satellite's identification and the second contains the orbital elements. As an example, a recent update of the Russian weather satellite `METEOR-M2` published by *CelesTrack* [17] is

```
METEOR-M 2
1 40069U 14037A 21055.81982948 -.00000032 00000-0 43009-5 0 9993
2 40069 98.4750 89.4221 0004367 270.6507 89.4161 14.20681096344048
```

This format is used as a standard input to algorithms that propagate the orbit of the satellite over time by simply using Kepler Laws or more sophisticated propagators which consider the orbit perturbations to a greater extent such as SGP4. The propagated state is extremely useful to predict next passes, schedule observations and respective antenna orientations and perform Doppler-shift frequency compensation.

To obtain the Orbital Elements description from ground observations, one noise-free measurement of a satellite's position and velocity suffices. A summary calculation of the transformations between Cartesian and Classical Elements is given in Appendices B and C. Further details and very pedagogical explanations are given in [16].

2.2.3 Orbit Perturbations

Recalling the Two-Body problem introduced in the previous section, the solution found for the trajectory of a satellite orbiting the Earth was based on the assumption that the only force acting on it was its weight and the Earth was assumed to be spherical, formed by concentric shells of constant density, which enabled the mathematical description of the force to be given by Newton's Gravitation Law. However, neither is gravity the only force acting on the satellite, nor is the Earth spherical. In fact, the gravitational force exerted by the Sun and the Moon, the atmospheric drag (with larger significance at

the Perigee of LEO satellites) and the solar radiation pressure (with larger significance in satellites with a large surface area) are also forces that affect the orbit.
A visual comparison of the magnitudes associated with each perturbing force is depicted in Fig. 2.6.
Nevertheless, the perturbation with the most significance (despite being three orders of magnitude weaker than the gravitational force) is the non-radial acceleration created by the oblateness of the Earth (since the equatorial radius R_E exceeds the polar radius by nearly $21\,\mathrm{km}$).

If one considers this perturbing force when modeling a satellite's orbit, the simple equation (2.7) becomes

$$\begin{bmatrix} \ddot{x} \\ \ddot{y} \\ \ddot{z} \end{bmatrix} = \begin{bmatrix} -\frac{\mu}{r^3}x \\ -\frac{\mu}{r^3}y \\ -\frac{\mu}{r^3}z \end{bmatrix} + \begin{bmatrix} J_2 \frac{3}{2}\left(\frac{R_E}{r}\right)^2 \left(\frac{5z^2}{r^2}-1\right) \\ J_2 \frac{3}{2}\left(\frac{R_E}{r}\right)^2 \left(\frac{5z^2}{r^2}-1\right) \\ J_2 \frac{3}{2}\left(\frac{R_E}{r}\right)^2 \left(\frac{5z^2}{r^2}-3\right) \end{bmatrix} \tag{2.11}$$

The additional perturbing vector is parameterized by J_2, which is a zonal coefficient (it affects equally, positions with equal latitude) that models the Earth's oblateness. This term is determined empirically by satellite observations.

Given the increased complexity of the additional perturbing terms, and observing the weak effect of these forces on the satellite for the problem at hand, the Two-Body assumptions are deemed to be sufficiently good to meet the accuracy expected for the type of position estimation methods envisaged in this work over a relatively short time horizon.

2.3 Opportunistic Measurements for Satellite Tracking

2.3.1 Pseudo-Range Measurement

Since in this scenario only passive measurements are available, distance information may be obtained from the difference between the time-stamp embedded in the messages sent by the satellite and the local station's clock.

Having the computed time difference and the propagation velocity of electromagnetic signals (speed of light c), the computed *pseudo-range* results from the multiplication of these two quantities, where the term *pseudo-range* arises to differentiate the true range from this indirect measurement.

Since the atmosphere is composed of several layers with different electromagnetic properties, the propagation of the signal is differently affected by each one. The interaction of electromagnetic waves with charged particles in the Ionosphere cause a signal's change of direction and velocity of propagation. This change of propagation velocity is linked with the electron density in the upper layers of the atmosphere, which is not homogeneous in space and changes with time.

Accounting for these variations is rather difficult since it requires knowledge of the refractive index along the path between satellite and station in order to take the integral and thus obtain the propagation time

$$\Delta t = \frac{1}{c}\int n\, ds \tag{2.12}$$

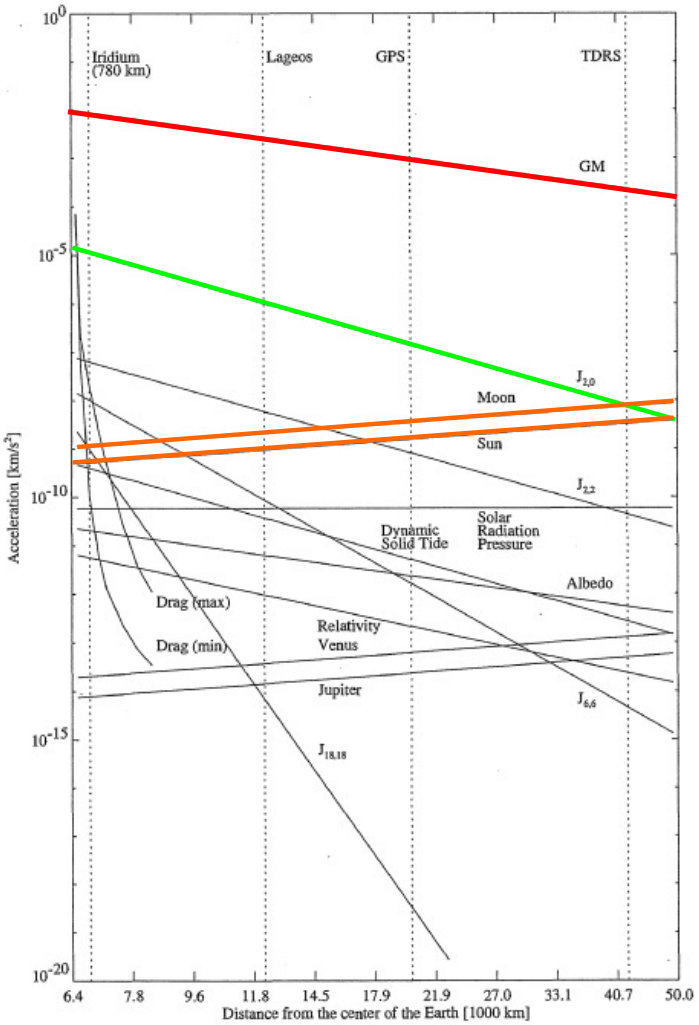

Figure 2.6: Graphical comparison of forces acting on a satellite. Gravity pull (Red) is three orders of magnitude stronger than Oblateness effect (Green) which in turn is four orders of magnitude stronger that Sun and Moon gravitational pull (Orange). (Image taken from [6]).

where n represents the refractive index. Nonetheless, ionospheric refraction and phase angle shifting are more important for lower frequencies and can almost be neglected at about 100 MHz [18].

Also, accurate distance calculations are dependent on keeping the local station's and satellite's clocks perfectly synchronized, otherwise, it may lead to erroneous time-difference computations and consequently wrongly computed ranges. To mitigate this error, periodic corrections should be made to the satellite's clock, preventing error integration over time.

It is also important to note that the obtained pseudo-range must be assigned to the time-stamp of the sent message since the satellite has moved a certain distance between the sent and the receiving events. The time travel for the exchanged message typically ranges from 5 ms for LEO orbits to 100 ms for geostationary satellites. For a satellite in low orbit with a velocity of $3\,\mathrm{ms}^{-1}$ this time difference corresponds to about 100 m of range difference. This requirement conflicts with the imperfect synchronization of both clocks and so may introduce ranging errors on the order of hundreds of meters [6]. Moreover, there is a small portion of the computed *pseudo-range* that results from the motion of the station along with Earth as it rotates. Considering once again a satellite in low orbit, a propagation time of 5 ms and

Earth's rotation rate ($7.3 \times 10^{-5}\,\mathrm{rad\,s^{-1}}$), the computed range error would be at most $3\,\mathrm{m}$ [19].

In addition to these non-ideal conditions, there are others (ground station displacement due to tidal perturbations and plate motion, solid Earth tides, etc.) which have a rather small influence (on the order of millimeters to centimeters) but must be taken into consideration for very precise orbit determination (which is not the case here).

2.3.2 Angle Measurement

At ground, an angle tracking system uses a beacon signal emitted by the satellite to feed the software that controls the antenna rotator, closing a feedback-loop that locks the antenna onto the direction corresponding to the maximum received signal power (this is known as step tracking). This technique may be complemented by the predicted satellite orbit, which speeds up the locking process since it provides a good initial guess for the satellite's position in the sky at a given time.

Recent studies even propose replacing the maximum signal power criterion in the step tracking method with Doppler-shift information [20]. This works by comparing the theoretical and practical Doppler curves. Since the theoretical curves are obtained from numerical orbit propagation (using a propagator such as SGP4), it certainly has some degree of error. It is expected that in this case, the curves are shifted in time. After comparing both curves and calculating the time difference, this difference is incremented/decremented to the Mean Anomaly (M) of the TLE element set and elevation and azimuth angles are recalculated, closing the tracking loop. The authors state in [20] that Doppler tracking is the most fruitful technique attaining an accuracy of 0.1° (in simulation) while being passive and not requiring sensitive antennas. When using step tracking, the resolution of angle determination depends on the beam-width (which itself depends on the frequency and antenna diameter) of the ground station antenna (the smaller the beam width, the better). The reported accuracy for small antenna rotors ranges from 0.5° to 2° [21].

There are some effects that may render more complex modeling of the angle. These arise from the finiteness of light velocity, which causes the geometric relative position at the time of signal reception to be different from the true signal path (due to Earth rotation). This effect is known as aberration.
The reported errors for this effect are very small compared to the non-linearities and systematic errors of the antenna's control mechanism. In [6] the aberration is reported to introduce an error of $0.6''$ (approx. $1.67 \times 10^{-4\circ}$).

2.3.3 Doppler-shift Measurement

This technique explores the physical property of the frequency shift between a radio signal emitted by a moving source and the apparent frequency detected by a receiver. This frequency difference poses a problem in communication since the receiver must compensate for this drift to send and receive signals at the right frequency. When the satellite state is known this is an easy calculation, but it is very difficult to determine the state solely from the Doppler-shift, as discussed later.

The measurement of the frequency drift is made by counting the number of cycles of the received

signal during a fixed number of periods of the reference signal, or instead, by multiplying the reference and the received signals, low-pass filtering the result and counting the number of cycles for a fixed time t_c. This relation can be converted to a range-rate measurement, which for S-Band signals (2 GHz) and $t_c = 1\,\mathrm{s}$, has an accuracy in determination of $1\,\mathrm{mm\,s^{-1}}$ (assuming ideal conditions) [6].

In a study published in [22], the one-way Doppler-shift frequency measured by a single station is used to estimate the orbit of a Micro-Satellite in LEO which carries a transmitter operating at $2.2\,\mathrm{GHz}$. The reported standard deviation for relative velocity was $0.1\,\mathrm{ms^{-1}}$, which for this particular transmission frequency translates to a standard deviation in measured frequency shift of $5.4\,\mathrm{Hz}$.

2.4 Mathematical Background

2.4.1 Random Variables

Given a set of discrete observations of a random variable (range, angle, frequency), it can be modeled by a probability density function, *pdf*, that in turn depends on a parameter $\boldsymbol{\theta}$.

To statistically describe the observations, one has to find an estimator $\hat{\boldsymbol{\theta}}$ for the parameter $\boldsymbol{\theta}$. Moreover, to ensure that, on average, the value of the estimator $\hat{\boldsymbol{\theta}}$ corresponds to the real value of the parameter, for all values of $\boldsymbol{\theta}$, the estimator must be *unbiased* which corresponds to

$$E(\hat{\boldsymbol{\theta}}) = \{\boldsymbol{\theta} \mid \boldsymbol{\theta} \in \mathcal{D}\} \tag{2.13}$$

where $\mathcal{D}$ is a compact domain.

2.4.2 Cramér-Rao Lower Bound

In order to determine the best performance achievable by an estimator and to benchmark it against other candidate estimators, it is necessary to have a statistical tool for efficiency evaluation. For an unbiased estimator, the easiest way to determine the lower bound for the variance of the estimator is the *Cramér-Rao Lower Bound* (CRLB) [23].
If a given unbiased estimator attains the CRLB, this provides a certificate of optimality, but in the case that it does not, an estimator can be found such that it attains the bound asymptotically.

According to the CRLB theorem, for a *pdf* $p(x;\theta)$ that satisfies the regularity condition

$$E\left[\frac{\partial \ln p(x;\theta)}{\partial \theta}\right] = 0 \tag{2.14}$$

for all θ, then, if an unbiased estimator for the *pdf* scalar parameter θ exists, its variance is lower bounded by

$$\mathrm{Var}[\hat{\theta}] \geq \frac{1}{-E\left[\frac{\partial^2 \ln p(x;\theta)}{\partial \theta^2}\right]}. \tag{2.15}$$

where the term $I(\theta) = -E\left[\frac{\partial^2 \ln p(x;\theta)}{\partial \theta^2}\right]$ is known as the *Fisher Information*.

If more parameters are to be determined, $\boldsymbol{\theta}$ is a vector and the variance for the estimator of each scalar parameter verifies

$$\mathrm{Var}[\hat{\theta}_i] \geq [\boldsymbol{I}^{-1}(\boldsymbol{\theta})]_{ii} \tag{2.16}$$

where $\boldsymbol{I}(\boldsymbol{\theta})$ is the *Fisher Information Matrix*, a symmetric matrix with the number of rows/columns equal to the number of parameters to be estimated.

Each entry of $\boldsymbol{I}(\boldsymbol{\theta})$ is then given by

$$\boldsymbol{I}(\boldsymbol{\theta})_{ij} = -E\left[\frac{\partial^2 \ln p(x;\boldsymbol{\theta})}{\partial\theta_i\,\partial\theta_j}\right]. \tag{2.17}$$

A more in-depth analysis is provided in Appendix D.

2.4.3 MLE Framework

The objective of Maximum-Likelihood estimation is to find $\hat{\boldsymbol{\theta}}$ that maximizes $p(\boldsymbol{x};\boldsymbol{\theta})$ *i.e.*, that makes the (particular) observed data, $\boldsymbol{x} \in \mathbb{R}^N$, most probable.

The problem can be formulated as

$$\hat{\boldsymbol{\theta}}_{ML} = \arg\max_{\boldsymbol{\theta}} p(\boldsymbol{x};\boldsymbol{\theta}) \tag{2.18}$$

Here, the *pdf* is viewed as a function of the unknown parameter and so is called the *likelihood-function* $L(\boldsymbol{\theta}) = p(\boldsymbol{x};\boldsymbol{\theta})$.

If the observations are independent and identically distributed (IID), the joint probability density function can be written as the product of the *pdf*'s for each observation, leading to

$$L(\boldsymbol{\theta}) = p(x(1),\ldots,x(N);\boldsymbol{\theta}) = \prod_{n=1}^{N} p(x(n);\boldsymbol{\theta}). \tag{2.19}$$

If $L(\boldsymbol{x};\boldsymbol{\theta})$ is strictly positive (which it certainly is for Gaussian distributions) the logarithm is applied to ease the computational implementation of the maximization problem, leading to

$$\hat{\boldsymbol{\theta}}_{ML} = \arg\max_{\boldsymbol{\theta}} \ell(\boldsymbol{\theta}) \tag{2.20}$$

where $\ell(\boldsymbol{\theta}) = \log\, L(\boldsymbol{x};\boldsymbol{\theta})$ is called the *log-likelihood function* which is related with (2.19) by

$$\ell(\boldsymbol{\theta}) = \log\, L(\boldsymbol{x};\boldsymbol{\theta}) = \sum_{n=1}^{N} \log p(x(n);\boldsymbol{\theta}). \tag{2.21}$$

Finally, (2.20) should be rewritten in the standard form of optimization problems which requires the minimization of the cost function. This modification is easily performed by negating the cost function in (2.20), resulting in

$$\hat{\boldsymbol{\theta}}_{ML} = \arg\min_{\boldsymbol{\theta}} \; -\ell(\boldsymbol{\theta}). \tag{2.22}$$

Using the MLE framework has the great advantage of producing an estimator that is unbiased or approaches the optimal one (attains the lower variance bound) for large datasets of observations and is therefore *asymptotically-efficient* according to the CRLB criterion [23].

2.4.4 Convex Optimization

The solution to the problem stated in (2.22) are the values of the parameter vector $\boldsymbol{\theta}$ for which the cost function $-\ell(\boldsymbol{\theta})$ attains it's minimum.
Since the formulated functions are generally highly non-linear, there is a high chance that there will exist multiple local minimizers of the cost function. The most straightforward method to solve the optimization problem is to perform an exhaustive search in the solution space although this is very time-consuming, and hence, not targeted for real-time applications.

To speed up the process, one may try to find the global minima using an iterative algorithm (*e.g.*, gradient method) which searches for a solution in the vicinity of an educated guess point provided by the user. In this case, it's not surprising that the algorithm may converge to a sub-optimal (local) solution, depending on the initial guess. However, if the cost function can be changed to ensure the existence of only one minimum, the iterateive algorithm will converge to the optimal solution. This technique is called *convex relaxation*.

To be convex, a function $f : \mathbb{R}^n \to \mathbb{R}$ whose domain is a convex set (Fig. 2.8), must verify, for all $x, y \in$ **dom** f and $0 \leq t \leq 1$, the following inequality [24]

$$f(\,t\,x + (1 - \,t\,)y) \leq \,t\,f(x) + (1 - \,t\,)f(y). \tag{2.23}$$

The geometric interpretation of this inequality is represented in Fig. 2.7.

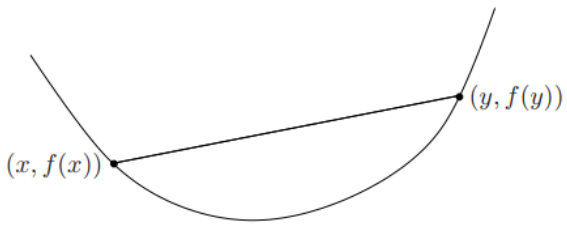

Figure 2.7: Geometric representation of a convex function . (Source [24]).

It means that: a line that connects the points $(x, f(x))$ and $(y, f(y))$ must be above the graph for every point on the interval $[x, y]$ [24].

(a) Convex Set. (b) Non Convex Set.

Figure 2.8: Illustration of a convex set. A set C is convex if the line segment between any two points in C lies in C. All convex sets must verify the condition: if $x_1, x_2 \in C$ then $t\,x_1 + (1 - t\,)x_2 \in C$ with $0 \leq t \leq 1$ (Adapted from [24]).

One of the most important aspects for this thesis is the set of rules that, when verified, enable one to conclude without further analysis if a function is convex or not.
This is particularly relevant because the convex optimization solver used in this work is implemented in a MATLAB® Toolbox called *CVX* that requires the optimized cost functions to be constructed under this set of rules (also called *Disciplined Convex Programming*).

The scheme presented in Fig. 2.9 summarizes the constructions that ensure the creation of a convex function.

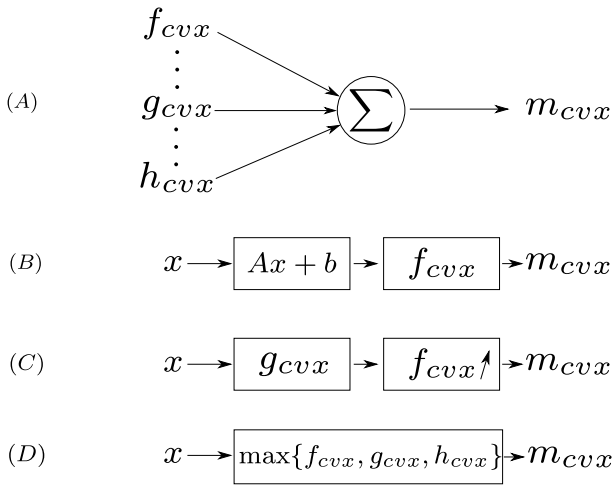

Figure 2.9: Disciplined Convex Programming rule-set.

The textual description of each rule is

(A) - The sum of convex functions is a convex function.

(B) - The composition of an affine map with a convex function, is a convex function.

(C) - The composition of a convex function with a non-decreasing convex function, is a convex function

(D) - The maximum of a set of convex functions, is a convex function.

2.5 Methods for Orbit Determination

Generally, the problem of obtaining the six orbital elements from astronomical observations may be split into two distinct problems: preliminary orbit determination and orbit estimation (or differential correction). While the former is used to directly compute the six parameters with no *a priori* knowledge of the spacecraft orbit, the latter assumes a previous parameter determination phase and performs successive improvements using a large set of tracking data. Classical methods for differential correction tend to use Least-Squares approaches, while more recent methods use Kalman Filter-based algorithms [6].

2.5.1 Preliminary Orbit Determination

There are several well-known algorithms to obtain an initial guess of the orbital elements. These are generally based on geometric relations between the observer and satellite positions and the measured angles and distances between them. When accurate distance information is not available, one may use Laplace or Gauss methods which only use angular information, although they are best suited for interplanetary missions. For near-Earth orbits, the Double-r method shows superior performance [5]. If distance measurements are available, and for sufficiently spaced observations, a common choice is to use Gibbs Method which calculates a velocity vector (in ECI frame) at instant t^k given three, equally spaced, satellite positions (also in ECI frame) at instants t^{k-1}, t^k and t^{k+1} as illustrated in Fig. 2.10 .

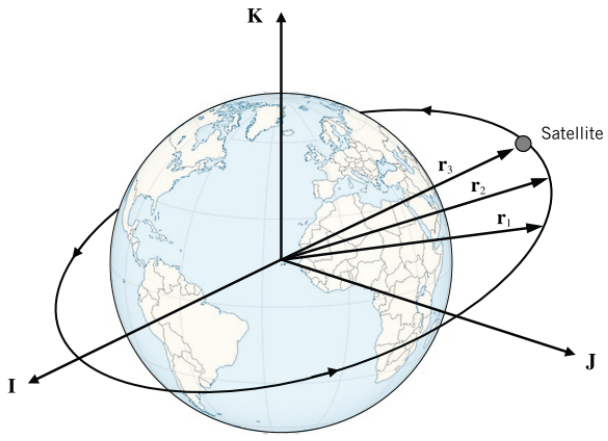

Figure 2.10: Gibbs method illustration. (Source [16]).

This algorithm is one of the simplest and more intuitive to apply. It is based on the assumption of coplanarity between the three successive position vectors to exploit the linear dependence between them. From a position and a velocity vector, the orbital elements are readily obtained from the algorithm summarized in Appendix B. This approach is only applicable to obtain an initial guess since the lack of redundant measurements makes these algorithms prone to errors arising from defective position vector estimates.

2.5.2 Orbit Estimation

Least Squares

Since one of the objectives in this thesis is to exploit the properties of Doppler-shift measurements to formulate a convex problem, a closer look is taken on the use of this kind of observation in orbit estimation. The classical use of Doppler-shift measurements is surveyed in this section, based on Least-Squares formulations.

The principle of Least-Squares is to find a set of model parameters that minimize the square of the difference between modeled observations and actual measurements, (minimize the square sum of the residuals). In particular for the case of Orbit determination, the LS method is generally used to refine the calculation of an initial state using the observations made at subsequent times.

Denoting $\boldsymbol{x}_0$ as the satellite's state at the reference epoch t_0 and z_k as an observation at instant k, their relation is given by

$$\underbrace{\begin{bmatrix} z_1 \\ \vdots \\ z_k \\ \vdots \\ z_n \end{bmatrix}}_{\boldsymbol{z}} = \underbrace{\begin{bmatrix} h_1(t_1, \boldsymbol{x}_0) \\ \vdots \\ h_k(t_k, \boldsymbol{x}_0) \\ \vdots \\ h_n(t_n, \boldsymbol{x}_0) \end{bmatrix}}_{\boldsymbol{h}(\boldsymbol{x_0})} + \underbrace{\begin{bmatrix} \epsilon_1 \\ \vdots \\ \epsilon_k \\ \vdots \\ \epsilon_n \end{bmatrix}}_{\boldsymbol{\epsilon}} \tag{2.24}$$

where the function $h_n(t_n, \boldsymbol{x_0})$ is the observation model which relates the observations at time k with the satellite's state at reference epoch t_0 and $\boldsymbol{\epsilon}$ accounts for the measurement errors which are assumed to be randomly distributed with zero mean, since the Least Squares method makes no probabilistic assumptions about the data [23] .
The associated residual $\boldsymbol{r} = \boldsymbol{z} - \boldsymbol{h}(\boldsymbol{x_0})$ is the difference between real and modeled observations. The Least Squares cost function is then written as the sum of the squared residuals

$$S(\boldsymbol{x_0}) = \boldsymbol{r}^T\boldsymbol{r} = (\boldsymbol{z} - \boldsymbol{h}(\boldsymbol{x}_0))^T(\boldsymbol{z} - \boldsymbol{h}(\boldsymbol{x}_0)) \tag{2.25}$$

and the goal is to find the initial state $\boldsymbol{x}_0$ that best approaches the modeled observations to the real ones.

Since $\boldsymbol{h}$ is highly non-linear, it is difficult to find the minimum of the cost function in (2.25), so $\boldsymbol{h}$ is often linearized around an initial guess for the reference state $\boldsymbol{x}_0^*$ and $\boldsymbol{r}$ becomes

$$\boldsymbol{r} \approx \Delta\boldsymbol{z} - \boldsymbol{H}\Delta\boldsymbol{x}_0 \tag{2.26}$$

where $\boldsymbol{H} = \frac{\partial \boldsymbol{h}(\boldsymbol{x}_0)}{\partial \boldsymbol{x}_0}|_{\boldsymbol{x}_0 = \boldsymbol{x}_0^*}$ denotes the Jacobian of the measurement model evaluated at the nominal state $\boldsymbol{x}_0^*$, $\Delta\boldsymbol{z} = \boldsymbol{z} - \boldsymbol{h}(\boldsymbol{x}_0^*)$ and $\Delta\boldsymbol{x}_0 = \boldsymbol{x}_0 - \boldsymbol{x}_0^*$.

Replacing (2.26) into (2.25), one can directly identify the normal equations and arrive at the LS

solution

$$\Delta x_0^{LS} = \left(\boldsymbol{H}^T \boldsymbol{H}\right)^{-1} \left(\boldsymbol{H}^T \Delta \boldsymbol{z}\right) \tag{2.27}$$

The best estimate for the reference state $\hat{\boldsymbol{x}}_0$ is then given by $\hat{\boldsymbol{x}}_0 = \boldsymbol{x}_0^* + \Delta x_0^{LS}$.
In the case where some measurements are known to be more accurate than others, a weighting factor can be introduced in the equation, resulting in

$$\Delta x_0^{WLS} = \left(\boldsymbol{H}^T \boldsymbol{W} \boldsymbol{H}\right)^{-1} \left(\boldsymbol{H}^T \boldsymbol{W} \Delta \boldsymbol{z}\right) \tag{2.28}$$

where $\boldsymbol{W}$ is a diagonal matrix containing the weights. This is known as *Weighted Least Squares*. There are several examples of this method in the older literature on orbit determination.
In [7], the author uses the Doppler-Shift measurements to get a representation of the radial velocity of a satellite tracked by three stations. The observations are used to fit a polynomial of 7$^{\text{th}}$ order that locally approximates the satellite radial velocity, and after integration, the position. Then, two instants are chosen in order to obtain six distance measurements along with the angles obtained from the geographic position of the tracking stations. The set of three pairs (distance, angle), enables the preliminary orbit determination using the *Gauss* method [6] to find the Keplerian orbit parameters.

In [8], the author assumes that the preliminary orbit determination was already made and focuses on improving the estimate by differential correction of the initial approximation for the orbit of a satellite which emits a radio signal. The Weighted Least Squares method is applied to minimize the residuals between the observed Doppler-shift and the expected frequency shift based on the pre-determined orbit. The resulting residuals are added to the current position and velocity estimates and the algorithm continues iteratively until the root mean square of the residuals reaches a minimum. This method provides very good results in the determination of the orbital plane and good determination of the shape of the ellipse, but poor results in estimating the orientation of the ellipse in the orbital plane. If the preliminary determination of the orbit is in the range of the differential corrector, positions can be determined to a few tens of kilometers from observations performed by a single station at just one pass, with improvements in subsequent transits.

In [9], the author proposes an approach similar to [8] describing a method to improve the estimation by differential correction of the pre-determined orbit. This method uses once again the current estimation of the position and velocity to compute the necessary variations to the state that minimizes the error between the predicted observations in the estimated orbit and the real ones. The difference between them resides in the fact that in this scenario the radio signal is sent by an emitting station on Earth, reflected by the satellite and received by a different station, which requires a different metric to measure the Doppler-shift. It is important to note that the direct use of the orbital parameters in the Least-Squares minimization may result in an ill-conditioned problem since the normal equations may not be sufficiently independent. The method converges provided that the initialization of each position coordinate does not exceed about $80\,\mathrm{km}$ and the velocity measurements are correct to within $0.8\,\mathrm{km/s}$ to $1.6\,\mathrm{km/s}$. However, if two tracking stations were used instead of just one, the convergence would be attained for errors up to $320\,\mathrm{km}$ in position and $1.6\,\mathrm{km/s}$ in velocity. This method was specifically developed for the DOPLOC

(DOppler Phase LOCk) system [25].

In [10] the author utilizes the same idea of the differential correction scheme presented in the above articles but calculates the theoretical Doppler-Shift measurements in two distinct ways: calculating the velocity of the satellite relative to the observer based on the estimated parameters or computing the rate of change of the distance between the observer and the satellite. The author concludes that, for observations performed by a single station, it is very difficult to estimate accurately the parameters e, i and ω_0 and suggests the use of the parameters from the prediction services of the world tracking networks. In this way, after estimating the remaining parameters, it should be possible to obtain the satellite position in the region of the observer within $20\,\mathrm{km}$.

This approach may also be found in more recent publications such as [22], where an accuracy evaluation is made about the tracking of a French Brazilian Micro-satellite using only one-way Doppler-shift information from measurements of a single station. For a satellite with $775\,\mathrm{km}$ circular orbit and near-equatorial inclination, a total of 8 passes were recorded with 600 frequency measurements per pass. After performing the Least Squares routine using a reference orbit previously determined, the resulting solution presented a standard deviation of $2\,\mathrm{km}$ in position.

Sequential Estimation

The Least Squares approach enables the processing of batches of measurements and may be easily adapted to incorporate new observations along with the last computed state correction. The drawback of this correction scheme is that the state which is being updated is at epoch t_0 instead of the last measurement instant.

Alternatively, a method of *sequential estimation* can be used based on the Kalman filter.

Denoting by x_i^{ref} the state vector that is obtained by propagating the reference state x_{i-1}^{ref} from epoch t_{i-1} to t_i and representing by Φ the transition matrix from epoch t_{i-1} to epoch t_i (obtained from satellite dynamics), the filter predicts a new state (without information of the new measurements) by the following equation.

$$x_i^- = x_i^{ref} + \Phi_i(x_{i-1}^+ - x_{i-1}^{ref}) \tag{2.29}$$

where x_{i-1}^+ represents the state vector at the previous epoch (including the information of the measurements at that epoch).

The a priori covariance matrix is given by

$$P_i^- = \Phi_i P_{i-1}^+ \Phi_i^T \tag{2.30}$$

where P_{i-1}^+ represents the covariance matrix at the previous epoch (including the information of the measurements at that epoch).

To incorporate the new measurements, the filter updates the current state using the observation at the current instant z_i, the observation predicted for that instant using a linearization for the observation model, h_i, (through a Taylor series expansion with jacobian H_i, around x_i^{ref}) and a vector of gains K_i

called the *Kalman Gain vector*.

The update of the state can then be written as

$$x_i^+ = x_i^- + K_i \left(z_i - h_i(x_i^{ref}) - H_i \left(x_i^- - x_i^{ref} \right) \right) \tag{2.31}$$

More details on the update process may be found in [6] and [5].
Since the algorithm requires the linearization of h_i, it is called as the *Linearized Kalman filter*.

According to (2.31), the state can be updated using only the measurement taken at the instant of computation, with the past information encoded in the previous state estimate. This enables the use of this algorithm in real-time applications and provides a propagation of the state and covariance matrix over time instead of updating the state at a reference epoch as Least Squares does.

Note, however, that for practical applications of the *Linearized Kalman Filter* the deviations between the reference state and the estimated state must be small enough to neglect any non-linearities in the system dynamics an thus enable the algorithm to converge. To alleviate this issue, the reference state x_{i-1}^{ref} can be reset to the state estimate x_{i-1}^+ at each iteration. Repeated linearization of the dynamics is the basis for *Extended Kalman Filter* (EKF).

Still, the EKF tends to quickly diverge if there are large linearization errors.

2.6 Maximum Likelihood Formulation

From the transformations summarized in Appendices B and C one may observe that the relation between the observations made by an observer in Cartesian coordinates and the satellite's orbital parameters are highly non-linear and non-convex. Although the techniques used for Precise Orbit Determination generally work with models that directly use the orbital elements to model the satellite's dynamics and observations [26], they produce rather intricate expressions which would introduce a huge complexity in this problem. Thus, it is much easier to formulate the estimation problem in Cartesian coordinates. However, the problem loses the favorable property of having 6 parameters to estimate at each instant but 5 of them being constant through all measurement instants.

A brief introduction to the MLE framework was presented in Sec. 2.4.3.

In the following sections, the measurement models in Cartesian coordinates are described and the known relaxations are discussed.

In a related work, albeit in a different context, the author in [27] formulates the problem of determination of an aircraft pose as it approaches an aircraft carrier. The plane has an IMU on-board from which it obtains measurements of acceleration, angular velocity, and local magnetic field. On the ground, there are three RF beacons from which it is possible to measure the pseudo-range, angle of transmission and the range-rate (from Doppler-Shift measurements). In order to obtain an estimate for the position and attitude (at each time instant) from the combination of the information extracted by the RF signals and the

IMU, a Maximum-Likelihood estimator was constructed. The estimator uses the measurements obtained in the past T instants up to the current instant, t_0. This technique is known as FHMLE (Finite Horizon Maximum-Likelihood Estimation). The MLE was computed numerically using a solver implemented in the MATLAB® Toolbox, TensCalc© [28].

Since part of the available measurements and estimation variables are common to the problem addressed in this thesis and even the problem formulation uses the Maximum-Likelihood framework as in this case, a closer analysis will be made with the respective adaptations.

Pseudo-Range

The *pseudo-range* (PR) is the distance between an emitter and a receiver computed from the travel time of a message exchanged between them. In this case, it corresponds to the difference between the time-stamp, t_s of a packet sent by a satellite and the time of reception by the ground station, t_r.
In the context of this thesis, the clock offset between the two agents will be considered negligible to simplify the problem. Moreover, the agents are a satellite and a ground station which typically have precise clocks and proper mechanisms for clock synchronization.

The expression that relates the position of the satellite $\boldsymbol{r}$ and the station $\boldsymbol{r}_{gs}$ at observation k with the (PR) measurement may be written as

$$\rho^k = c\,(t_r^k - t_s^k). \tag{2.32}$$

Modeling the measurement error introduced by the RF system as a random variable with Gaussian distribution with zero mean and variance σ_ρ^2, the likelihood function for the pseudo-range may be written as

$$L(\rho^k; \boldsymbol{r}^k) = \frac{\exp\left(-\frac{\left(\rho^k - \left\|\boldsymbol{r}^k - \boldsymbol{r}_{gs}^k\right\|\right)^2}{2\sigma_\rho^2}\right)}{\sqrt{2\pi}\sigma_\rho}. \tag{2.33}$$

Angle-of-Transmission

The angle-of-transmission corresponds to the unit vector pointing from the ground station's antenna to the satellite. Under the assumption of an ideal emission/receiving system, the angle-of-transmission is related to the position of the ground station and the position of the satellite by

$$AoT^k = \frac{\boldsymbol{r} - \boldsymbol{r}_{gs}}{\|\boldsymbol{r} - \boldsymbol{r}_{gs}\|} \tag{2.34}$$

To obtain a closer model of the reality that accounts for the noise introduced by the RF systems and by the mechanical antenna's control system, the AoT measurements may be modeled as a random variable described by some *pdf* that is able to handle directional data (since the measurements are most naturally expressed as vectorial quantities, although they are most commonly given by a pair of azimuth/elevation angles). The "equivalent" of the Normal distribution for directional data is the Von-Mises Fisher distribution.

The Von-Mises Fisher distribution (VMF) is a class of multidimensional directional distributions with support in the unit sphere of order $(p-1)$ for a p-dimensional space [29].

The probability density function of a p-dimensional random vector $\boldsymbol{x}$ is given by

$$f_p(x;\mu,\kappa) = C_p(\kappa)e^{\kappa\mu^T\boldsymbol{x}} \tag{2.35}$$

where μ denotes the mean direction, κ represents the concentration parameter (analogous to the inverse of the variance $\left(\sigma^2 \approx \frac{1}{\kappa}\right)$ [29] in the Normal distribution) and $C_p(k)$ is a normalization factor.

For a three-dimensional vector $\boldsymbol{x}$, as in this case, the VMF is supported on a three-dimensional sphere and the normalization factor can be written as

$$C_3(\kappa) = \frac{\kappa}{4\pi\sinh(\kappa)} \tag{2.36}$$

Fig. 2.11 shows the behavior of the distribution as the concentration parameter varies. The simulations were based on a publicly available MATLAB® function to generate random samples from a VMF distribution [30].

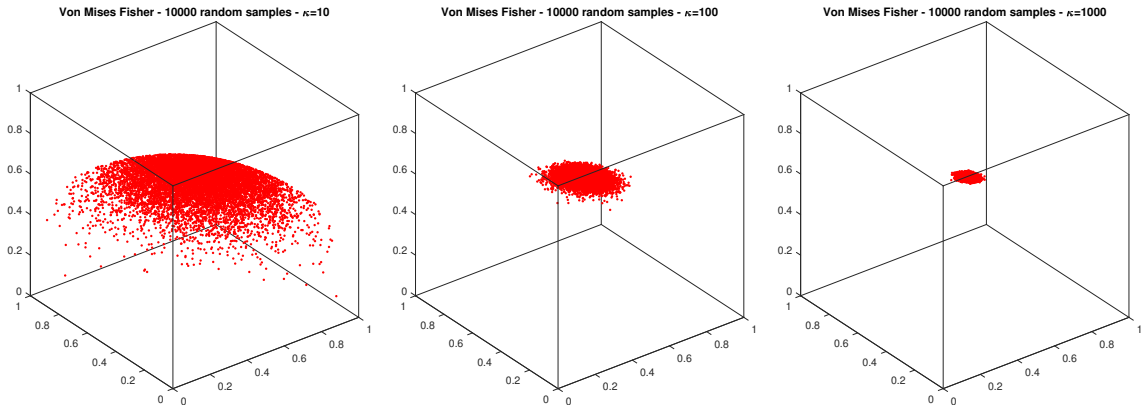

(a) 1000 random samples of Von-Mises Fisher distribution with concentration parameter $\kappa = 10$.

(b) 1000 random samples of Von-Mises Fisher distribution with concentration parameter $\kappa = 100$.

(c) 1000 random samples of Von-Mises Fisher distribution with concentration parameter $\kappa = 1000$.

Figure 2.11: Comparison of a random sampling of the Von-Mises Fisher distribution with mean vector $\mu^T = [1,1,1]$ and different values of the concentration parameter, κ.

Using the Von-Mises Fisher distribution with mean given by (2.34) and $\kappa > 0$ to model an AoT measurement from a ground station at instant k , the likelihood function may then be written as

$$L(AoT^k;\boldsymbol{r}^k) = \frac{\exp\left(\kappa\frac{(\boldsymbol{r}^k-\boldsymbol{r}_{gs}^k)^T AoT^k}{\left\|\boldsymbol{r}^k-\boldsymbol{r}_{gs}^k\right\|}\right)}{2\pi(e^{\kappa}-e^{-\kappa})}. \tag{2.37}$$

Doppler-shift

An emitter that sends a signal while it is approaching/moving away from a receiver, causes a frequency change in the emitted signal that increases/decreases its frequency, respectively.

The diagram of velocities of a spacecraft in a straight trajectory is presented in Fig. 2.12.

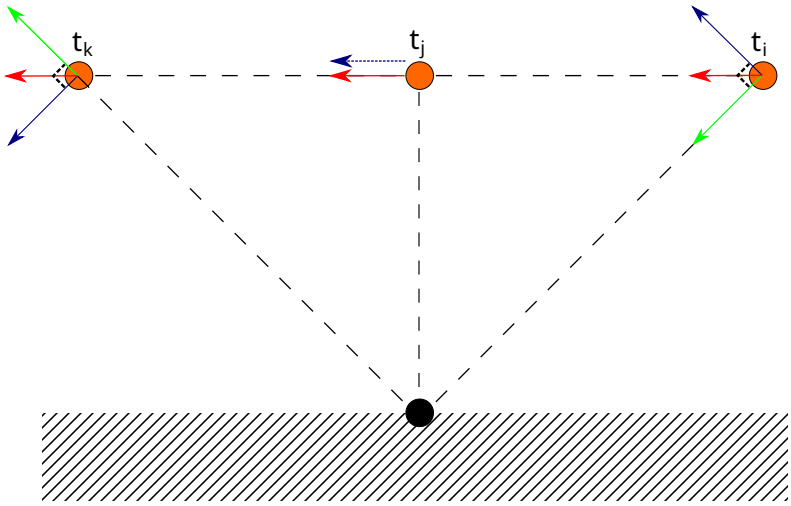

Figure 2.12: Diagram of velocities at instants t^i, t^j and t^k between a spacecraft in a straight trajectory (orange circles) and a static receiver on the ground (black circle). The arrow (red) is the sum of the radial velocity (green) and the tangential velocity (blue). Adapted from [31].

The relation between the radial velocity (or range-rate) of the spacecraft, the frequency of the transmitted signal, f_t^k, and the frequency of the received signal, f_r^k, may be written as [27]

$$\dot{\rho}^k = c\left(1 - \frac{f_r^k}{f_t^k}\right) \tag{2.38}$$

The radial velocity $\dot{\rho}^k$ is positive when the relative distance between the two objects is decreasing and is negative if they are moving apart.

If the spacecraft travels at a constant speed, the behavior of the received frequency is illustrated in Fig. 2.13 for an ideal case with noiseless measurements.

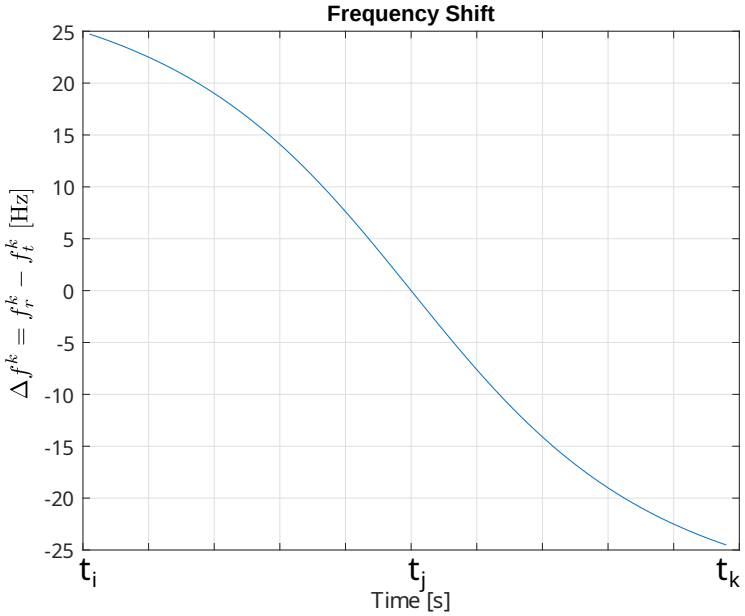

Figure 2.13: Illustration of the frequency shift in the received signal for the spacecraft's trajectory depicted in Fig. 2.12. This shape is known as the Doppler-shift curve.

An alternative equation that follows from (2.38) relates the Doppler-shift $\Delta f^k = f_r^k - f_t^k$ measured at ground station $\boldsymbol{r}_{gs}^k$ with the position of the satellite $\boldsymbol{r}^k$

$$\Delta f^k = -\frac{f_t^k}{c}\frac{d}{dt}\left\|\boldsymbol{r}^k - \boldsymbol{r}_{gs}^k\right\| \tag{2.39}$$

which indicates that the measured Doppler-shift is proportional to the range-rate.

Taking the derivative in (2.39) and expanding, results in

$$\Delta f^k = -\frac{f_t^k}{c}\frac{(\boldsymbol{r}^k - \boldsymbol{r}_{gs}^k)^T \cdot (\boldsymbol{v}^k - \boldsymbol{v}_{gs}^k)}{\left\|\boldsymbol{r}^k - \boldsymbol{r}_{gs}^k\right\|}. \tag{2.40}$$

To obtain an intuitive geometric interpretation of (2.40) one may observe that Δf^k is proportional to the projection of the relative velocity $(\boldsymbol{v}^k - \boldsymbol{v}_{gs}^k)$ onto the relative direction vector $\frac{\boldsymbol{r}^k - \boldsymbol{r}_{gs}^k}{\left\|\boldsymbol{r}^k - \boldsymbol{r}_{gs}^k\right\|}$.

To enable the representation of the perturbations added by the RF system, the Doppler-shift error measurement may be represented by a random variable modeled by a Gaussian distribution with zero mean and variance σ_f^2.

The likelihood function may then be written as

$$L\left(\Delta f^k; \boldsymbol{v}^k\right) = \frac{\exp\left(-\frac{\left(\Delta f^k + \frac{f_t^k}{c}\frac{(\boldsymbol{r}^k - \boldsymbol{r}_{gs}^k)^T(\boldsymbol{v}^k - \boldsymbol{v}_{gs}^k)}{\left\|\boldsymbol{r}^k - \boldsymbol{r}_{gs}^k\right\|}\right)^2}{2\sigma_f^2}\right)}{\sqrt{2\pi}\sigma_f} \tag{2.41}$$

2.6.1 Complete ML formulation

The individual log-likelihood functions follow from applying the logarithm to (2.33), (2.37) and (2.41)

$$\ell(\rho^k; \boldsymbol{r}^k) = \log L(\rho^k; \boldsymbol{r}^k) = \log(\sqrt{2\pi}\sigma_\rho) - \frac{\left(\rho^k - \left\|\boldsymbol{r}^k - \boldsymbol{r}_{gs}^k\right\|\right)^2}{2\sigma_\rho^2} \tag{2.42}$$

$$\ell(AoT^k; \boldsymbol{r}^k) = \log L(AoT^k; \boldsymbol{r}^k) = \log(2\pi(e^\kappa - e^{-\kappa})) + \kappa\frac{(\boldsymbol{r}^k - \boldsymbol{r}_{gs}^k)^T AoT^k}{\left\|\boldsymbol{r}^k - \boldsymbol{r}_{gs}^k\right\|} \tag{2.43}$$

$$\ell\left(\Delta f^k; \boldsymbol{r}^k, \boldsymbol{v}^k\right) = \log L\left(\Delta f^k; \boldsymbol{r}^k, \boldsymbol{v}^k\right) = \log(\sqrt{2\pi}\sigma_f) - \frac{\left(\Delta f^k + \frac{f_t^k}{c}\frac{(\boldsymbol{r}^k - \boldsymbol{r}_{gs}^k)^T(\boldsymbol{v}^k - \boldsymbol{v}_{gs}^k)}{\left\|\boldsymbol{r}^k - \boldsymbol{r}_{gs}^k\right\|}\right)^2}{2\sigma_f^2} \tag{2.44}$$

According to (2.19), the total log-likelihood function may then be written as

$$\ell(\boldsymbol{r}, \boldsymbol{v}) = \sum_{k=1}^{N} \ell(\rho^k; \boldsymbol{r}^k) + \ell(AoT^k; \boldsymbol{r}^k) + \ell\left(\Delta f^k; \boldsymbol{r}^k, \boldsymbol{v}^k\right) \tag{2.45}$$

and the problem of finding the ML estimator follows from (2.20),

$$\hat{\boldsymbol{\theta}}_{ML} = \underset{\boldsymbol{r}^k, \boldsymbol{v}^k}{\arg\max}\ \ell(\boldsymbol{r}, \boldsymbol{v}) \tag{2.46}$$

which is equivalent to

$$\hat{\boldsymbol{\theta}}_{ML} = \arg\min_{\boldsymbol{r},\boldsymbol{v}} \sum_{k=1}^{N} \frac{1}{2\sigma_\rho^2} \underbrace{\left(\rho^k - \left\|\boldsymbol{r}^k - \boldsymbol{r}_{gs}^k\right\|\right)^2}_{F_\rho^k} - \kappa \underbrace{\frac{(\boldsymbol{r}^k - \boldsymbol{r}_{gs}^k)^T AoT^k}{\left\|\boldsymbol{r}^k - \boldsymbol{r}_{gs}^k\right\|}}_{F_\alpha^k} + \frac{1}{2\sigma_f^2} \underbrace{\left(\Delta f^k + \frac{f_t^k}{c} \frac{(\boldsymbol{r}^k - \boldsymbol{r}_{gs}^k)^T (\boldsymbol{v}^k - \boldsymbol{v}_{gs}^k)}{\left\|\boldsymbol{r}^k - \boldsymbol{r}_{gs}^k\right\|}\right)^2}_{F_f^k} \tag{2.47}$$

The following sections are dedicated to study possible relaxations that may be applied to F_ρ^k, F_α^k and F_f^k in order to solve an approximation of the optimization problem (2.47) using a convex solver, so it can estimate the satellite's position and velocity over time from the observations of ρ^k, AoT^k and Δf^k. The emitted signal's frequency, f_t^k, and propagation velocity, c, are assumed to be known as well as the variance of the noise affecting the observations which is assumed to be estimated externally.

2.6.2 Known relaxations

Pseudo-range

The function in (2.33) is non-convex due to the argument of the exponential term in the numerator. According to the definition of convex function given in Sec. 2.4.4, any chord between two points of a function should be above that function (in the domain between the points), which is not verified in this case, as depicted in Fig. 2.15a.

To overcome this issue, a relaxation technique developed in [32] may be adapted to this case to formulate an alternative convex function. Instead of trying to minimize de difference between the real distance and the measured distance between the agents, the requirement is relaxed to minimize the difference only for positions that are outside the circle with a radius equal to the measurement value, d, as depicted in Fig. 2.14.

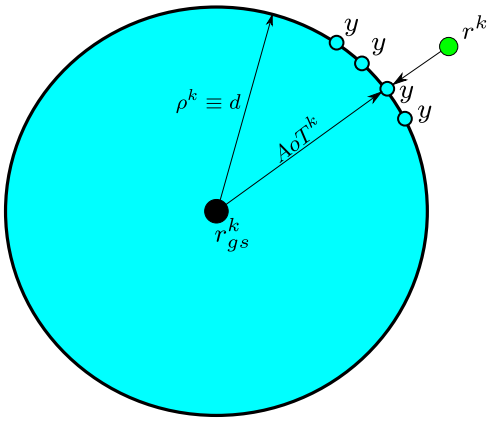

Figure 2.14: Visual representation of the convex relaxation for distance and angle measurement. A disk was used for simplicity of representation but the conclusions are identical for higher dimensions. The range measurement ρ^k obtained from the sensor k now defines the value of d while $\boldsymbol{y} \in \mathcal{D}(r_{gs}^k, d)$. Based on [15].

Beyond the naturally required estimated position variable $\boldsymbol{r}^k$ a new variable $\boldsymbol{y}$ is introduced in [32]. The intention is that $\boldsymbol{y}$ should be as close as possible to the real position $\boldsymbol{r}^k$ but it cannot leave the disk with radius d which corresponds to the raw range measurement. Although in [15] this modification

enables a parallel implementation of the localization algorithm, in this centralized case there is no need to introduce this new estimation variable since, equivalently, the difference $\left\|\boldsymbol{r}^k - \boldsymbol{r}_{gs}\right\| - \rho^k$ may simply be clipped to zero when it takes on negative values.

The simplified likelihood function may be written as

$$L(\rho^k; \boldsymbol{r}^k) = \frac{\exp\left(-\frac{\left[\left(\left\|\boldsymbol{r}^k - \boldsymbol{r}_{gs}^k\right\| - \rho^k\right)_+\right]^2}{2\sigma_\rho^2}\right)}{\sqrt{2\pi}\sigma_\rho} \tag{2.48}$$

where $[x]_+ = \max(0, x)$.

The new relaxed contribution to the likelihood is represented in Fig. 2.15b.

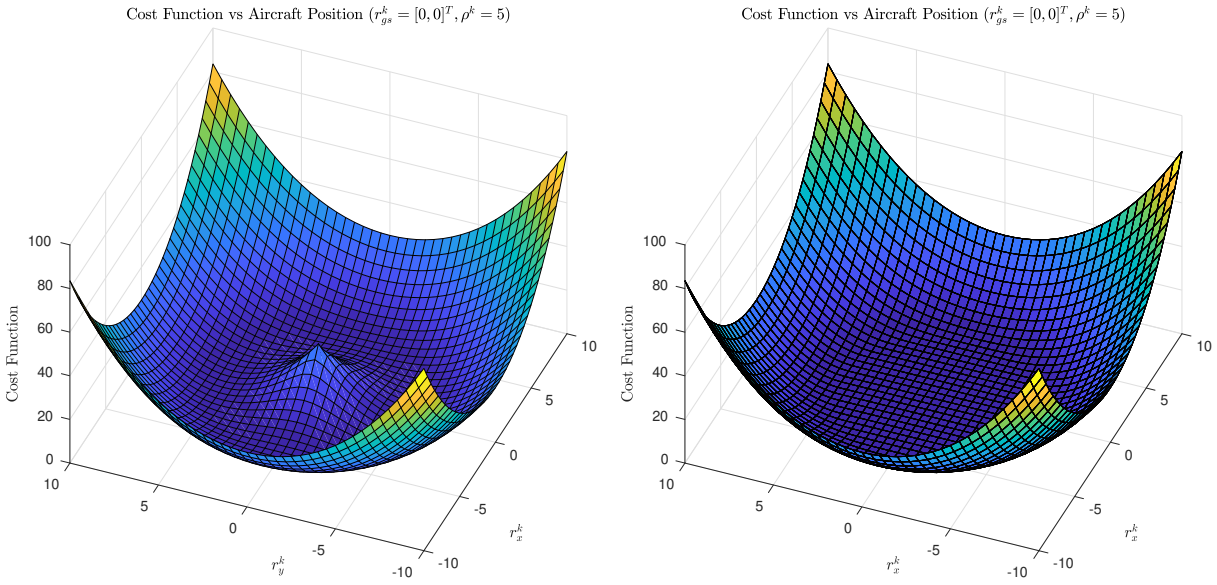

(a) Representation of the argument of the exponential $\left(\left\|\boldsymbol{r}^k - \boldsymbol{r}_{gs}^k\right\| - \rho^k\right)^2$.

(b) Representation of the argument of the exponential $\left[\left(\left\|\boldsymbol{r}^k - \boldsymbol{r}_{gs}^k\right\| - \rho^k\right)_+\right]^2$.

Figure 2.15: Visual comparison between the original cost function (2.33) and its relaxed version (2.48).

Angle of Transmission

The cost function in (2.37) is also non-convex due to the denominator term $\|\boldsymbol{r} - \boldsymbol{r}_{gs}\|$ in the argument of the exponential. A relaxation for the angle term was developed in [15] based on the same reasoning made for the distance term.

According to Fig. 2.14, since $\boldsymbol{y}$ corresponds to the projection of $\boldsymbol{r}^k$ onto the disk when $\boldsymbol{r}^k$ is outside of it, $\frac{\boldsymbol{y}}{d}$ will be a unit norm vector that encodes the angle between the two agents, so, the non-convex term $\frac{(\boldsymbol{r}^k - \boldsymbol{r}_{gs}^k)^T AoT^k}{\left\|\boldsymbol{r}^k - \boldsymbol{r}_{gs}^k\right\|}$ can be approximated by $\frac{\boldsymbol{y}^T AoT^k}{d}$ [2]. For a problem with multiple agents, this formulation is very advantageous since $\boldsymbol{y}$ will be adjusted to cope with the angular measurements and (for positions outside the disk), $\boldsymbol{y}$ will maintain the nice property $\|\boldsymbol{y}\| = d$.

[2] Adding this term that depends on $\boldsymbol{y}$ biases the global likelihood function such that the original geometric interpretation for $\boldsymbol{y}$ becomes only approximate. This will not seriously degrade the performance unless perhaps range/angle measurements are extremely noisy. In fact, the bias term is shown to be beneficial in [33] under most conditions when compared to range-only measurements

On the other hand, when $\|\boldsymbol{y}\| \leq d$ the relaxation loses accuracy since the result $\frac{\boldsymbol{y}}{d}$ is no longer a unit vector.

Adapting this formulation to the problem addressed in this thesis where the range error is a tiny fraction of the true range between the agents (since range measurement errors are on the order of a few kilometers, while a satellite's closest approach to the ground station is on the order of hundreds of kilometers; see Appendix E.2), the normalization may be simply approximated by $\frac{\boldsymbol{r}-\boldsymbol{r}_{gs}}{\rho^k}$ and introducing the additional variable $\boldsymbol{y}$ becomes unnecessary. Given the differences in the magnitude of the measured range and the true range, the impact of this approximation on the minimization is small since the denominator is acting almost like a normalization constant with the great advantage of having just half of the variables to optimize. The resulting likelihood function of applying this relaxation to (2.37) is

$$L(AoT^k; \boldsymbol{r}^k) = \frac{\exp\left(\kappa \frac{(\boldsymbol{r}^k - \boldsymbol{r}_{gs}^k)^T AoT^k}{\rho^k}\right)}{2\pi(e^{\kappa} - e^{-\kappa})}. \tag{2.49}$$

Doppler Relaxations

Several examples can be found in the literature that incorporate Doppler-shift information for purposes of localization and tracking of a target, not specifically a satellite. Also, the majority of the relaxations found in this survey are targeted for cases where simultaneous Doppler-shift measurements are available, and so, they can't be directly used but rather serve as inspiration for the work developed in the next sections. In [34] the author addresses the problem of localization of a target, moving in a 2D plane, which emits a constant but unknown tone and maintains a constant-course and speed. The tone is detected by a network of five sensors and the best fitting position is found by maximizing a Doppler-shift cost function using grid search with subsequent filtering in order to reduce the search space. This approach is computationally expensive and prone to sub-optimal solutions.
On the other hand, in [35] the author develops a closed-form solution to determine the initial position and velocity of a moving target in a 2D scenario from only three measurements of Doppler-shift taken by a static observer and the initial angle between the two. An algorithm that only uses the minimum necessary measurements to compute the solution is more prone to errors introduced by noisy observations, which is the case here. However, the main limitation of this algorithm is that the solution was developed for a 2D scenario, and so, the resulting expressions are attached to the geometry of the problem making it not generalizable for 3D. In [36] and [37] the solutions are obtained using statistical estimation tools but the 2D scenario assumption is also present making it not suitable for the current problem.

The literature found which most closely resembles the problem of developing a convex relaxation to incorporate Doppler information in a localization problem was [38] and [39].

In [38] a comparison is made between a relaxation of the Doppler term into a SOCP or SDP formulation and also includes a relaxation of TDOA terms to augment the available information. It was concluded that SOCP provides a slightly better result in obtaining a target's localization but is prone to failure when the target is outside the convex hull of the observers. On the other hand, when the problem

is written in the form of an SDP, it provides an acceptable result for any position of the observers at the expense of increased computational cost. However, these relaxations cannot be directly applied in the case of this thesis since the scenario in which these relaxations are developed assume static targets and more than one moving observers to ensure observability (in this case there are two observers, which is the minimum required to ensure observability in a 2D scenario). Also, by knowing that the target is static, its velocity does not need to be estimated, and more importantly, there is only one target position to be estimated over all observation window.

In [39] only Doppler-shift measurements are used to localize a moving target with an unknown trajectory, observed by M stationary sensors. The ML cost function is reformulated as a Constrained Weighted Least Squares (CWLS) and then relaxed into an SDP problem. The resultant solution is used to initialize a non-linear solver (Levenberg–Marquardt) and the two solutions are compared to ensure that the iterative algorithm has achieved convergence. Similarly to the previous work, it was found that this relaxation is accurate even when the target is outside the convex hull of the sensors. Once again, this relaxation cannot be used in the context of this thesis since it was developed in an environment with 8 observers and one target, requiring more simultaneous measurements than those available in the present scenario.

Chapter 3

Implementation

3.1 Simplifying assumptions

According to [6], the required level of orbit estimation accuracy employed in space missions that is necessary to transmit and receive mission operation data, antenna pointing and attitude control, ranges from $1\,\mathrm{km}$ to $10\,\mathrm{km}$, therefore this range will be used to decide about the quality of the estimation for this application.

To streamline the implementation, and considering the level of accuracy intended, some simplifying assumptions regarding satellite movement and ground-based observations can be made.

When considering an observation window of a few minutes (which is the typical pass duration for satellites in LEO), the orbit perturbations discussed in Sec. 2.2.3 are negligible. Regarding distance measurements described in Sec. 2.3.1, it is assumed that the bias introduced by clock offset is sufficiently small to be neglected and the only error sources are the satellite's and station's transceivers.

Errors associated with angular information are assumed to arise from inaccuracies in the antenna's control system and modeled by a von-Mises Fisher distribution. Biases associated with mechanical defects of the antenna's rotator are not considered. Other angular error sources presented in Sec. 2.3.2 are not taken into account given their reduced effect.

The satellite's transceiver frequency is assumed to be sufficiently stable or periodically corrected so that the error due to oscillator drift has little effect on the range-rate measurement. Considering a frequency of operation of $425\,\mathrm{MHz}$ (which is frequent in CubeSat missions [40]) errors related to the signal propagation path such as ionospheric refraction effects, are not considered for analysis due to the physical properties discussed in Sec. 2.3.1.

Finally, the station's position is assumed to be absolutely determined without error.

The remaining sources of error are assumed to be well represented by Gaussian distributions.

3.2 Doppler cost function relaxations

The objective of this section is to investigate the possible relaxations to a cost function based on the Doppler-shift measurement model. Fig. 3.1 summarizes the names of the variables used in the next sections.

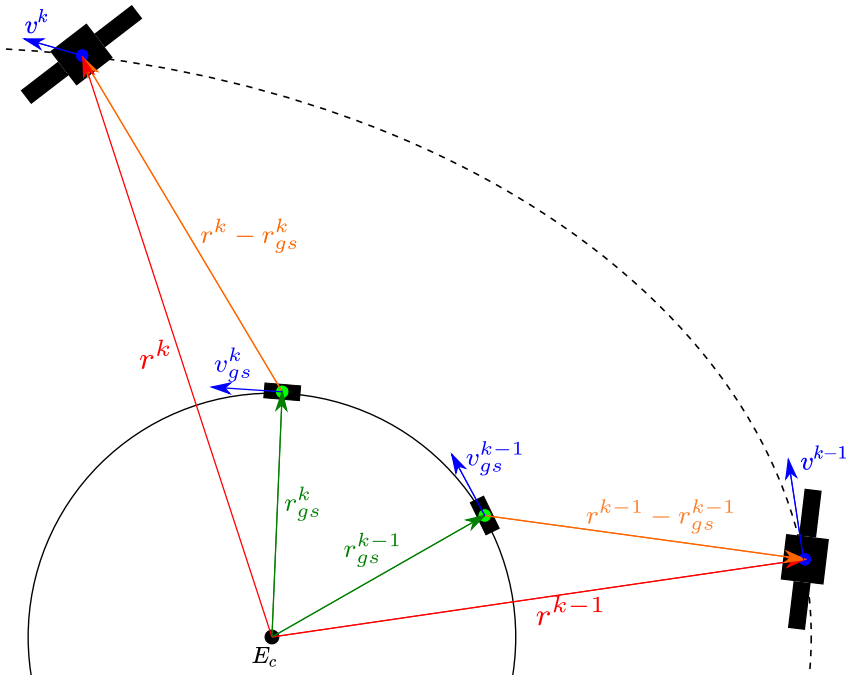

Figure 3.1: Representation of vectorial components that form the satellite's position vector.

3.2.1 Relaxation Overview

Doppler Information

The Doppler-shift term, F^k_f, in (2.47) does not fit the framework of *Disciplined Convex Programing* problems since its construction does not follow the rules summarized in Sec. 2.4.4.

In fact, it's easy to spot two terms that can't be constructed according to those rules, namely, a bi-linear term $(\boldsymbol{r}^k - \boldsymbol{r}^k_{gs})^T(\boldsymbol{v}^k - \boldsymbol{v}^k_{gs})$ and a vector norm in the denominator $\left\|\boldsymbol{r}^k - \boldsymbol{r}^k_{gs}\right\|$.

These terms also introduce a nonlinear relation between the two unknown variables, ($\boldsymbol{r}$,$\boldsymbol{v}$), which obfuscate their dependence on the measurements. This increased difficulty may also be perceived when looking at the complex shape of Fig. 3.2a (simplified cost function associated with the Doppler-shift measurements). Moreover, in order to solely use Doppler-shift observations to localize a spacecraft in a 3D scenario, it would require a minimum of 6 simultaneous and independent measurements to have a finite number of solutions for satellite's position and velocity [41].

This intuitive exploration shows that Doppler information can't be used alone for purposes of localization using only one observation site at a given instant. With more simultaneous observations this conclusion is no longer valid [39].

This creates a limitation on the usefulness of Doppler-shift measurements and it is expected that the

introduction of this information to improve position estimation will have little influence on the final result except if the consecutive range measurements are too irregular.

Since the MLE framework produces an estimator that is asymptotically unbiased when used with a large number of observations, the CRLB may provide some insight about the amount of information provided by the Doppler-shift observations. The hypothesis is that, since CRLB gives the best attainable variance for an unbiased estimator (if it exists), then the variance of the estimator, $\hat{\theta}_{\rho\alpha f}$, which uses information about the range, ρ, the angle, α, and the Doppler-shift measurements, f, should be smaller than the one which just uses distance and angular information $\hat{\theta}_{\rho\alpha}$. Some preliminary results of the theoretical CRLB calculation are described in Appendix D. From the analysis made for a complete pass with very high elevation (the case where Doppler-shift should contribute with more information) the calculations show that, with good quality pseudo-range measurements, the Doppler-shift model approximation with the bigger potential to improve the information quantity is the one that uses the velocity approximation by differences in positions. For a case with noisier pseudo-range measurements, both show some degree of improvement. Note however that, this is only a best case study, i.e., the calculated values only corresponds to the best achievable standard deviation, and does not necessarily reflect the real-world performance of any given estimator.

Doppler function relaxation options

At this point, two possible ways were explored to manipulate the expression in (2.39) and obtain an approximate but convex function:

Discrete derivative relaxation The derivative term in (2.39) is approximated by an expression which uses discrete-time position terms followed by a suitable convex relaxation.

Analytical derivative relaxation The analytical derivative in (2.40) is used and some convex relaxation strategy is employed to overcome the non-convexity described in Sec. 3.2.1.

To streamline the presentation, all the optimization problems formulated in this section only focus on the Doppler-shift cost term, but the remaining terms relative to angle and distance presented in Sec. 2.6.1 are implicit in the complete problem formulation, with the correspondent modifications required by the Doppler-relaxation scheme in use and which will be pointed out in the respective sections.

3.2.2 Discrete derivative relaxation

Since the measurements are taken in discrete time, the derivative term can't be directly used. The first and most intuitive approach is to approximate the continuous-time derivative by its discrete counterpart. Even then, there are several options to approximate the derivative term depending on the intended accuracy and the causality constraint in the case of position estimation in real-time.

For a generic function f, an approximate second-order finite-divided-difference first derivative, $f'(x_k)$,

may be obtained from 4 consecutive values of $f(x_k)$ from instant $(k-2)$ to $(k+2)$ using

$$f'(x_k) = \frac{-f(x_{k+2}) + 8f(x_{k+1}) - 8f(x_{k-1}) + f(x_{k-2})}{12\Delta t} + O(\Delta t^4) \tag{3.1}$$

Since these expressions are obtained from Taylor series expansion, they implicitly introduce an error caused by the truncation of higher-order terms of the series. In particular, for the approximation in (3.1), the error is proportional to the fourth power of the step-size. This is not useful to assess the accuracy of the approximation alone but it provides insight into the importance of the sampling time, which should be decreased (to the expent possible) to ensure small truncation errors.
An empirical analysis based on simulated data is given in Appendix E, allowing one to conclude that the error obtained with a centered finite-divided-difference term of second order is less than 5%, even if positions are separated by intervals of 4 minutes (for orbits with small eccentricities) which represents a close approximation. Moreover, the more position terms enter the expression, the greater is the correlation between them, which in turn creates redundancy in the measurements, resulting in better position estimates.
Higher-order approximations and further discussion may be found in [42].

Substituting (3.1) in (2.39), the resulting term for F_f^k in (2.47) becomes

$$F_f^k = \left(\Delta f^k + \frac{f_t^k}{c} \frac{- \left\| \boldsymbol{r}^{k+2} - \boldsymbol{r}_{gs}^{k+2} \right\| + 8 \left\| \boldsymbol{r}^{k+1} - \boldsymbol{r}_{gs}^{k+1} \right\| - 8 \left\| \boldsymbol{r}^{k-1} - \boldsymbol{r}_{gs}^{k-1} \right\| + \left\| \boldsymbol{r}^{k-2} - \boldsymbol{r}_{gs}^{k-2} \right\|}{12\Delta t} \right)^2 \tag{3.2}$$

Inspecting (3.2), it becomes clear that it can't be built from the rules in Sec. 2.4.4 since there is a term containing the difference of two convex functions which is not guaranteed to be convex.

Graphical approach

The graphical description of the cost function is a valuable starting point to grasp the function's behavior and get inspiration to construct a relaxed version of it.
Since (3.2) maps a space in $\mathbb{R}^{12}$ to $\mathbb{R}$, it's impossible to sketch it in a graph. However, it is possible to use a discrete derivative approximation of smaller order and also consider only the position's representation in $1D$. Following this idea, the function (3.2) may be modified to accept a domain in $\mathbb{R}^2$

$$F_f^k = \left| \Delta f^k + \frac{f_t^k}{c} \frac{|x| - |y|}{\Delta t} \right| = \left| \Delta f^k + f_i^k \left[|x| - |y| \right] \right| \tag{3.3}$$

where $f_i^k = \frac{f_t^k}{c\,\Delta_t}$ and the variables x and y (schematically) represent the satellite's position in a $1D$ line, at two consecutive instants. Also, the squaring operation was substituted by the absolute value to simplify the following illustrations.

The two plots in Fig. 3.2 illustrate a toy example with $f_i^k = 1$ and with positive and negative Δf^k, respectively.

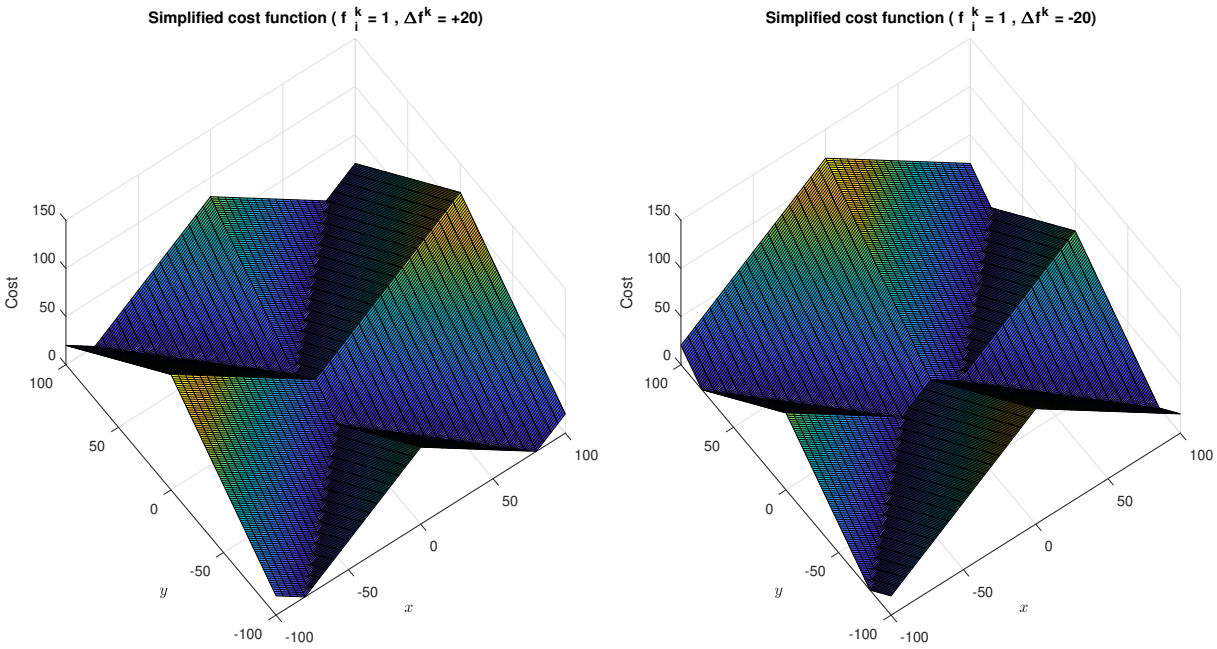

(a) Simplified cost function 3.3 with Δf^k positive.

(b) Simplified cost function (3.3) with Δf^k negative.

Figure 3.2: Illustration of the modified cost function (3.3).

Comparing both plots with the one corresponding to the distance's cost function in Fig. 2.14 one may find that the former present a more complex behavior than the latter. This finding dissuades one from pursuing the graphical approach.

Epigraph relaxation

With the graphical method off the table, the most direct analytical approach to the convex relaxation problem is the well-known epigraph relaxation.

The method consists in substituting the convex functions (which form the full cost function) with a new set of variables and enforcing the solution of the problem for the new variables to be contained on the epigraph of the convex functions replaced by them.

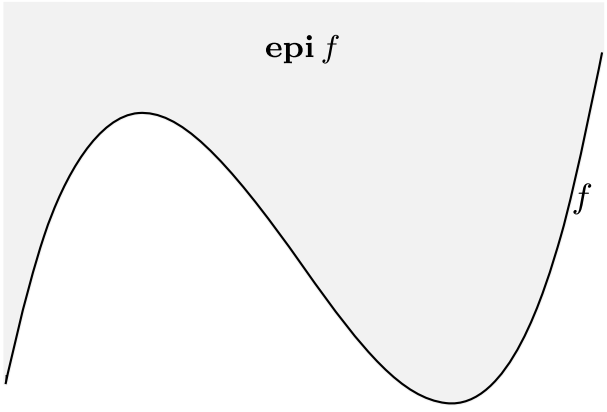

Figure 3.3: Epigraph illustration. The formal definition of the epigraph of a function f is stated in [24] as **epi** $f = \{(x,t) \,|\, x \in \textbf{dom}\ f,\ f(x) < t\}$.

The approximated problem written in the canonical form of a convex optimization problem is

$$\begin{aligned} \underset{\boldsymbol{r},\boldsymbol{t}}{\text{minimize}} \quad & \sum_{k=2}^{N-2} \frac{1}{2\sigma_f^2} \underbrace{\left(\Delta f^k + \frac{f_t^k}{c} \frac{-t^{k+2} + 8t^{k+1} - 8t^{k-1} + t^{k-2}}{12\Delta t} \right)^2}_{F_f^k} + \delta \mathbf{t}^T \mathbf{t} \\ \text{subject to} \quad & \left\| \boldsymbol{r}^k - \boldsymbol{r}_{gs}^k \right\| < t^k \qquad k = 1, \ldots, N \end{aligned} \tag{3.4}$$

which is now a convex optimization problem since it has a convex cost function (composition of an affine function with a convex function) and second-order cone constraints which amounts to requiring that the affine function $(\boldsymbol{r}^k - \boldsymbol{r}_{gs}^k, t^k)$ lie in a convex cone in $\mathbb{R}^4$.

Note also that in (3.4) a penalization term, $\delta \boldsymbol{t}^T \boldsymbol{t}$, is required for the vector $\boldsymbol{t}$ [43]. To understand why, let's suppose that there is no penalization term. Then, if the same constant $c > 0$ is added all elements of $\boldsymbol{t}$, the optimal value of the cost function is unchanged due to the cancellation of $-t^{k+2} - c + 8t^{k+1} + 8c - 8t^{k-1} - 8c + t^{k-2} + c$ but the constraints become loose for a sufficiently large constant. Note also that a weighting factor must be applied to the penalizing term otherwise the norm terms in inequality constraints would be strangled to zero since the penalization term has a much bigger value than the Doppler cost term.

Direct substitution by measurements

Another possible way to ensure convexity in (3.2) is to remove the term that ruins the convexity of the expression. As stated in the previous section, the difference of norms is not guaranteed to be convex. In the case where range measurements are available, they may be used to replace the norm being subtracted, leading to a modified convex optimization problem written as

$$\underset{\boldsymbol{r}}{\text{minimize}} \quad \sum_{k=2}^{N-2} \frac{1}{2\sigma_f^2} \underbrace{\left(\underbrace{\left[\Delta f^k + \frac{f_t^k}{c} \frac{-\rho^{k+2} + 8\left\| \boldsymbol{r}^{k+1} - \boldsymbol{r}_{gs}^{k+1} \right\| - 8\rho^{k-1} + \left\| \boldsymbol{r}^{k-2} - \boldsymbol{r}_{gs}^{k-2} \right\|}{12\Delta t} \right]_+}_{g} \right)^2}_{F_f^k}. \tag{3.5}$$

The drawback is: this creates a strong influence of the range measurement error on the Doppler-shift equation which is in itself already affected by the error in received signal frequency. Moreover, since the expression g is convex but not affine, it requires the function involved in the composition to be convex and non-decreasing to comply with the rules presented in Sec. 2.4.4. For this application, $f(x) = x^2$ was modified to $f(x) = max(0, x)^2$.

In practice, the composition of g with f, $g \circ f$, is equivalent to consider the cost of g only when it's positive. Yet, this choice imposes a limitation: the cost function does not act on the full space of possible solutions since positions that correspond to a greater frequency drift than the measured one don't contribute to the overall cost (since the g is negative in that case). This type of drawback was already encountered in the problem of source localization based on range measurements as found on the Disk Relaxation method presented in Sec. 2.6.2.

Spherical-like Coordinates

The discrete approximation of range-rate would be more practical to use if the expression involving norms was affine, so, in that case, the requirement of a non-decreasing convex function could be dropped. This suggests the separation of the problem into two independent sub-problems for distance estimation and direction estimation, something that could be accomplished by using spherical coordinates.

Ideally, the spherical coordinate system would have the same origin as the ECI frame. However, since all measurements are taken from a ground station, the origin's placement of the spherical coordinate frame is forced to lie at the station's location.

This eases the use of the Doppler-shift cost function but severely limits any constraint relative to satellite dynamics since these constraints are expressed in the ECI frame as presented in Sec. 2.2.1. In this manner $\boldsymbol{r}^k - \boldsymbol{r}_{gs}^k$ is written in terms of its magnitude and direction vector given by r^k and $\hat{\boldsymbol{u}}^k$ respectively. Now it is straightforward to use the Doppler cost function with these new variables since it only involves the information about the range which is represented by r.

With this coordinate transformation, the Doppler cost function only contributes to the range estimation, while the angular information is only determined by the antenna's measured angles. The terms associated with distance and angle are modified accordingly and the resulting optimization problem becomes

$$\begin{aligned} \underset{r,\hat{\boldsymbol{u}}}{\text{minimize}} \quad & \sum_{k=2}^{N-2} \frac{1}{2\sigma_\rho^2} \underbrace{\left(r^k - \rho^k\right)^2}_{F_\rho^k} - \kappa \underbrace{AoT^k \cdot \hat{\boldsymbol{u}}^k}_{F_\alpha^k} + \frac{1}{2\sigma_f^2} \underbrace{\left(\Delta f^k + \frac{f_t^k}{c} \frac{-r^{k+2} + 8r^{k+1} - 8r^{k-1} + r^{k-2}}{12\Delta t}\right)^2}_{F_f^k} \\ \text{subject to} \quad & \left\|\hat{\boldsymbol{u}}^k\right\| \leq 1 \qquad k = 2, \ldots, N-2. \end{aligned} \tag{3.6}$$

3.2.3 Analytical derivative relaxation

The previously introduced equation (2.40) uncovers a new unknown quantity: the satellite's velocity.

Again, this expression cannot directly be used to build a convex cost function since it depends on the bi-linear term $(\boldsymbol{r}^k - \boldsymbol{r}_{gs}^k)^T(\boldsymbol{v}^k - \boldsymbol{v}_{gs}^k)$ and contains the already mentioned problematic norm term in the denominator.

Substitution by estimated positions

Taking inspiration from the previous section, the first approach to approximate cost function (2.44) using a convex relaxation may be to replace the positions, $\boldsymbol{r}^k$, by the respective measurements, $\hat{\boldsymbol{r}}^k$, and approximate $\hat{\boldsymbol{v}}^k$ according to (3.1). If $\boldsymbol{r}^k$ is chosen to be replaced, the problem of the denominator is solved and the expression ends up as an affine function with the satellite's velocity as the unknown variable. Nevertheless, this can be transformed to a problem whose estimation variables are only positions if the velocity term is approximated by its discrete derivative, as in (3.2). So, after the substitution by position

measurements and the addition of the velocity discrete derivative constraint, the convex optimization problem becomes

$$\begin{aligned} \underset{\boldsymbol{r}}{\text{minimize}} \quad & \sum_{k=2}^{N-2} \frac{1}{2\sigma_f^2} \underbrace{\left(\Delta f^k + \frac{f_t^k}{c} \frac{(\hat{\boldsymbol{r}}^k - \boldsymbol{r}_{gs}^k)^T (\boldsymbol{v}^k - \boldsymbol{v}_{gs}^k)}{\left\| (\hat{\boldsymbol{r}}^k - \boldsymbol{r}_{gs}^k) \right\|} \right)^2}_{F_f^k} \\ \text{subject to} \quad & \boldsymbol{v}^k = \frac{-\boldsymbol{r}^{k+2} + 8\boldsymbol{r}^{k+1} - 8\boldsymbol{r}^{k-1} + \boldsymbol{r}^{k-2}}{12\Delta t} \qquad k = 2, \ldots, N-2. \end{aligned} \tag{3.7}$$

Ping-Pong Position-Velocity

An attempt to reduce the influence of the distance measurement errors on the cost function in (3.7) is to resort to alternating projections, commonly known as the ping-pong method. Beginning with raw position estimates from sensors $\hat{\boldsymbol{r}}$, the optimization problem is solved first with $\boldsymbol{v}$ as the optimization variable but introducing a regularization term to induce agreement between position and velocity, weighted with a penalizing term δ that should be chosen according to the quality of the estimates

$$\underset{\boldsymbol{v}}{\text{minimize}} \quad \sum_{k=2}^{N-2} \frac{1}{2\sigma_f^2} \underbrace{\left(\Delta f^k + \frac{f_t^k}{c} \frac{(\hat{\boldsymbol{r}}^k - \boldsymbol{r}_{gs}^k)^T (\boldsymbol{v}^k - \boldsymbol{v}_{gs}^k)}{\left\| (\hat{\boldsymbol{r}}^k - \boldsymbol{r}_{gs}^k) \right\|} \right)^2}_{F_f^k} + \delta \left\| \boldsymbol{v}^k - \frac{-\hat{\boldsymbol{r}}^{k+2} + 8\hat{\boldsymbol{r}}^{k+1} - 8\hat{\boldsymbol{r}}^{k-1} + \hat{\boldsymbol{r}}^{k-2}}{12\Delta t} \right\|^2 . \tag{3.8}$$

Note that the angle and distance terms of the cost function are not included in this optimization problem since they are not relative to the estimation variable, $\boldsymbol{v}$.

After that, the problem is solved again with the same cost function and the same regularization term, but alternating the optimization variable to $\boldsymbol{r}$ and using $\hat{\boldsymbol{v}}$ from the previous iteration

$$\underset{\boldsymbol{r}}{\text{minimize}} \quad \sum_{k=2}^{N-2} \frac{1}{2\sigma_f^2} \underbrace{\left(\Delta f^k + \frac{f_t^k}{c} \frac{(\boldsymbol{r}^k - \boldsymbol{r}_{gs}^k)^T (\hat{\boldsymbol{v}}^k - \boldsymbol{v}_{gs}^k)}{\left\| (\hat{\boldsymbol{r}}^k - \boldsymbol{r}_{gs}^k) \right\|} \right)^2}_{F_f^k} + \delta \left\| \hat{\boldsymbol{v}}^k - \frac{-\boldsymbol{r}^{k+2} + 8\boldsymbol{r}^{k+1} - 8\boldsymbol{r}^{k-1} + \boldsymbol{r}^{k-2}}{12\Delta t} \right\|^2 . \tag{3.9}$$

The case when $\boldsymbol{r}$ is to be estimated is more problematic since the norm in the denominator is no longer a constant. To circumvent this problem, that norm is approximated with the estimated position vector $\hat{\boldsymbol{r}}$ of the previous iterations.

The iteration index is omitted for simplicity. The cycle repeats until the changes in position and velocity are negligible between iterations or in the worst case, if the algorithm diverges (or oscillates).

As in typical alternating minimization methods, each sub-problem converges to its minimum but there are no guarantees that a global optimum is ever reached.

Substitution by measured angle

Still in the spirit of direct substitution by measurements, another natural possibility is to experiment with the direct substitution of the directional unit vector $\left(\frac{\boldsymbol{r}^k - \boldsymbol{r}_{gs}^k}{\left\| \boldsymbol{r}^k - \boldsymbol{r}_{gs}^k \right\|} \right)$ by the direction angle output obtained

from the tracking antennas.

Considering a discrete approximation for the velocity as previously done, one obtains the following optimization problem

$$\begin{aligned} \underset{\boldsymbol{r}}{\text{minimize}} \quad & \sum_{k=2}^{N-2} \frac{1}{2\sigma_f^2} \underbrace{\left(\Delta f^k + \frac{f_{emm}}{c} \left(\boldsymbol{v}^k - \boldsymbol{v}_{gs}^k \right)^T \hat{\boldsymbol{u}}^k \right)^2}_{F_f^k}. \\ \text{subject to} \quad & \boldsymbol{v}^k = \frac{-\boldsymbol{r}^{k+2} + 8\boldsymbol{r}^{k+1} - 8\boldsymbol{r}^{k-1} + \boldsymbol{r}^{k-2}}{12\Delta t} \qquad k = 2, \ldots, N-2 \end{aligned} \tag{3.10}$$

Ping-Pong Position-Angle

The motivation for the iterative algorithm with alternating position and velocity is also valid for the case with position and angle. Using the direct angle output from the antennas one solves for $\boldsymbol{r}$ as

$$\begin{aligned} \underset{\boldsymbol{r}}{\text{minimize}} \quad & \sum_{k=2}^{N-2} \frac{1}{2\sigma_f^2} \underbrace{\left(\Delta f^k + \frac{f_t^k}{c} \left(\boldsymbol{v}^k - \boldsymbol{v}_{gs}^k \right)^T \hat{\boldsymbol{u}}^k \right)^2}_{F_f^k} - \delta \, \boldsymbol{r}^{k^T} \hat{\boldsymbol{u}}^k \\ \text{subject to} \quad & \boldsymbol{v}^k = \frac{-\boldsymbol{r}^{k+2} + 8\boldsymbol{r}^{k+1} - 8\boldsymbol{r}^{k-1} + \boldsymbol{r}^{k-2}}{12\Delta t} \qquad k = 2, \ldots, N-2 \end{aligned} \tag{3.11}$$

Afterwards, the estimate of $\hat{\boldsymbol{r}}$ is substituted to solve the same optimization problem for $\boldsymbol{u}$

$$\begin{aligned} \underset{\boldsymbol{u}}{\text{minimize}} \quad & \sum_{k=2}^{N-2} \frac{1}{2\sigma_f^2} \underbrace{\left(\Delta f^k + \frac{f_t^k}{c} \left(\boldsymbol{v}^k - \boldsymbol{v}_{gs}^k \right)^T \boldsymbol{u}^k \right)^2}_{F_f^k} - \delta \, \left(\hat{\boldsymbol{u}}^k \right)^T \boldsymbol{u}^k \\ \text{subject to} \quad & \boldsymbol{v}^k = \frac{-\hat{\boldsymbol{r}}^{k+2} + 8\hat{\boldsymbol{r}}^{k+1} - 8\hat{\boldsymbol{r}}^{k-1} + \hat{\boldsymbol{r}}^{k-2}}{12\Delta t} \qquad k = 2, \ldots, N-2 \\ & \left\| \boldsymbol{u}^k \right\| \leq 1 \qquad k = 2, \ldots, N-2 \end{aligned} \tag{3.12}$$

Note again that the angle and distance terms of the cost function are not included in this optimization problem since they are not relative to the estimation variable, $\boldsymbol{u}$.

The procedure is analogous to the position-velocity case with the advantage of directly obtaining a convex function in each iteration since the norm term in the denominator has vanished.

Again, a term was added to ensure agreement between the two alternating variables to enhance convergence. Due to the large distance between the satellite and the Earth's surface, a small variation in $\boldsymbol{u}$ produces a large position offset of the satellite. This requires a special regularization term that approximates $\boldsymbol{u}$ from the measured value $\hat{\boldsymbol{u}}$ for the case when $\boldsymbol{u}$ is to be estimated.

As in the ping-pong position-velocity approach, there are no global convergence guarantees, and indeed divergence may occur for sufficiently large errors.

SDP based relaxation

One of the most common choices to tackle a non-convex problem with quadratic constraints is to transform it into a Semidefinite Program (SDP). In semidefinite programming, one minimizes a linear function

subject to the constraint that an affine combination of symmetric matrices is positive semidefinite. Such a constraint is non-linear and non-smooth, but convex, so semidefinite programs are convex optimization problems [44].

The relaxation developed below does not lead to an SDP since it produces a quadratic cost function (instead of a linear one) but borrows the techniques used in that class of problems. In particular, the idea to leverage the complicated handling of non-convex bi-linear terms which appear when one expands (2.40), by encoding them as entries of a suitably constructed matrix, $\boldsymbol{G}$.
Expanding (2.40) one obtains

$$\Delta f^k = -\frac{f_t^k}{c}\frac{(\boldsymbol{r}^k - \boldsymbol{r}_{gs}^k)^T(\frac{\boldsymbol{r}^{k+1}-\boldsymbol{r}^k}{\Delta t} - \boldsymbol{v}_{gs}^k)}{\left\|\boldsymbol{r}^k - \boldsymbol{r}_{gs}^k\right\|} + \epsilon \tag{3.13}$$

$$\Delta f^k + \frac{f_t^k}{c}\frac{(\boldsymbol{r}^k - \boldsymbol{r}_{gs}^k)^T(\frac{\boldsymbol{r}^{k+1}-\boldsymbol{r}^k}{\Delta t} - \boldsymbol{v}_{gs}^k)}{\left\|\boldsymbol{r}^k - \boldsymbol{r}_{gs}^k\right\|} = \epsilon \tag{3.14}$$

$$\frac{1}{\rho}\left(\Delta f^k \left\|\boldsymbol{r}^k - \boldsymbol{r}_{gs}^k\right\| + \frac{f_t^k}{c}(\boldsymbol{r}^k - \boldsymbol{r}_{gs}^k)^T\left(\frac{\boldsymbol{r}^{k+1} - \boldsymbol{r}^k}{\Delta t} - \boldsymbol{v}_{gs}^k\right)\right) = \epsilon \tag{3.15}$$

$$\frac{1}{\rho}\left(\Delta f^k \left\|\boldsymbol{r}^k - \boldsymbol{r}_{gs}^k\right\| + \frac{f_t^k}{c}\left(\frac{{\boldsymbol{r}^k}^T\boldsymbol{r}^{k+1}}{\Delta t} - \frac{{\boldsymbol{r}^k}^T\boldsymbol{r}^k}{\Delta t} - {\boldsymbol{r}^k}^T\boldsymbol{v}_{gs}^k - \frac{{\boldsymbol{r}_{gs}^k}^T\boldsymbol{r}^{k+1}}{\Delta t} + \frac{{\boldsymbol{r}_{gs}^k}^T\boldsymbol{r}^k}{\Delta t} + {\boldsymbol{r}_{gs}^k}^T\boldsymbol{v}_{gs}^k\right)\right) = \epsilon \tag{3.16}$$

Here, a first-order forward finite-divided-difference approximation was chosen for velocity to simplify the derivation and to ease the and implementation under the condition that this formulation is only valid for small time intervals (see Appendix E). The approximated velocity at instant k may then be written as $\boldsymbol{v}^k = \frac{\boldsymbol{r}^{k+1}-\boldsymbol{r}^k}{\Delta t}$.

To overcome the non-convexity introduced by the norm in the denominator of (3.14), the norm is factored out of the expression and approximated by the range measurement, as proposed in [45]. Although this seems a good approximation, it is important to note that a norm term appears in (3.16) multiplying the measured noisy frequency difference, Δf^k, which in the end may amplify the error in measured Doppler-shift.

A suitable choice for $\boldsymbol{G}$ could be

$$\mathbf{G} = \boldsymbol{g}\boldsymbol{g}^T \tag{3.17}$$

where $\boldsymbol{g}$ is a vector that concatenates the problem variables, such that the dyad $\boldsymbol{g}\boldsymbol{g}^T$ creates all the contributions that are needed to build the linear and quadratic terms in the cost function. Specifically,

$$\boldsymbol{g} = \begin{bmatrix} a_x & a_y & a_z & b_x & b_y & b_z & c_x & c_y & c_z & n_1 & n_2 & n_3 & 1 \end{bmatrix}. \tag{3.18}$$

where

$$\boldsymbol{a} = \boldsymbol{r}^{k-1} \tag{3.19}$$

$$\boldsymbol{b} = \boldsymbol{r}^{k} \tag{3.20}$$

$$\boldsymbol{c} = \boldsymbol{r}^{k+1} \tag{3.21}$$

$$n_1 = \left\|\boldsymbol{r}^{k-1} - \boldsymbol{r}_{gs}^{k-1}\right\| \tag{3.22}$$

$$n_2 = \left\|\boldsymbol{r}^{k} - \boldsymbol{r}_{gs}^{k}\right\| \tag{3.23}$$

$$n_3 = \left\|\boldsymbol{r}^{k+1} - \boldsymbol{r}_{gs}^{k+1}\right\| \tag{3.24}$$

To create this illustration, only three time instants were considered creating a matrix $\boldsymbol{G}$ with dimension $4 \times 3 + 1$, but in reality, $\boldsymbol{G}$ is a square matrix of dimension $4N + 1$, with N the number of Doppler-shift observations.

The expanded form of $\boldsymbol{G}$ is then

$$\boldsymbol{G} = \begin{bmatrix}
a_x^2 & a_x a_y & a_x a_z & a_x b_x & a_x b_y & a_x b_z & a_x c_x & a_x c_y & a_x c_z & a_x n_1 & a_x n_2 & a_x n_3 & a_x \\
a_x a_y & a_y^2 & a_y a_z & a_y b_x & a_y b_y & a_y b_z & a_y c_x & a_y c_y & a_y c_z & a_y n_1 & a_y n_2 & a_y n_3 & a_y \\
a_x a_z & a_y a_z & a_z^2 & a_z b_x & a_z b_y & a_z b_z & a_z c_x & a_z c_y & a_z c_z & a_z n_1 & a_z n_2 & a_z n_3 & a_z \\
a_x b_x & a_y b_x & a_z b_x & b_x^2 & b_x b_y & b_x b_z & b_x c_x & b_x c_y & b_x c_z & b_x n_1 & b_x n_2 & b_x n_3 & b_x \\
a_x b_y & a_y b_y & a_z b_y & b_x b_y & b_y^2 & b_y b_z & b_y c_x & b_y c_y & b_y c_z & b_y n_1 & b_y n_2 & b_y n_3 & b_y \\
a_x b_z & a_y b_z & a_z b_z & b_x b_z & b_y b_z & b_z^2 & b_z c_x & b_z c_y & b_z c_z & b_z n_1 & b_z n_2 & b_z n_3 & b_z \\
a_x c_x & a_y c_x & a_z c_x & b_x c_x & b_y c_x & b_z c_x & c_x^2 & c_x c_y & c_x c_z & c_x n_1 & c_x n_2 & c_x n_3 & c_x \\
a_x c_y & a_y c_y & a_z c_y & b_x c_y & b_y c_y & b_z c_y & c_x c_y & c_y^2 & c_y c_z & c_y n_1 & c_y n_2 & c_y n_3 & c_y \\
a_x c_z & a_y c_z & a_z c_z & b_x c_z & b_y c_z & b_z c_z & c_x c_z & c_y c_z & c_z^2 & c_z n_1 & c_z n_2 & c_z n_3 & c_z \\
a_x n_1 & a_y n_1 & a_z n_1 & b_x n_1 & b_y n_1 & b_z n_1 & c_x n_1 & c_y n_1 & c_z n_1 & n_1^2 & n_1 n_2 & n_1 n_3 & n_1 \\
a_x n_2 & a_y n_2 & a_z n_2 & b_x n_2 & b_y n_2 & b_z n_2 & c_x n_2 & c_y n_2 & c_z n_2 & n_1 n_2 & n_2^2 & n_2 n_3 & n_2 \\
a_x n_3 & a_y n_3 & a_z n_3 & b_x n_3 & b_y n_3 & b_z n_3 & c_x n_3 & c_y n_3 & c_z n_3 & n_1 n_3 & n_2 n_3 & n_3^2 & n_3 \\
a_x & a_y & a_z & b_x & b_y & b_z & c_x & c_y & c_z & n_1 & n_2 & n_3 & 1
\end{bmatrix} \tag{3.25}$$

Now it is possible to find the linear and bi-linear terms to construct (3.16) since these appear directly in specific entries of $\boldsymbol{G}$.

At this point, it seems that this is a good formulation to solve the problem since the Doppler equation is very close to the true one and can be written as a linear expression using the right entries of $\boldsymbol{G}$. However, there is a fundamental detail that must be addressed: without additional constraints, the $\boldsymbol{G}$ matrix is viewed by the solver as a set of non related variables. The representation in (3.25) just a mental construction to help the encoding of (3.16) with the entries of $\boldsymbol{G}$. To solve this problem, one has to add constraints that make the entries of $\boldsymbol{G}$ tightly related, according to (3.16).

To make the position variables appear unchanged in the last row and column of the $\boldsymbol{G}$ matrix, it is necessary to force the last entry of its diagonal to be one. Also, the construction of $\boldsymbol{G}$ according to (3.17)

automatically implies that this matrix is symmetric positive semidefinite and has an unitary rank (since all columns are linearly dependent) as noted in [45].
These three properties of $\boldsymbol{G}$ may be written as

$$\boldsymbol{G}(4N+1, 4N+1) = 1 \tag{3.26}$$

$$\mathbf{G} \succeq 0 \tag{3.27}$$

$$\mathrm{rank}(\boldsymbol{G}) = 1 \tag{3.28}$$

respectively.

These constraints can't be used yet to build a convex optimization problem since (3.26) and (3.27) are convex constraints but (3.28) is not. The most common solution is to simply drop this constraint, although there are alternative approaches based on statistical properties of the solution, as discussed in [46].

Also, one may observe that the squared norm terms in the diagonal and the position terms in the last column of $\boldsymbol{G}$ may be used to create the following additional constraints

$$\left\|\boldsymbol{r}^k - \boldsymbol{r}_{gs}^k\right\|^2 = \left\|\boldsymbol{r}^k\right\|^2 - 2{\boldsymbol{r}_{gs}^k}^T \boldsymbol{r}^k + \left\|\boldsymbol{r}_{gs}^k\right\|^2 \qquad k = 1, \ldots, N. \tag{3.29}$$

Finally, an additional constraint arrives from satellite dynamics by forcing the cross-product between position and velocity (known as the *angular momentum per unit mass*) to be constant over time

$$\boldsymbol{r}^k \times \boldsymbol{v}^k = \boldsymbol{q} \Leftrightarrow \tag{3.30}$$

$$\boldsymbol{r}^k \times \frac{\boldsymbol{r}^{k+1} - \boldsymbol{r}^k}{\Delta t} = \boldsymbol{q} \Leftrightarrow \tag{3.31}$$

$$\boldsymbol{r}^k \times \boldsymbol{r}^{k+1} = \boldsymbol{q}\,\Delta t \Leftrightarrow \tag{3.32}$$

$$\begin{bmatrix} q_1 \\ q_2 \\ q_3 \end{bmatrix} = \frac{1}{\Delta t} \begin{bmatrix} \boldsymbol{r}_y^k \boldsymbol{r}_z^{k+1} - \boldsymbol{r}_z^k \boldsymbol{r}_y^{k+1} \\ \boldsymbol{r}_z^k \boldsymbol{r}_x^{k+1} - \boldsymbol{r}_x^k \boldsymbol{r}_z^{k+1} \\ \boldsymbol{r}_x^k \boldsymbol{r}_y^{k+1} - \boldsymbol{r}_y^k \boldsymbol{r}_x^{k+1} \end{bmatrix} \tag{3.33}$$

It is then possible to add $\boldsymbol{q}$ as a new variable to the optimization problem and create a constraint to force $\boldsymbol{q}$ to be constant and satisfy (3.33) for every time instant resulting in the following optimization

problem

$$\underset{\boldsymbol{G},\boldsymbol{q}}{\text{minimize}} \quad \sum_{k=1}^{N-1} \frac{1}{2\sigma_f^2} \left[\frac{1}{\rho^k} \left(\Delta f^k \left\| \boldsymbol{r}^k - \boldsymbol{r}_{gs}^k \right\| + \frac{f_t^k}{c} \left(\frac{{\boldsymbol{r}^k}^T \boldsymbol{r}^{k+1}}{\Delta t} - \frac{{\boldsymbol{r}^k}^T \boldsymbol{r}^k}{\Delta t} - {\boldsymbol{r}^k}^T \boldsymbol{v}_{gs}^k - \frac{{\boldsymbol{r}_{gs}^k}^T \boldsymbol{r}^{k+1}}{\Delta t} + \frac{{\boldsymbol{r}_{gs}^k}^T \boldsymbol{r}^k}{\Delta t} + {\boldsymbol{r}_{gs}^k}^T \boldsymbol{v}_{gs}^k \right) \right) \right]^2 \tag{3.34}$$

$$\text{subject to} \quad \boldsymbol{q} = \begin{bmatrix} \boldsymbol{r}_y^k \boldsymbol{r}_z^{k+1} - \boldsymbol{r}_z^k \boldsymbol{r}_y^{k+1} \\ \boldsymbol{r}_z^k \boldsymbol{r}_x^{k+1} - \boldsymbol{r}_x^k \boldsymbol{r}_z^{k+1} \\ \boldsymbol{r}_x^k \boldsymbol{r}_y^{k+1} - \boldsymbol{r}_y^k \boldsymbol{r}_x^{k+1} \end{bmatrix} \qquad k = 1, \ldots, N-1$$

$$\left\| \boldsymbol{r}^k - \boldsymbol{r}_{gs}^k \right\|^2 = \left\| \boldsymbol{r}^k \right\|^2 - 2{\boldsymbol{r}_{gs}^k}^T \boldsymbol{r}^k + \left\| \boldsymbol{r}_{gs}^k \right\|^2 \qquad k = 1, \ldots, N$$

$$\boldsymbol{G}(4N+1, 4N+1) = 1$$

$$\mathbf{G} \succeq 0$$

Note that, for clarity of representation, the terms were written in symbolic form but the implemented code substitutes each symbol by its correspondent entry on $\boldsymbol{G}$. For completeness, the version of the problem written in terms of the entries of $\boldsymbol{G}$ is given in Appendix F.

The represented cost function is only relative to the Doppler-shift information. The terms related to range (2.42) and angle (2.43) may be easily adapted to this new set of variables since the satellite positions conveniently appear at the last column and row of $\boldsymbol{G}$.

3.3 Dynamics based regularization functions

Until now, the cost functions developed were based only on the available measurements (except in the SDP based formulation, with the introduction of the angular momentum constraint). However, some complementary cost functions may be combined with each Doppler-shift cost function obtained with the convex relaxations discussed in previous sections. These complementary functions contain information about the satellite's dynamics and thus may be used to improve the position estimation as they introduce correlation between positions.

Once again, given the rigorous set of rules regarding the construction of convex cost functions, it is hard to find admissible regularization terms based on the dynamic's properties. The next sections are devoted to the investigation of admissible cost functions, $F(\boldsymbol{r})$, for regularization regarding the satellite's movement.

3.3.1 Dynamics relaxation

Although measurements are obtained in a station's local frame (LT), the laws governing the satellite's motion are most naturally described in ECI frame, and so, unless all sensor outputs are described in ECI, the constraints imposed by celestial mechanics can't be exploited.

Moreover, the gravitation law does not fit in the *Disciplined Convex Programming* framework as can

be verified in (2.6). To tackle this problem two approaches were considered:

Substitution by position estimates - Perform a direct substitution of $\boldsymbol{r}^k$ either by the value obtained in the previous estimation step or directly by a raw estimate from the sensor outputs.

Linearization - Linearize the dynamics around the previously estimated position.

Substitution by position estimates

As in previous sections, direct substitution by the measurements vector, $\hat{\boldsymbol{r}}$, solves the non-convexity problem but is prone to large errors due to observation noise.

The cost function that, when minimized, finds the satellite positions that best describe the calculated acceleration (based on raw measured values) is

$$F(\boldsymbol{r}) = \sum_{k=4}^{N} \left\| \ddot{\boldsymbol{r}}^k - \hat{\ddot{\boldsymbol{r}}}^k \right\|^2 + \delta \left\| \boldsymbol{r} - \hat{\boldsymbol{r}} \right\| \tag{3.35}$$

where the relation between the satellite's positions and the acceleration may be once more approximated resorting to the centered finite-divided-difference formulas, but this time for second-order derivatives [42]

$$\ddot{\boldsymbol{r}}^k = \frac{-\boldsymbol{r}^{k+2} + 16\boldsymbol{r}^{k+1} - 30\boldsymbol{r}^k + 16\boldsymbol{r}^{k-1} - \boldsymbol{r}^{k-2}}{12\Delta t^2} + O(\Delta t^4). \tag{3.36}$$

The estimated acceleration is simply calculated substituting the raw position measurements, $\hat{\boldsymbol{r}}^k$, into (2.7), resulting in $\hat{\ddot{\boldsymbol{r}}}^k = \frac{-\mu}{\|\hat{\boldsymbol{r}}^k\|^3}\hat{\boldsymbol{r}^k}$, based on Newton's law for the two body problem.

Linearization

It is possible to do better than just substitute for raw sensor estimates. If measurement errors are of small magnitude, one may use the linearized acceleration function to allow some extra flexibility. The partial derivative $\frac{\partial \ddot{\boldsymbol{r}}}{\partial \boldsymbol{r}}$ is given in [6] as

$$\frac{\partial \ddot{\boldsymbol{r}}}{\partial \boldsymbol{r}} = \frac{\mu}{\|\boldsymbol{r}\|^5} \begin{bmatrix} 3r_x^2 - \|\boldsymbol{r}\|^2 & 3r_x r_y & 3r_x r_z \\ 3r_y r_x & 3r_y^2 - \|\boldsymbol{r}\|^2 & r_y r_z \\ 3r_z r_x & 3r_z r_y & 3r_z^2 - \|\boldsymbol{r}\|^2 \end{bmatrix}. \tag{3.37}$$

The linearization follows the first-order Taylor expansion

$$\ddot{\boldsymbol{r}}(\boldsymbol{r}) \approx \ddot{\boldsymbol{r}}(\boldsymbol{r})|_{\hat{\boldsymbol{r}}} + \left.\frac{\partial \ddot{\boldsymbol{r}}(\boldsymbol{r})}{\partial \boldsymbol{r}}\right|_{\hat{\boldsymbol{r}}} (\boldsymbol{r} - \hat{\boldsymbol{r}}). \tag{3.38}$$

Moreover, it is possible to employ an iterative method to sequentially improve the position estimate but in that case, an additional regularization term is needed to allow only small increments in position. That is necessary to limit the validity of the linearization to a small region where it still describes the true acceleration with sufficient accuracy. Also, the regularization cost may be simply captured by the Euclidean norm between the current estimate and the linearization point.

The cost function associated with this complementary term may be written as

$$F(\boldsymbol{r}) = \sum_{k=2}^{N-2} \left\| \frac{-\boldsymbol{r}^{k+2} + 16\boldsymbol{r}^{k+1} - 30\boldsymbol{r}^{k} + 16\boldsymbol{r}^{k-1} - \boldsymbol{r}^{k-2}}{12\Delta t^2} - \ddot{\boldsymbol{r}}(\boldsymbol{r})|_{\hat{\boldsymbol{r}}^k} - \left.\frac{\partial \ddot{\boldsymbol{r}}(\boldsymbol{r})}{\partial \boldsymbol{r}}\right|_{\hat{\boldsymbol{r}}^k} (\boldsymbol{r} - \hat{\boldsymbol{r}}^k) \right\|^2 + \delta \left\| \boldsymbol{r} - \hat{\boldsymbol{r}} \right\| \tag{3.39}$$

Once again, there are no guarantees of convergence for the global problem, only for the one with linearized dynamics. However, if the algorithm is having difficulty to converge, it is possible to influence the position update magnitude by tweaking δ.

3.3.2 Polynomial smoothing

Although the dynamics equation cannot be used in standard form, requiring some degree of approximation, there is one certainty regarding satellite's position and velocity: for a satellite moving with no other forces beyond gravity, consecutive positions won't describe a "spiky" behavior. This implicitly introduces a smoothness constraint that position and velocity must obey.

The most natural approach is to force the positions to be described by a polynomial. The particular value of the coefficients is not relevant, what matters is that they act as a link between all positions and force them to describe a smooth path.

Since in a fairly long trajectory arc the velocity is not assumed to be linear, the second best assumption is that velocity may be accurately described by a second-order polynomial and, as a consequence, positions should be described by a third-order polynomial.

The equation for positions may then be written as

$$\boldsymbol{r}^k = \boldsymbol{c_1} + \boldsymbol{c_2}\,\boldsymbol{T}(k) + \boldsymbol{c_3}\;\boldsymbol{T}(k)^2 + \boldsymbol{c_4}\,\boldsymbol{T}(k)^3 + \epsilon_r^k \tag{3.40}$$

where $\boldsymbol{T}$ is an array of normalized times between 0 and 1 with N steps. This removes possible numerical instabilities when time values are too large. The sampling time step is not relevant. The residuals ϵ_r^k and ϵ_v^k describe the error of the fitting model.

These equations may be used to construct a cost function with additional estimation variables corresponding to the new constant vector coefficients $\boldsymbol{c_1}, \boldsymbol{c_2}, \boldsymbol{c_3}$ and $\boldsymbol{c_4}$ of the polynomials. To find the best fitting coefficients (and, consequently, the best fitting positions) one just has to minimize

$$F(\boldsymbol{c_1}, \boldsymbol{c_2}, \boldsymbol{c_3}, \boldsymbol{c_4}, \boldsymbol{r}) = \sum_{k=1}^{N} \left\| \boldsymbol{c_1} + \boldsymbol{c_2}\,\boldsymbol{T}(k) + \boldsymbol{c_3}\;\boldsymbol{T}(k)^2 + \boldsymbol{c_4}\,\boldsymbol{T}(k)^3 - \boldsymbol{r}^k \right\|^2. \tag{3.41}$$

3.3.3 Angular momentum constraint (slack variable)

The angular momentum constraint was used previously when dealing with the SDP formulation but this property may be also used to improve the convergence of the iterative solution presented in Sec. 3.2.3. Once again, this equation can't be used directly in the convex problem formulation since the cross product is not a convex operator. This may be observed if one writes the equivalent matrix expression

$$\boldsymbol{r} \times \boldsymbol{v} = \underbrace{\begin{bmatrix} 0 & -r_x & r_y \\ r_z & 0 & -r_x \\ -r_y & r_x & 0 \end{bmatrix}}_{A(\boldsymbol{r})} \underbrace{\begin{bmatrix} v_x \\ v_y \\ v_z \end{bmatrix}}_{b(\boldsymbol{v})}. \tag{3.42}$$

Once more, an iterative approach with alternating optimization variables may be used. Exploiting the dynamic property which forces $\boldsymbol{r} \times \boldsymbol{v}$ to be constant, then a positive slack variable may be added to the problem in order to force the cross-product term to be zero.

The constraint may be translated by the following cost functions

$$F(\boldsymbol{s}, \boldsymbol{v}) = \sum_{k=2}^{N-2} \|A(\hat{\boldsymbol{r}})b(\boldsymbol{v}) + s\| + \left\| \frac{-\hat{\boldsymbol{r}}^{k+2} + 8\hat{\boldsymbol{r}}^{k+1} - 8\hat{\boldsymbol{r}}^{k-1} + \hat{\boldsymbol{r}}^{k-2}}{12\Delta t} - \boldsymbol{v}^k \right\|^2 \tag{3.43}$$

$$F(\boldsymbol{r}) = \sum_{k=2}^{N-2} \|A(\boldsymbol{r})b(\hat{\boldsymbol{v}}) + s\| + \left\| \frac{-\boldsymbol{r}^{k+2} + 8\boldsymbol{r}^{k+1} - 8\boldsymbol{r}^{k-1} + \boldsymbol{r}^{k-2}}{12\Delta t} - \hat{\boldsymbol{v}}^k \right\|^2. \tag{3.44}$$

Again, it is worth noting the introduction of the penalization term to force the agreement between velocity and positions.

3.3.4 Nuclear Norm

As stated previously, the two-body problem constrains the position of the orbiting body to a plane. Again, no convex cost function was found to exactly enforce this constraint, but there are approximate ways to do it.

If positions were written as columns of a matrix $P \in \mathbb{R}^{3\times N}$, then, the condition that would place all positions in the same plane would be $\mathrm{rank}(P) = 2$ since every position could be written as the combination of two fixed linearly independent vectors lying on that plane.

One way to evaluate the rank of a matrix A is by counting the non-zero singular values, σ_i, of A. The notation is such that σ_i denotes the i^{th} largest singular value of A, defined as $\sigma_i(A) = \sqrt{\lambda_i}$ in which λ_i corresponds to the i^{th} largest eigenvalue of $A^T A$. However, it is well known that a rank equality constraint is not convex (the set of matrices with $\mathrm{rank}(A) = n \in \mathbb{N}$ is not convex).

Nevertheless, the *nuclear norm*, which is a convex envelop of the rank operator, may be used to approximate this constraint [47].

The *Nuclear norm* corresponds to the sum of nonzero singular-values of A

$$\|A\|_* = \sum_{i=1}^{\mathrm{rank}(A)} \sigma_i(A). \tag{3.45}$$

This can be used as a regularizer function with the addition of a weighting term δ leading to

$$F(\boldsymbol{r}) = \delta \|P\|_*. \tag{3.46}$$

The rationale beyond this approximation is that for a sufficiently small δ and for a set of solutions

which includes near co-planar positions, the penalization term will drive the solution to lie on a plane without greatly affecting the minimization of the remaining cost function terms.

3.3.5 Plane projection

Recalling the need for co-planar positions in a satellite's orbit, a more intuitive method is to use the raw estimates of position (only feasible when distance and angular information are simultaneously available) and do some pre-processing to determine the best fitting plane.
Parameterizing the plane as $H(\boldsymbol{\alpha}, \beta) = \left\{\boldsymbol{r} \in \mathbb{R}^3 : \boldsymbol{\alpha}^T \boldsymbol{r} = \beta\right\}$, the computation of parameters $\{\boldsymbol{\alpha}, \beta\}$ that leads to the least squared distances between positions set and the estimated plane is given by

$$R = \frac{1}{N} \sum_{k=1}^{N} (\bar{\boldsymbol{r}} - \boldsymbol{r}^k)(\bar{\boldsymbol{r}} - \boldsymbol{r}^k)^T \tag{3.47}$$

$$\boldsymbol{\alpha} = \lambda_{min}(R) \tag{3.48}$$

$$\beta = \boldsymbol{\alpha}^T \bar{\boldsymbol{r}} \tag{3.49}$$

After that, it is straightforward to include an additional constraint to the optimization problem to drive the solution to lie on that plane. The additional cost function term is constructed by noting that the squared norm between a point and its projection in the plane is

$$d\left(\boldsymbol{r}, H(\boldsymbol{\alpha}, \beta)\right)^2 = \left(\frac{\beta - \boldsymbol{\alpha}^T \boldsymbol{r}}{\|\boldsymbol{\alpha}\|}\right)^2. \tag{3.50}$$

which is the composition of an affine map with a convex function, and thus, convex.
From this, one may write

$$F(\boldsymbol{r}) = \sum_{k=1}^{N} \left(\frac{\beta - \boldsymbol{\alpha}^T \boldsymbol{r}^k}{\|\boldsymbol{\alpha}\|}\right)^2. \tag{3.51}$$

Chapter 4

Results

4.1 Simulation Setup

The simulation environment chosen to generate the satellite's orbit data and respective observations was the MATLAB® Toolbox ODTBX © [48] developed at NASA Goddard Space Flight Center.

The orbit parameters and the ground station observations were shaped to meet a typical orbit of a LEO satellite. Values are summarized in Tab. 4.1.

Orbit parameters	Value
Semimajor axis (a)	7078 km
Perigee	700 km
Eccentricity (e)	0.01
Inclination (i)	5°
RAAN (Ω)	33°
Arg. Perigee (ω)	90°
True anomaly (θ)	0°

Table 4.1: Orbital elements of fictitious LEO satellite in simulation.

In particular, the simulation was envisioned such that the inclusion of the Doppler term in the estimation would have the best chance to improve the solution. This is because the orbit comprises a pass with very high elevation (Fig. 4.1), above the ground station which corresponds to the case where the variations in the range are more pronounced.

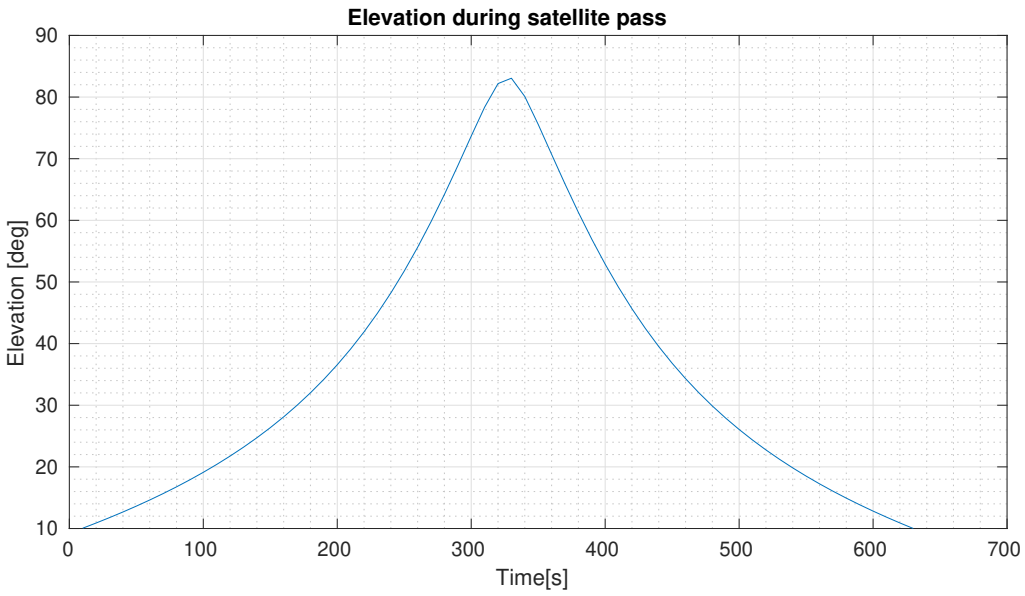

Figure 4.1: Elevation evolution over a complete pass.

Moreover, the standard deviation associated with Doppler was chosen to be very small in all simulations so that the information contained in the cost function could be fully exploited. To speed-up the optimization routine, the set of measurements obtained in simulation with a time interval of $1\,\mathrm{s}$ were subsampled to intervals of $10\,\mathrm{s}$ so that the number of optimization variables could be reduced approximately 10 times while still accounting for the full pass.

4.2 Optimization scheme setup

The following sections contain the solutions of the optimizations problems whose cost functions are composed by the convex relaxation for the distance term in (2.48), $F_\rho^k(\boldsymbol{r})$, the convex relaxation for the angular term in (2.49), $F_\alpha^k(\boldsymbol{r})$, the convex relaxation of the Doppler-shift cost function developed in Sec. 3.2.2 and Sec. 3.2.3, $F_f^k(\boldsymbol{r})$, and the complementary regularization functions based on satellite's dynamics developed in Sec. 3.3, $F(\boldsymbol{r})$. This is encoded in the following formulation

$$\underset{\boldsymbol{r}}{\text{minimize}} \sum_{k=1}^{N} \frac{1}{2\sigma_\rho^2} \underbrace{\left[\left(\rho^k - \left\|\boldsymbol{r}^k - \boldsymbol{r}_{gs}^k\right\|\right)_+\right]^2}_{F_\rho^k} - \kappa \underbrace{\frac{(\boldsymbol{r}^k - \boldsymbol{r}_{gs}^k)^T AoT^k}{\rho^k}}_{F_\alpha^k} + \frac{1}{2\sigma_f^2} F_f^k(\boldsymbol{r}) + \gamma F(\boldsymbol{r}). \tag{4.1}$$

The weights applied to each measurement — distance, angle and frequency — are taken from the ML formulation in (2.47) as $1/(2\sigma_\rho^2)$, κ and $1/(2\sigma_f^2)$, respectively and γ is the weighting term applied to the complementary regularizing function.

To investigate the improvement introduced by Doppler-shift information, the first simulation did not use any complementary function. This provides insight into the information obtained for each Doppler-shift term relaxation, alone.

Subsequent simulations are intended to test the improvement of the estimation by introducing complementary functions used to regularize the positions estimates based on the known dynamics of the

satellite and all relaxations presented for Doppler-shift cost are tested with one complementary function at a time, according to the scheme presented in Tab. 4.2.

	Sim. 1	Sim. 2	Sim. 3	Sim. 4	Sim. 5	Sim. 6
	No CF	Poly. Smooth. (3.41)	Dyn. Relax. (3.35)	Slack Var. (3.43)/(3.44)	Nuc. Norm (3.46)	Plane Proj. (3.51)
No Doppler	✓	✓	✓	✗	✓	✓
Epigraph (3.4)	✓	✓	✓	✗	✓	✓
Range Subs (3.5)	✓	✓	✓	✗	✓	✓
Spherical-like Coordinates (3.6)	✓	✓	✗	✗	✗	✗
Position Subs (3.7)	✓	✓	✓	✗	✓	✓
Ping-Pong Pos-Vel (3.8)/(3.9)	✓	✓	✓	✓	✓	✓
Ping-Pong Pos-Ang (3.11)/(3.12)	✓	✓	✓	✗	✓	✓
SDP based (3.34)	✓	✓	✓	✗	✓	✓

Table 4.2: Simulated combinations of relaxations and complementary functions.

In order to provide a more complete picture of the comparison between methods without sacrificing conciseness, two noise levels were examined (except for Doppler measurements, as mentioned above). A very small one to have a primary insight on the performance of each estimator, and an extreme case with large noise standard deviation to test the stability of each method.

To better visualize the results, for the same simulation, these were split into the best and the worst obtained such that one may clearly distinguish the colors and the pattern of each line. The legend at the right side of each figure indicates which lines are active (black font) and inactive (gray font).

4.3 Simulation results

The simulations used the environment setup presented above to generate the ground-truth measurements, which were then used as mean values for Gaussian distributions with the standard deviations given in Tab. 4.3.

Standard Deviation	Small Noise	Large Noise
Range (σ_p)	0.2 km	10 km
Angle (σ_a)	0.1°	5°
Frequency (σ_f)	0.01 Hz	0.01 Hz

Table 4.3: Summarized standard deviations.

4.3.1 No Complementary Function

This simulation is the result of solving the optimization problem in (4.1) without adding any of the convex complementary functions based on satellite's dynamics developed in Sec. 3.3.1.

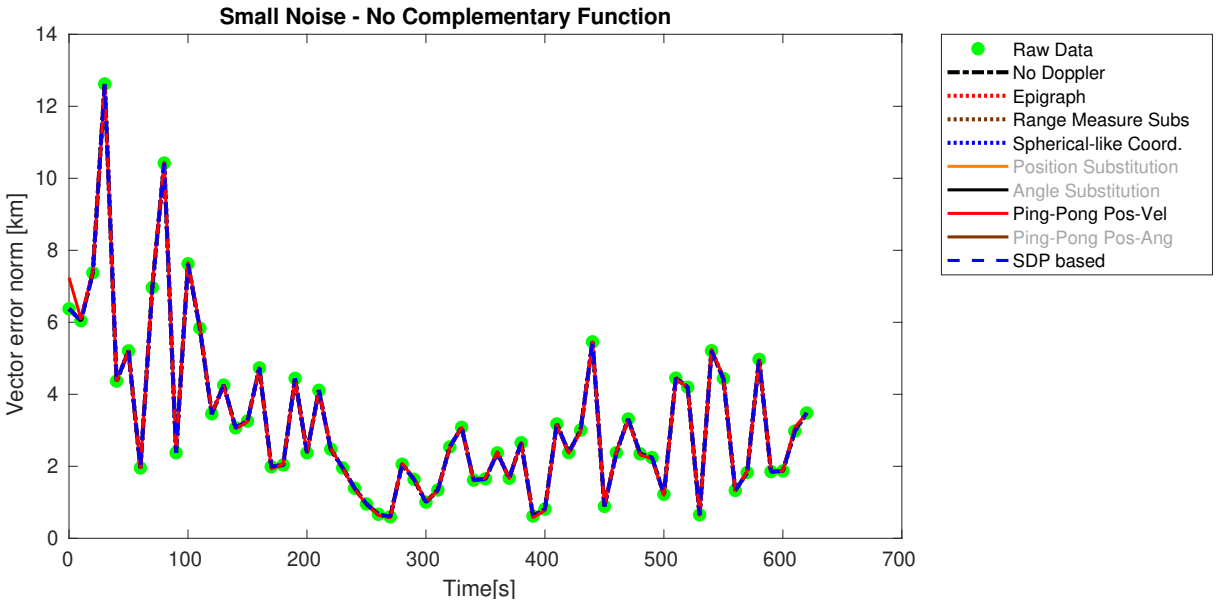

Figure 4.2: Simulation 1 - Small Noise - No Complementary Function - Comparing best performing cost functions without additional terms to regularize position estimates. All the active lines are overlapping and are identical to the raw position measurements given by the station's sensors.

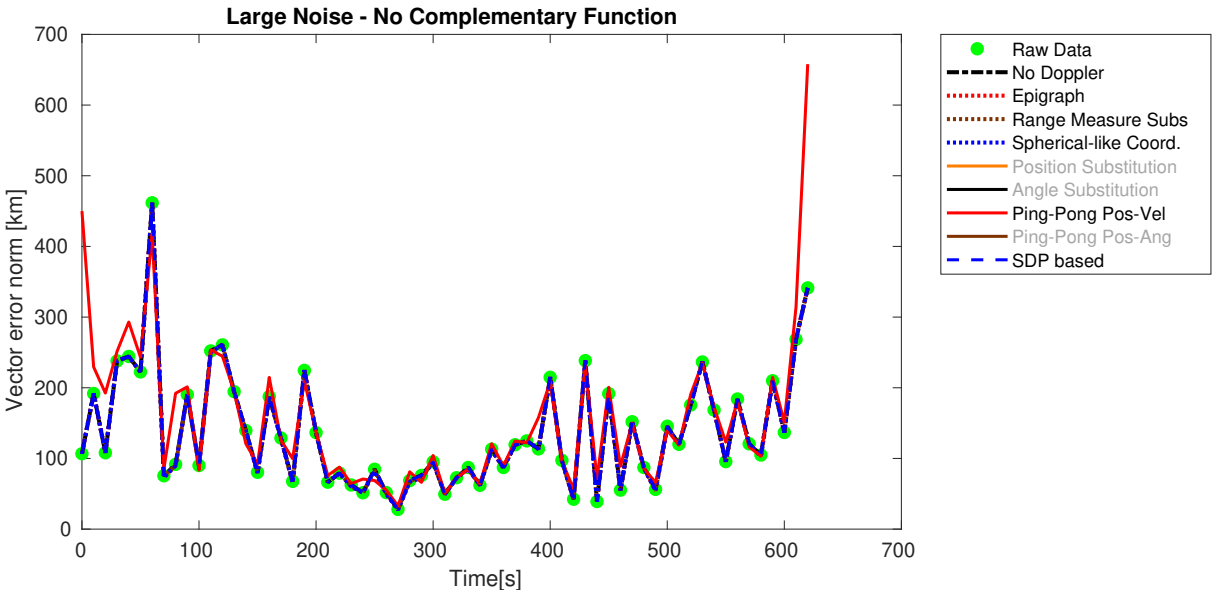

Figure 4.3: Simulation 1 - Large Noise - No Complementary Function - Comparing best performing cost functions without additional terms to regularize position estimates. The active lines relative to the ”No Doppler”, ”Epigraph”, ”Range Measure Subs”, ”Spherical-like Coord.” and ”SDP based” are overlapping.

From Fig. 4.2 and Fig. 4.3 one can take a major conclusion about the developed relaxations for the Doppler-shift measurement model: with the most favorable conditions to use Doppler information (pass with high elevation and frequency measurements with small added noise) but just one station and a satellite at a time and no complementary functions to regularize the position estimates, none of the relaxations found could improve the position estimates significantly.

Each of the remaining possible relaxations leads to an estimation worse than the raw output of the sensors.

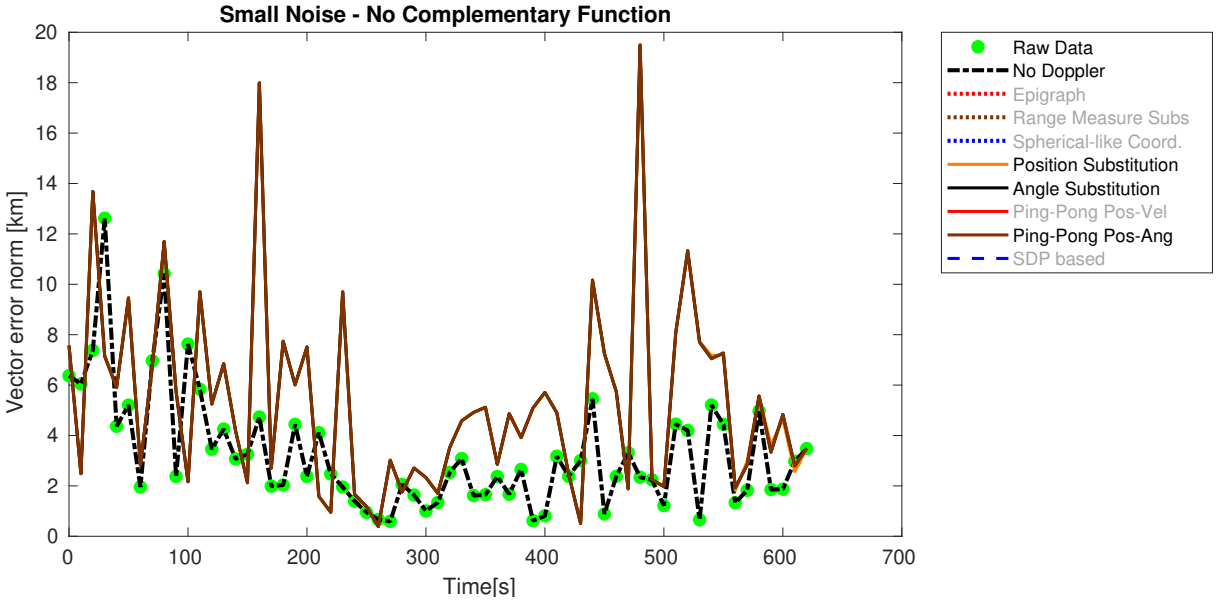

Figure 4.4: Simulation 1 - Small Noise - No Complementary Function - Comparing worst performing cost functions without additional terms to regularize position estimates. The active lines relative to ”Position Substitution”, ”Angle Substitution” and ”Ping-Pong Pos-Ang” are overlapping.

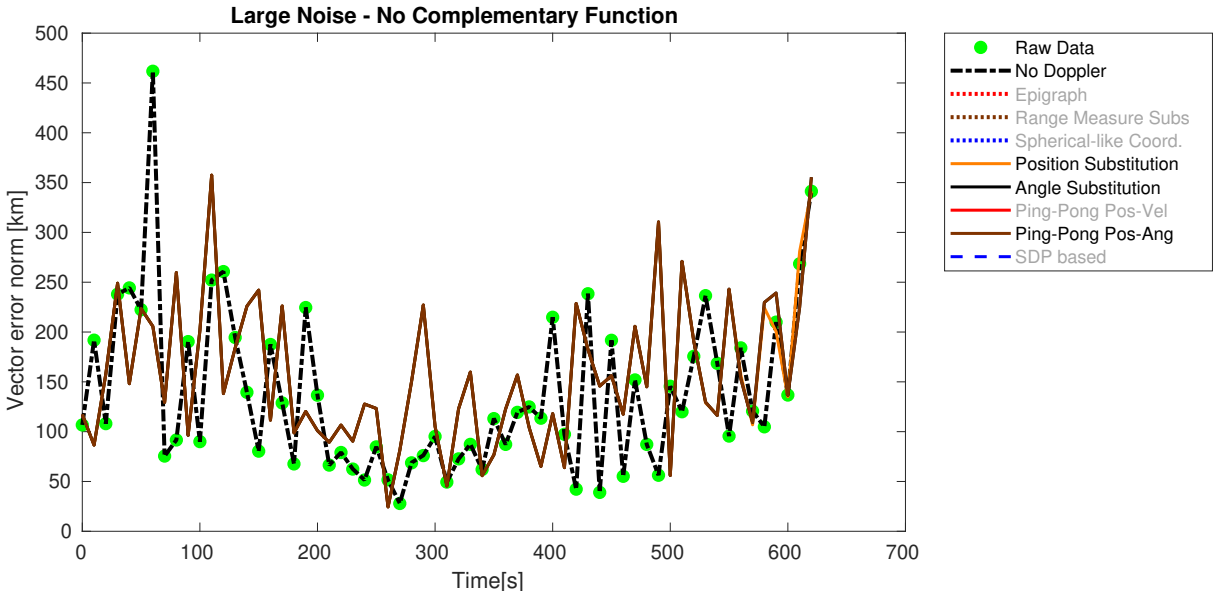

Figure 4.5: Simulation 1 - Large Noise - No Complementary Function - Comparing worst performing cost functions without additional terms to regularize position estimates. The active lines relative to ”Position Substitution”, ”Angle Substitution” and ”Ping-Pong Pos-Ang” are overlapping.

It is interesting to note that all the functions with the worst performance share the convexification scheme presented in Sec. 3.2.3. This suggests that this kind of convex relaxation amplifies the pre-existing measurement error. One possible explanation to this bad behavior is the fact that the weighting term associated to the Doppler-shift term is always very high (due to the assumed low noise in frequency measurements). This may amplify the error for non-tight relaxations. Looking at (3.7) and (3.10) one can see that the raw direction vectors are forcing the estimated positions to be noisy via the inner product computation. As position vectors have a large magnitude, the directional noise is amplified to a large positional noise.

This is also a sign that the non-tightness of the relaxation is negatively impacting the performance of the estimator since it contradicts the theoretical results which attribute a better performance to the relaxations developed in Sec. 3.2.3 relative to the ones developed in Sec. 3.2.2.

Nonetheless, an iterative correction may help to mitigate this noise by forcing an agreement between the alternating variables, thus driving the solution to a more accurate one (which only happens for Ping-Pong Position-Velocity (red line)).

The same iterative correction procedure does not work for the Position-Angle case, even in less aggressive noise conditions (orange line). This happens due to the direct estimation of $\boldsymbol{u}$ which, as previously mentioned, has a huge influence in the satellite's position computation so, even for small variations of $\boldsymbol{u}$, a huge position offset is created. Even so, the Achilles heel of these iterative methods is visible when the experience is repeated for measurements with large added noise. In this case, the Ping-Pong strategy fails to correct the estimates leading to a sub-optimal solution.

4.3.2 Polynomial Smoothing

The weight ,γ, of the polynomial smoothing term applied to the cost function in (3.41) was chosen to be equal across all formulations so that it forms a base to compare the results.

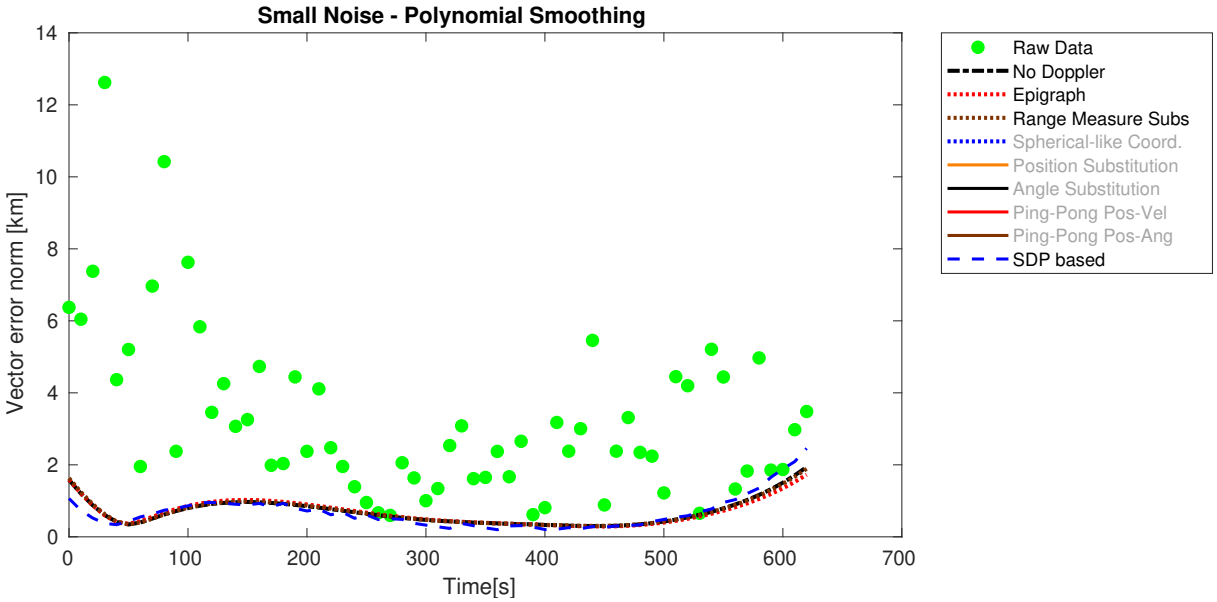

Figure 4.6: Simulation 2 - Small Noise - Polynomial Smoothing - Comparing best performing cost functions with additional polynomial terms to penalize non-smoothness of estimates. The three first active lines are overlapping.

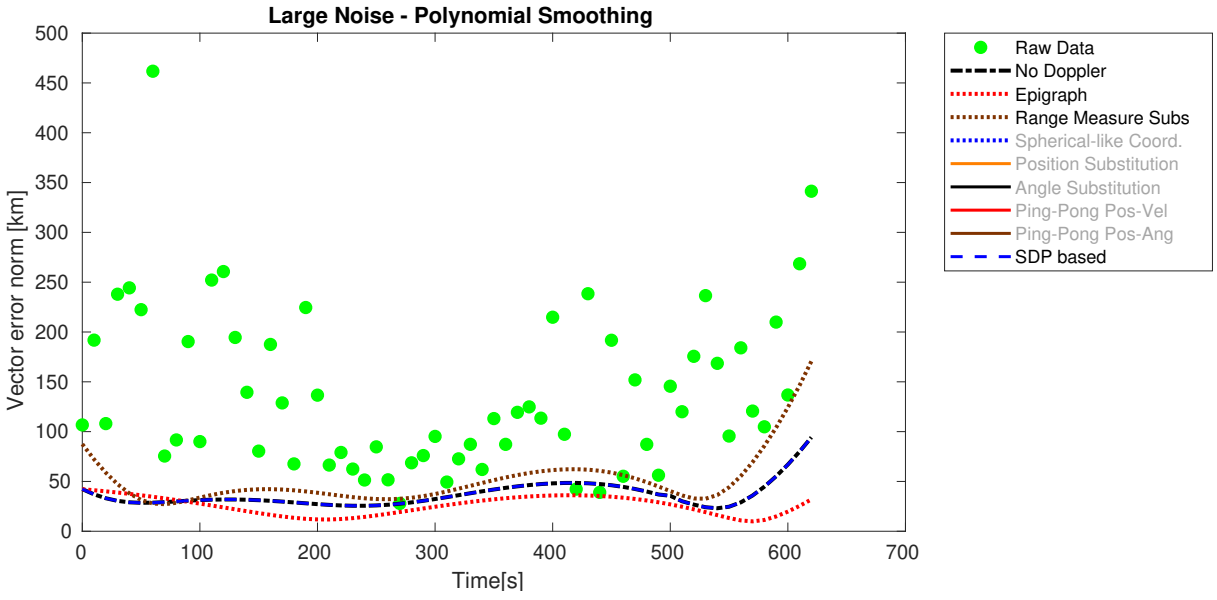

Figure 4.7: Simulation 2 - Large Noise - Polynomial Smoothing - Comparing best performing cost functions with additional polynomial terms to penalize non-smoothness of estimates. The lines relative to "No Doppler" and "SDP based" are overlapping.

Once more, the best performing relaxations, aided by the regularization term, do not significantly outperform the equivalent optimization problem without Doppler information. However, the introduction of the smoothing requirement presents a major improvement from the previous case since now there is

a correlation between positions which better matches the reality (compared to the case without correlation).

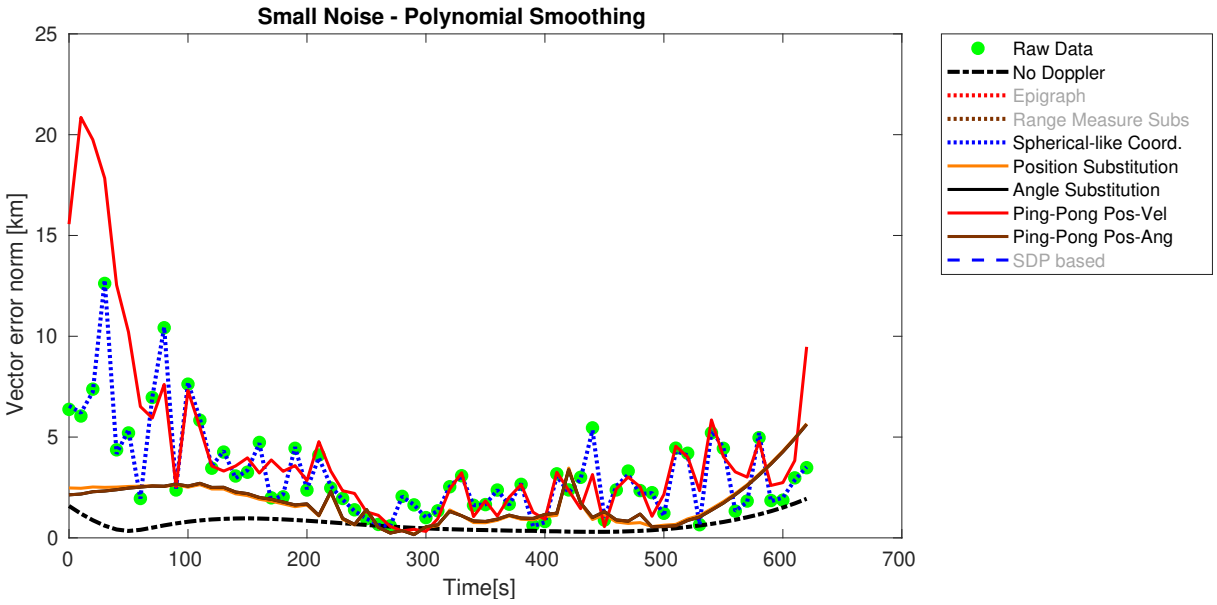

Figure 4.8: Simulation 2 - Small Noise - Polynomial Smoothing - Comparing worst performing cost functions with additional polynomial terms to penalize non-smoothness of estimates.

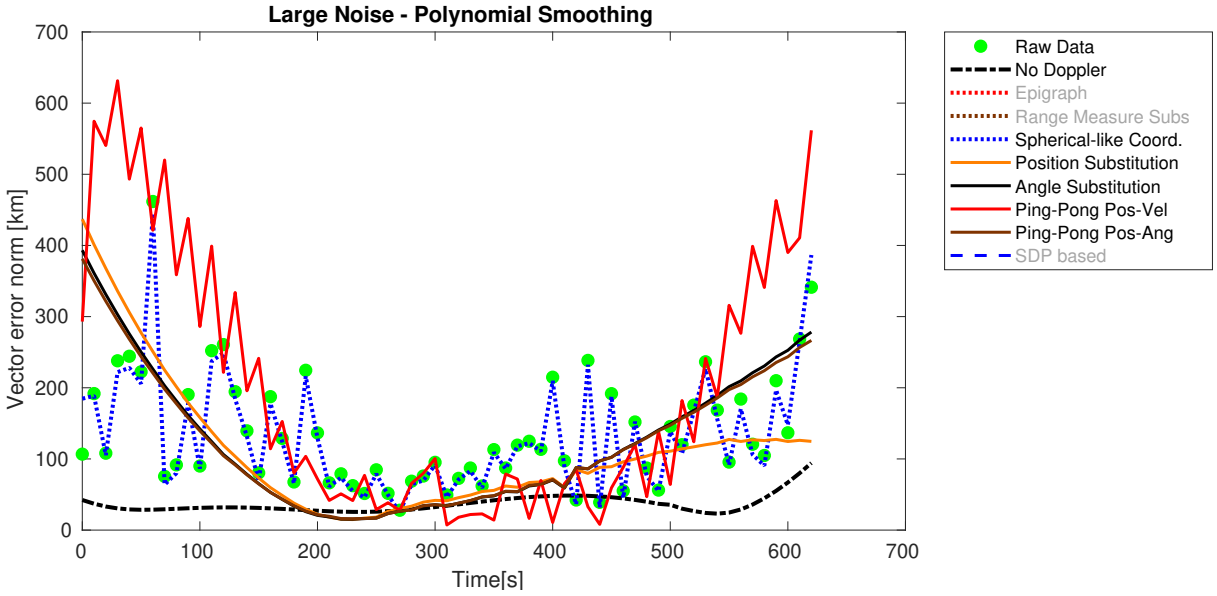

Figure 4.9: Simulation 2 - Large Noise - Polynomial Smoothing - Comparing worst performing cost functions with additional polynomial terms to penalize non-smoothness of estimates

There is however a drawback hidden behind by the good results of Fig. 4.6. Beyond the problem of the error amplification and the possibility of non-converging iterative algorithms, the weighting applied to the regularization term must change according to the noise magnitude.

Moreover, the order of the polynomial is dependent on the time of observation. Small orders generally lead to better results since there are fewer degrees of freedom, but may struggle for large observation windows. On the other hand, large orders can cope with long passes but, even for small noise observa-

tions, they may lead to poor results due to overfitting of the noisy data. Note also that, because of the introduction of this new term in the cost function, none of the iterative correction methods work, exposing again the fragility of this kind of approach.

4.3.3 Dynamics relaxation

As in the previous setting, the weight, γ, applied to the dynamics regularizing function in (3.35) was chosen to be equal across all formulations so that it forms a base to compare the results.

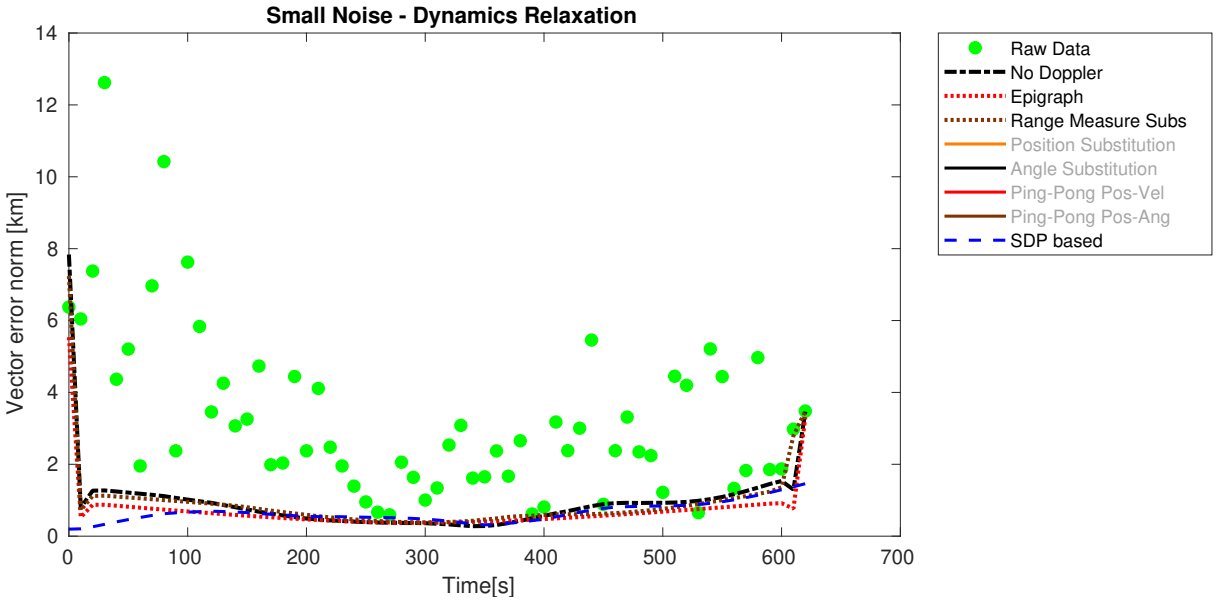

Figure 4.10: Simulation 3 - Small Noise - Dynamics Relaxation - Comparing best performing cost functions with additional term to regularize position estimates using linearized dynamics equations.

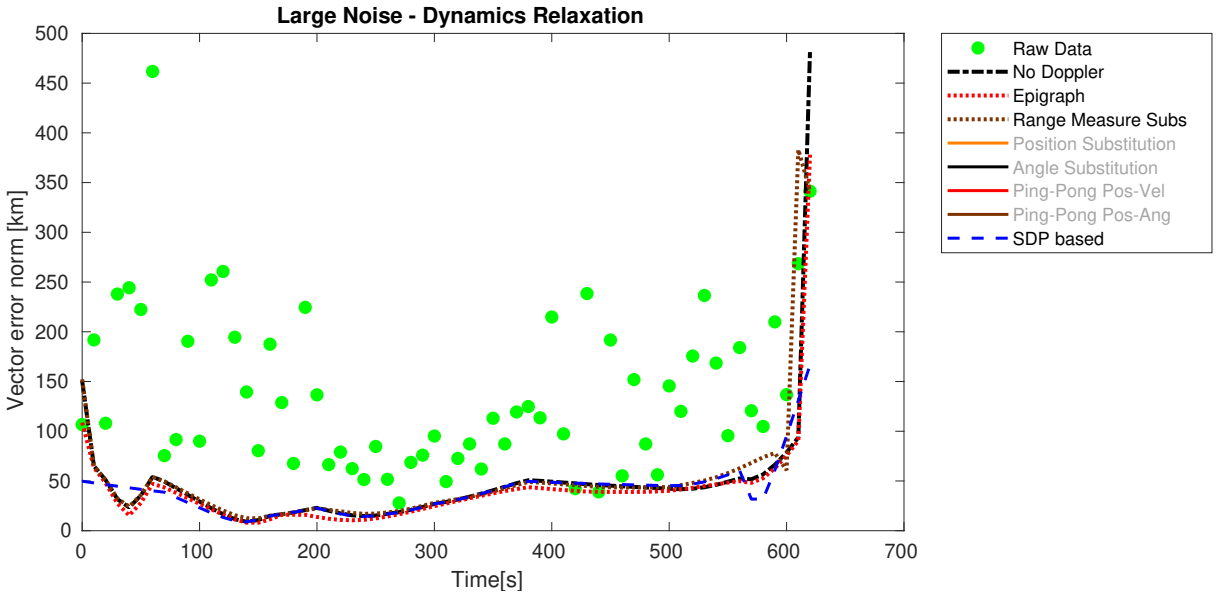

Figure 4.11: Simulation 3 - Large Noise - Dynamics Relaxation - Comparing best performing cost functions with additional term to regularize position estimates using linearized dynamics equations.

The best performing combinations are plotted in Fig. 4.10 and Fig. 4.11. This result mirrors the one

obtained with polynomial regularization but also shares the common problem of the weighting term. However, this formulation is independent of the observation window since the entire movement is dependent on the same law (gravitation law). The price to pay is the same as in the case of sequential estimation filters: since it is based on a linearized function it relies on a linearization point sufficiently close to the true value, otherwise, the quality of the penalizing cost-function deteriorates and one ends up with a useless result.

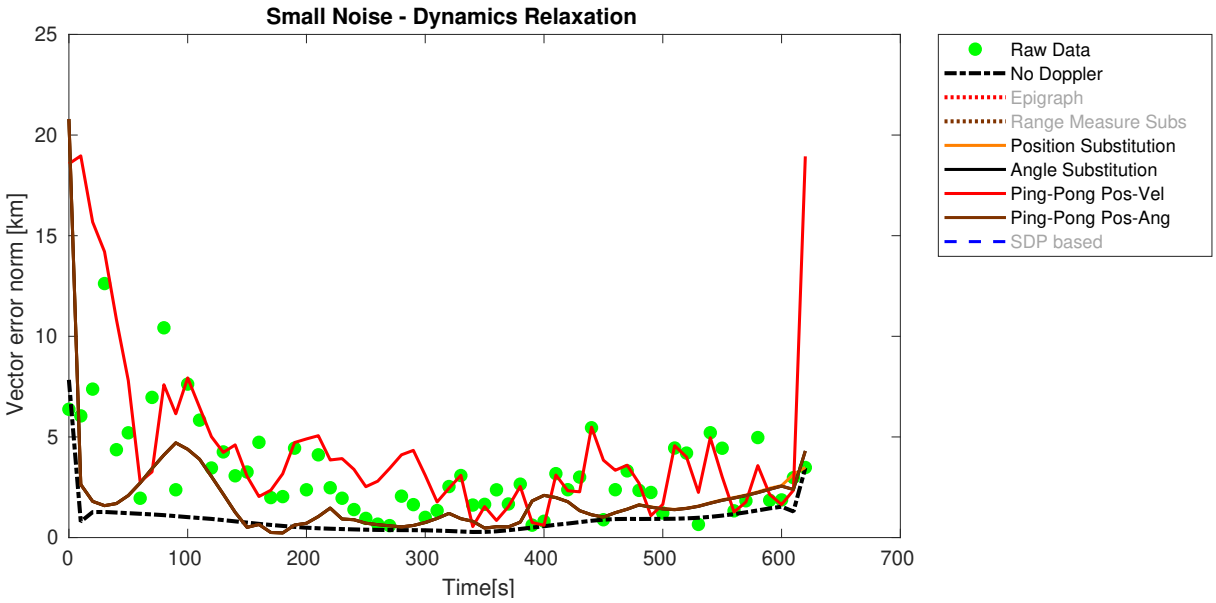

Figure 4.12: Simulation 3 - Small Noise - Dynamics Relaxation - Comparing worst performing cost functions with additional term to regularize position estimates using linearized dynamics equations. The lines relative to ”Position Substitution”, ”Angle Substitution” and ”Ping-Pong Pos-Ang” are overlapped.

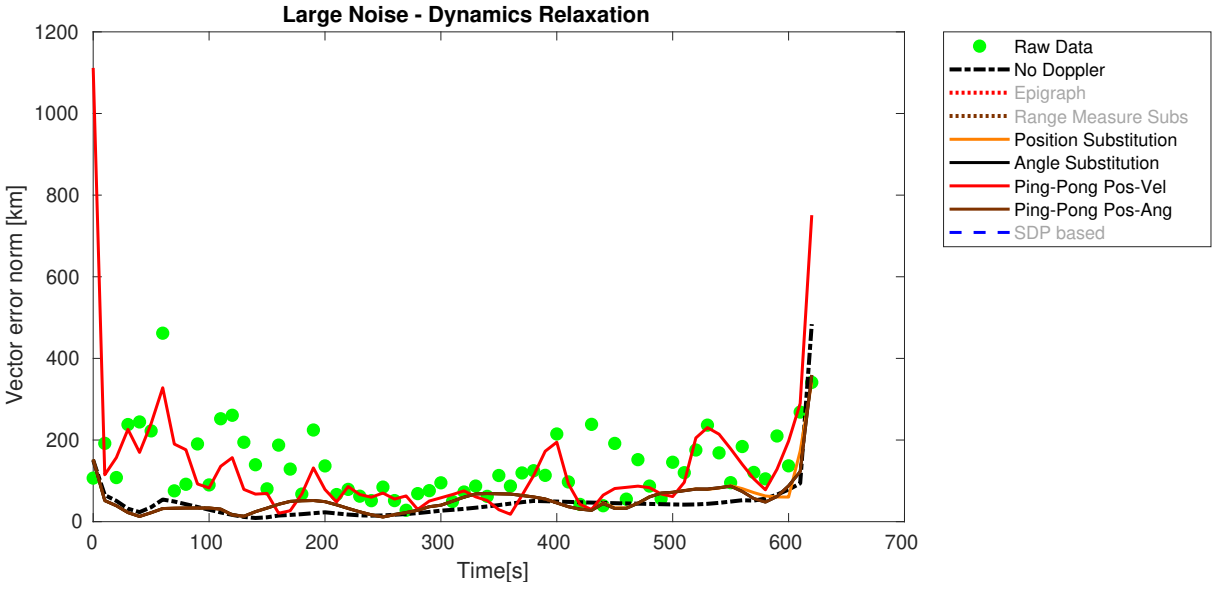

Figure 4.13: Simulation 3 - Large Noise - Dynamics Relaxation - Comparing worst performing cost functions with additional term to regularize position estimates using linearized dynamics equations. The lines relative to ”Position Substitution”, ”Angle Substitution” and ”Ping-Pong Pos-Ang” are overlapped.

Fig. 4.12 and Fig. 4.13 show the erratic behavior of the ping-pong scheme for position-velocity es-

timation (red line), even when aided with a smoothing regularization function. These are additional examples of the fragility in convergence of the iterative correction methods discussed above.

4.3.4 Slack variable

The addition of the angular momentum constraint using a slack variable in (3.43)/(3.44) to every formulation may be observed in Fig. 4.14 as a lower bound of the raw sensor measurements.

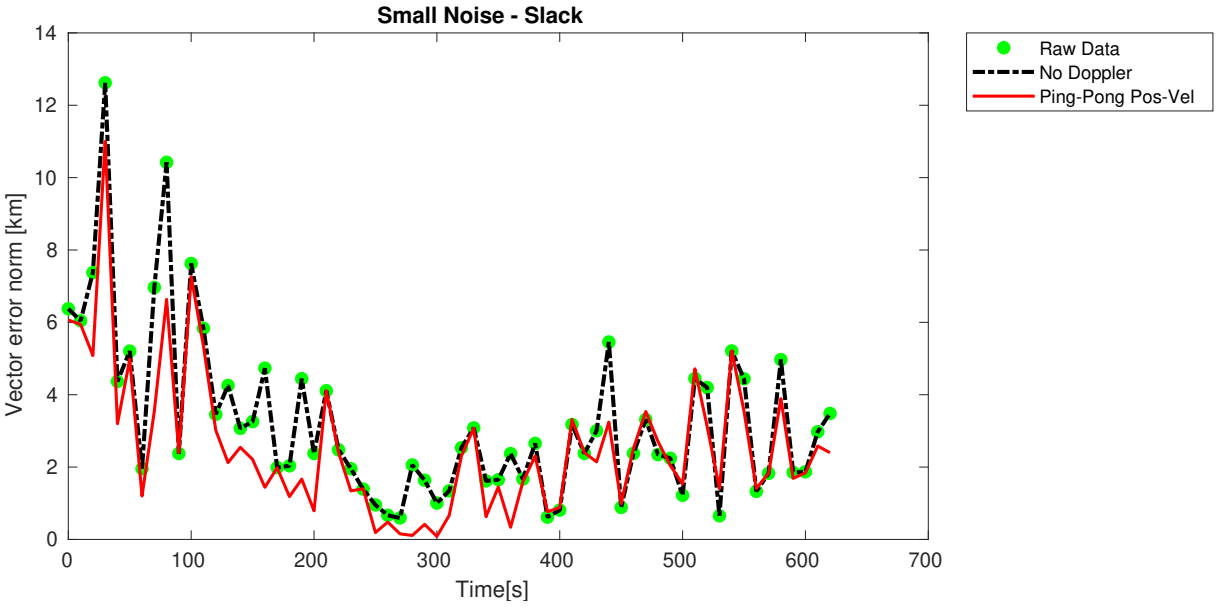

Figure 4.14: Simulation 4 - Small Noise - Slack Variable - Comparing position estimation performance with additional term to regularize position estimates using constant satellite's angular momentum property.

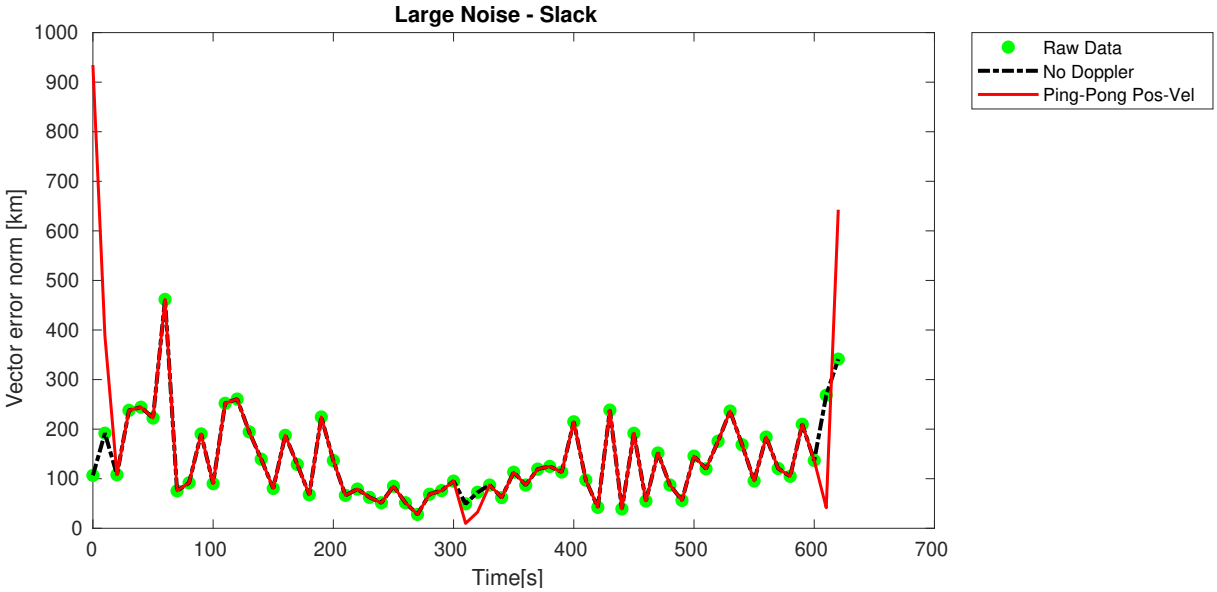

Figure 4.15: Simulation 4 - Large Noise - Slack Variable - Comparing eligible cost functions performance with additional term to regularize position estimates using constant satellite's angular momentum property.

The introduction of the *angular momentum* constraint is producing the intended effect: driving the positions set to a plane (verified by plotting 3-D estimated positions and confirming that they indeed belong to a plane). However, without an additional term to relate the positions over time, this formulation still produces far from smooth results and cannot be used to obtain a correct estimate of satellite's position.

4.3.5 Nuclear norm

The best results obtained with the introduction of the Nuclear Norm regularizer term in (3.46) are depicted in Fig. 4.16 and Fig. 4.17.
In this case, the weighting term was selected to dynamically penalize the deviation of the positions from a planar structure. This was done by making the penalizing term proportional to σ_3/σ_1.

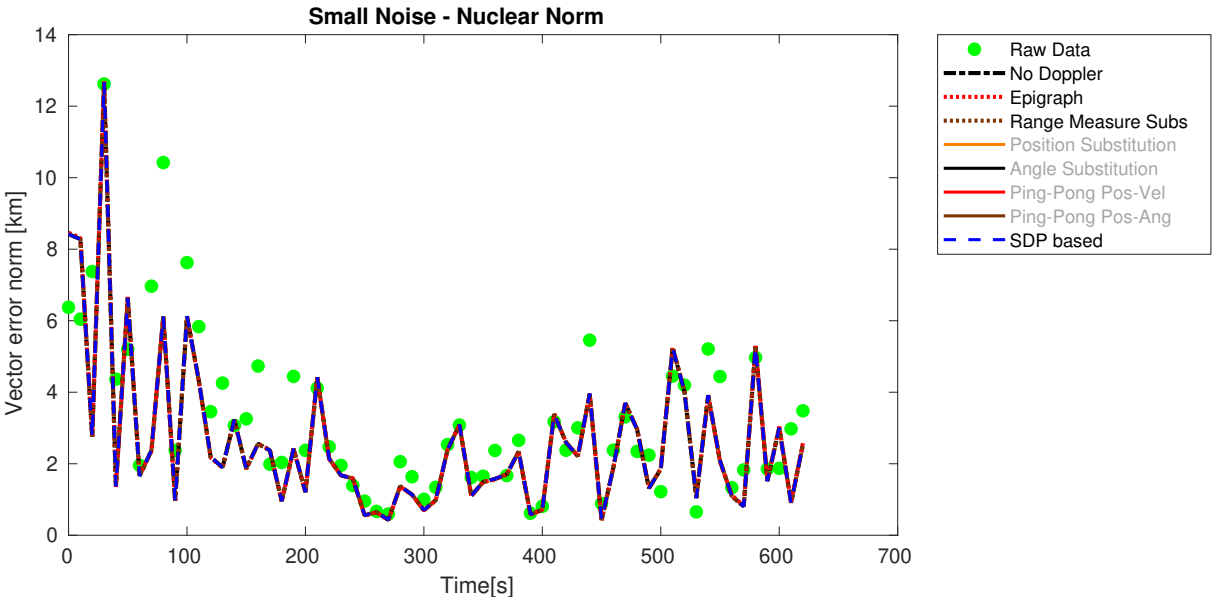

Figure 4.16: Simulation 5 - Small Noise - Nuclear Norm - Comparing best performing cost functions with additional term to regularize position estimates using nuclear norm drive solutions to a plane. All the active lines are overlapped

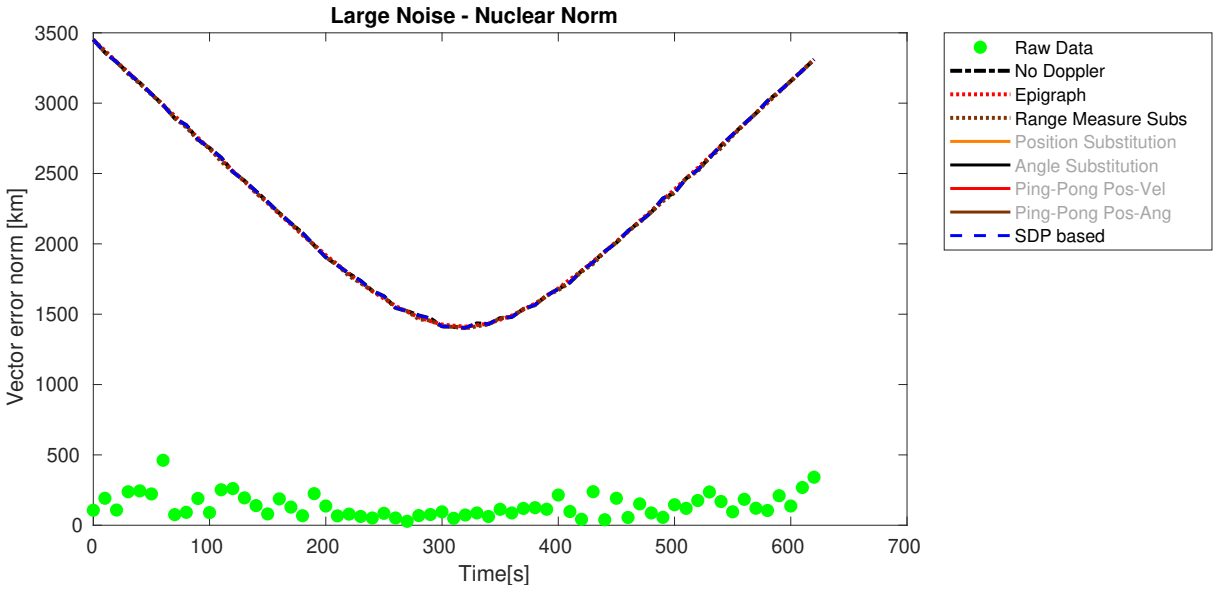

Figure 4.17: Simulation 5 - Large Noise - Nuclear Norm - Comparing best performing cost functions with additional term to regularize position estimates using nuclear norm drive solutions to a plane. All the active lines are overlapped.

This cost term is particularly difficult to use since by minimizing the nuclear norm there is no fine control of which singular values are being minimized because it seeks to minimize the sum of all. Finding a weighting term that meets the balance between minimization of σ_3 without greatly affecting σ_1 and σ_2 is hard.

Analyzing Fig. 4.16, it is evident that for the selected weighting technique some estimates are even degraded by this penalization.

The extreme case is evidenced in Fig. 4.17 where the estimated positions have an absurd error. This is explained by the increased value of σ_3 (due to the larger deviation of positions from a planar structure in a high noise condition) which in turn increases the weighting factor applied to the Nuclear Norm cost function.

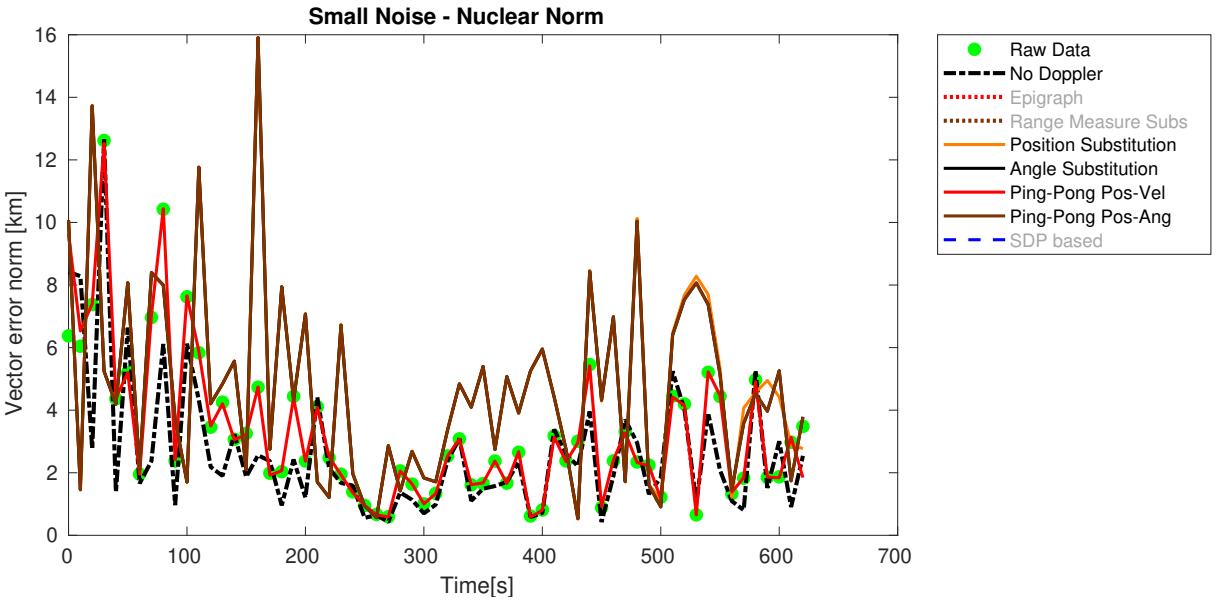

Figure 4.18: Simulation 5 - Small Noise - Nuclear Norm - Comparing worst performing cost functions with additional term to regularize position estimates using nuclear norm drive solutions to a plane. The lines relative to ”Position Substitution”, ”Angle Substitution” and ”Ping-Pong Pos-Ang” are overlapped.

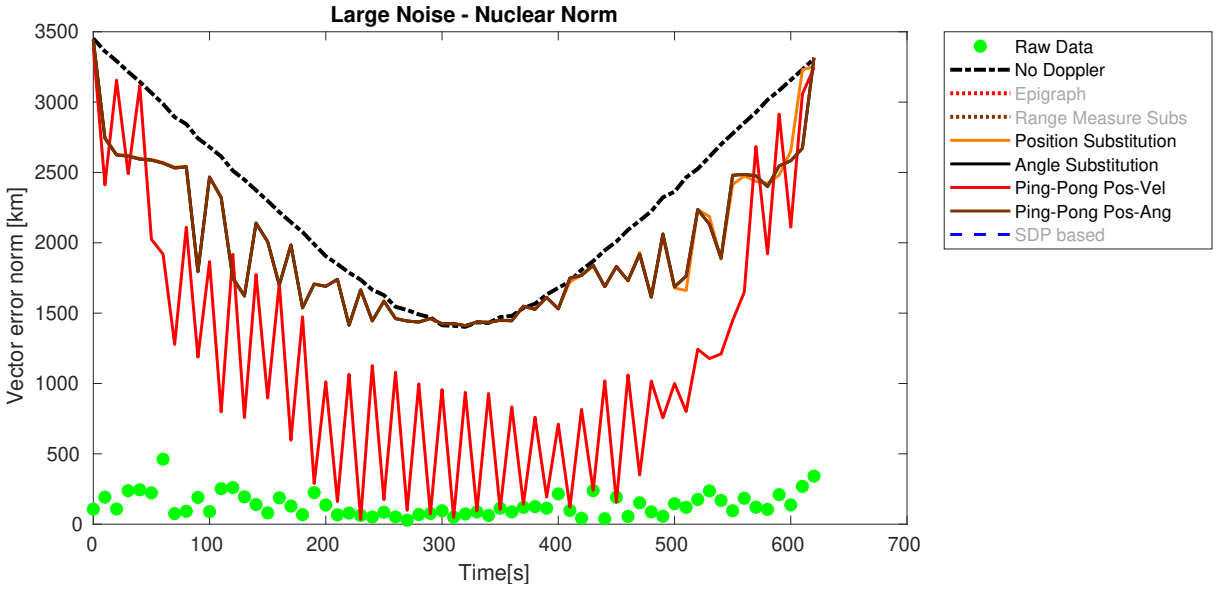

Figure 4.19: Simulation 5 - Large Noise - Nuclear Norm - Comparing worst performing cost functions with additional term to regularize position estimates using nuclear norm drive solutions to a plane.

As before, the cases which have positions and angles directly substituted, depicted in Fig. 4.18 and Fig. 4.19 do not improve their performance with the introduction of an additional penalizing term, performing equal or worse than the case with no Doppler information.

4.3.6 Plane projection

The projection in a plane aims to mitigate the problem of unconstrained rank minimization experimented in the Nuclear Norm problem by substituting the analytical rank property with a more intuitive geometric

method.

The weighting term, γ, applied to the regularizer function in (3.51) was chosen to be equal across all formulations so that it forms a base to compare the results.

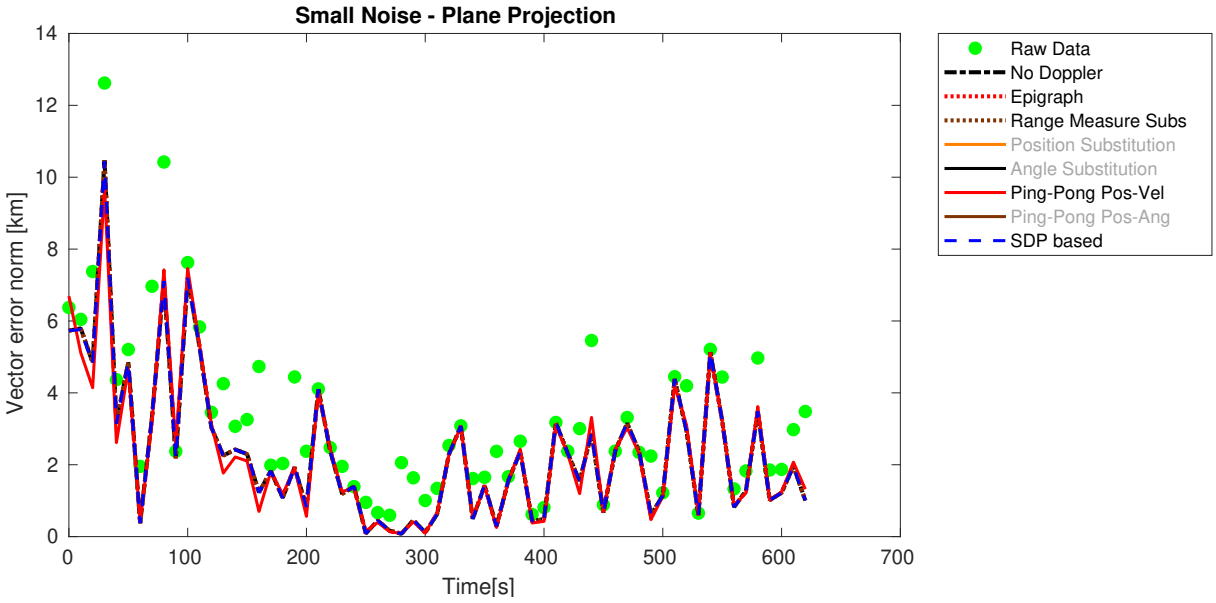

Figure 4.20: Simulation 6 - Small Noise - Plane Projection - Comparing best performing cost functions with additional term to regularize position estimates using distance to a previously computed best fitting plane.

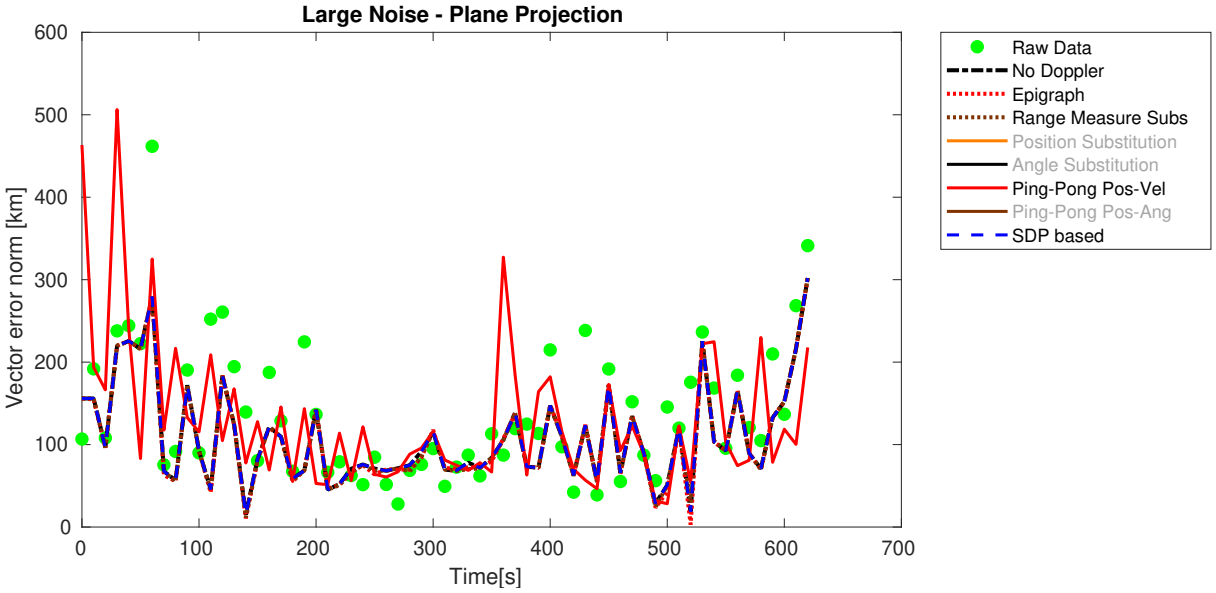

Figure 4.21: Simulation 6 - Large Noise - Plane Projection - Comparing best performing cost functions with additional term to regularize position estimates using distance to a previously computed best fitting plane. The three first active lines are overlapped.

Looking at the best results obtained with this penalizing metric, plotted in Fig. 4.20 and Fig. 4.21, it may be observed that, for a small noise case, it corresponds to a lower bound of the raw sensor outputs and so gives equal or better results compared to the minimization with no complementary function. However, for large noise, this property is lost and there is no advantage of using this complementary

function.

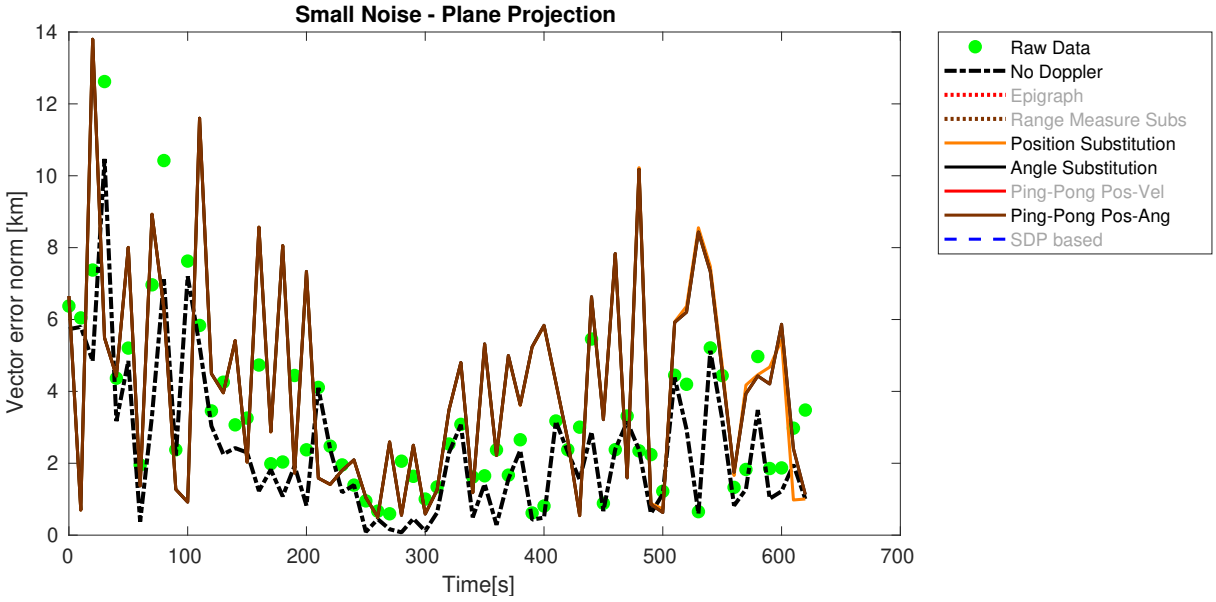

Figure 4.22: Simulation 6 - Small Noise - Plane Projection - Comparing worst performing cost functions with additional term to regularize position estimates using distance to a previously computed best fitting plane. The lines relative to ”Angle Substitution” and ”Ping-Pong Pos-Ang” are overlapped.

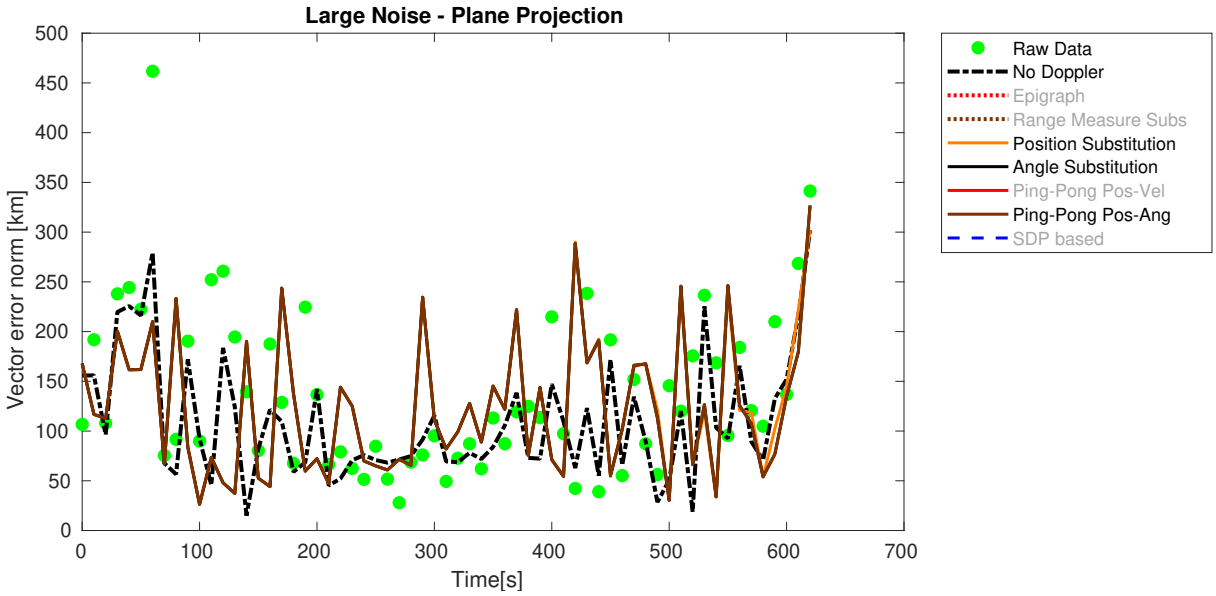

Figure 4.23: Simulation 6 - Large Noise - Plane Projection - Comparing worst performing cost functions with additional term to regularize position estimates using distance to a previously computed best fitting plane. The lines relative to ”Angle Substitution” and ”Ping-Pong Pos-Ang” are overlapped.

As expected, the terms with poor performance found in previous sections maintain their behavior.

Chapter 5

Conclusions

The study presented in Appendix D strongly suggests that the use of approximate functions for the Doppler-shift cost function introduces additional information to the estimation problem. However, this study is not sufficient to conclude about the tightness of the developed relaxations which may degrade the estimator performance. In fact, this problem was verified numerically, since by either approximating the range-rate by finite-dived-differences of ranges or positions there was no significant gain of information, and so Doppler relaxations are not expected to provide major improvements in the accuracy of position estimates when compared to the case with no frequency information . This study assumes that both range and angular data are always available, and if that is not the case the above conclusion on the marginal contribution of Doppler may not hold. Also, the ultimate test to find how much the Doppler-shift measurements could improve the estimation would be to solve a non-linear optimization problem with the, non-convex, original measurement model. But in that case, at each instant, six variables would have to be estimated from only three measurements which is not feasible.

Nevertheless, this analysis was made with only two agents at a time, so the conclusion may not hold when several stations are observing a single satellite at the same time while sharing their information. Nonetheless, in the case with little information studied in this thesis, the alternative found to circumvent the lack of redundant information was to introduce complementary functions based on the known properties of satellite dynamics. Interestingly, the best results were obtained with the simplest ones, namely, the polynomial smoothing and dynamics relaxation.

For a case with no outliers and for an adequate weighting factor, the introduction of a polynomial to regularize the position estimates is beneficial. However, there are hyper-parameters such as the order of the polynomial which are dependent on the observation window length which introduces a processing overhead when one has to employ grid searching methods to obtain a guess about the best order and the best weight to apply. One possible solution to overcome these limitations is to use splines that enable the use of an assemblage of smaller order polynomials in smaller partitions of the observation window.

On the other hand, in order to use dynamics relaxation, it is necessary to have good estimates of the satellite position beforehand so the linearization can approximate the real function with an acceptable

level of accuracy, otherwise it may introduce wrong information on the global optimization problem which in the end, corrupts the results.
Finally, there is an issue transversal to every optimization problem formulation, not for this particular case, but in a general sense. The problem is that solving convex optimization problems does not generally produce the true best solution for the original (non-convex) problem. Instead, it produces the best solution for the mathematical formulation that was developed to encode that question. This appears in practice when one has to decide what are the best weighting factors to apply to each term of the global cost function, in the case where the global cost function is composed of the sum of convex functions. This poses an additional challenge of firstly determining these hyper-parameters. In this case, the parameters were found by grid search methods, but these are cumbersome. Moreover, these hyper-parameters are generally dependent on the intrinsic characteristics of the input data which compounds the problem even further since it requires a new grid search for different noise levels.

5.1 Achievements

In this work, a study was made on the usage of information of opportunity to obtain a coarse position estimation of a satellite using convex optimization methods. Several relaxations for the Doppler cost function were found so that they could use the position and angle estimates along with the frequency provided by the sensors to improve the position estimation accuracy.
A preliminary theoretical study strongly suggests that the use of approximate functions for the Doppler-shift cost function introduces additional information to the estimation problem. However, this study is not sufficient to conclude about the tightness of the developed relaxations which may degrade the estimator performance. This suspicion was confirmed in the simulations where no relaxation method could significantly outperform the formulation without Doppler-shift information. Nonetheless, some formulations appear to be good candidates to generate position estimates to initialize sequential estimation algorithms that may provide a finer result.
The application of the discussed methods to localize a single satellite may have poor results but when the scenario includes a formation of satellites, these collaborative localization algorithms may add a significant contribution.

5.2 Future Work

A more promising idea is to investigate if any of the Doppler-shift cost function relaxations presented in this thesis is useful in the case where several stations observe the satellite at the same time and share the measurements so that some information redundancy is obtained.
Beyond studying a scenario with more ground-stations, it would be valuable to study a scenario with a formation of CubeSats (since this is the way they are normally used) in which each one can perform the same kind of measurements used in this thesis and also communicate to determine their relative position. This problem would be much more close to a sensor network optimization problem for which

there is extensive literature published.

Bibliography

[1] M. Naeimi and J. Flury. *Global Gravity Field Modeling from Satellite-to-Satellite Tracking Data*. Springer, 2017.

[2] A. Jäggi, U. Hugentobler, and G. Beutler. Pseudo-stochastic orbit modeling techniques for low-Earth orbiters. *Journal of Geodesy*, 80(1):47–60, 2006. doi: 10.1007/s00190-006-0029-9.

[3] I. Vertat, R. Linhart, M. Pokorny, J. Masopust, P. Fiala, and J. Mraz. Small satellite ground station in Pilsen - Experiences with VZLUSAT-1 commanding and future modifications toward open reference ground station solution. *28th International Conference Radioelektronika, RADIOELEKTRONIKA 2018*, pages 1–6, 2018. doi: 10.1109/RADIOELEK.2018.8376393.

[4] W. H. Guier and G. C. Weiffenbach. Genesis of satellite navigation. *Johns Hopkins APL Technical Digest (Applied Physics Laboratory)*, 19(1):14–17, 1998. ISSN 02705214.

[5] D. A. Vallado and W. D. Mcclain. *Fundamentals of Astrodynamics and Applications, Fourth Edition*. Microcosm Press, 2013. ISBN 9781881883180.

[6] O. Montenbruck, E. Gill, and F. Lutze. *Satellite Orbits: Models, Methods, and Applications*. Springer-Verlag, 2000.

[7] I. G. Izsak. Orbit determination from simultaneous doppler-shift measurements. *SAO Special Report*, 38, 1960.

[8] R. Hart. Single-station Tracking for Orbit Determination of Small Satellites. In *Technical Session VI: Small Satellites - Support Systems (Small Satellite Conference)*, 1987.

[9] R. B. Patton. Orbit determination from single pass doppler observations. *IRE Transactions on Military Electronics*, MIL-4(2/3):336–344, 1960. doi: 10.1109/IRET-MIL.1960.5008246.

[10] E. Golton. The use of the Doppler effect to deduce an accurate position for an artificial earth satellite. *Planetary and Space Science*, 9(10):607–623, 1962. ISSN 00320633. doi: 10.1016/0032-0633(62)90122-8.

[11] M. C. Dykstra. Single Station Doppler Tracking for Satellite Orbit Prediction and Propagation. Master's thesis, University of Texas, 2015.

[12] I. Klinkert. Satellite Orbit Determination with the Global Educational Network for Satellite Operations (GENSO). Master's thesis, Open Universiteit Nederland, 2010.

[13] L. Ansalone. *A search algorithm for stochastic optimization in initial orbit determination*. PhD thesis, Sapienza University of Rome, 2013.

[14] A. Almeida. A study on probabilistic satellite localization using messages metadata. Master's thesis, IST, Universidade de Lisboa, 2019.

[15] F. Valdeira. Hybrid Localization in Underwater Environment. Master's thesis, IST, Universidade de Lisboa, 2018.

[16] C. A. Kluever. *Space Flight Dynamics*. John Wiley and Sons Ltd, 2018.

[17] NORAD two-line element sets current data. `https://www.celestrak.com/NORAD/elements/weather.txt`, Last Update: 2021 Feb 25 10:06:05 UTC (Day 056). [Online; accessed 25-February-2021].

[18] J. Mass and E. Vassy. Doppler Effect of Artificial Satellites. *Advances in Space Science and Technology (Volume 4)*, 4:1–38, 1962. doi: 10.4324/9780203883068.

[19] M. Petovello. How does earth's rotation affect GNSS orbit computations? `https://insidegnss.com/how-does-earths-rotation-affect-gnss-orbit-computations/`, April 5, 2018. [Online; accessed 11-November-2020].

[20] H. Rouzegar, M. Nasirian, and M. Ghanbarisabagh. Novel Algorithm for Tracking LEO Satellites Using Doppler Frequency Shift Technique. *Wireless Personal Communications*, 96(2):2161–2178, 2017. ISSN 1572834X. doi: 10.1007/s11277-017-4291-3.

[21] N. Hongyim and S. Mitatha. Building automatic antenna tracking system for low earth orbit(LEO) satellite communications. *ICSEC 2015 - 19th International Computer Science and Engineering Conference: Hybrid Cloud Computing: A New Approach for Big Data Era*, 2016. doi: 10.1109/ICSEC.2015.7401448.

[22] H. Kuga and V. Orlando. Assessing Orbit Determination Through One Way Doppler Signals. *International Symposium on Space Dynamics - 17*, (January):1–7, 2003. URL `https://www.researchgate.net/publication/43654931_Assessing_orbit_determination_through_one_way_doppler_signals`.

[23] S. M. Kay. *Fundamentals of statistical signal processing*. Prentice Hall PTR, 1993.

[24] S. Boyd and L. Vandenberghe. *Convex optimization*. Cambridge university press, 2004.

[25] A. L. G. DeBey and V. W. Richard. The DOPLOC dark satellite tracking system. Technical report, In Ballistic Research Laboratories, 1963.

[26] R. M. D. Oliveira. Orbit Determination for Low-Altitude Satellites Using Semianalytical Satellite Theory. Master's thesis, IST, Universidade de Lisboa, 2021.

[27] S. Shankar, K. Ezal, and J. P. Hespanha. Finite horizon maximum likelihood estimation for integrated navigation with rf beacon measurements. volume 21, pages 1470–1482. Wiley Online Library, 2019.

[28] J. Hespanha. Tenscalc - a matlab toolbox for nonlinear optimization using symbolic tensor calculus. https://github.com/hespanha/tenscalc, 2010-2017. [Online; accessed 2-January-2020].

[29] H. Nurminen, L. Suomalainen, S. Ali-Löytty, and R. Piché. 3D Angle-of-Arrival Positioning Using von Mises-Fisher Distribution. In *21st International Conference on Information Fusion, FUSION 2018*, 2018. ISBN 9780996452762. doi: 10.23919/ICIF.2018.8455205.

[30] D. Muir. vmrand - function draw random variates from the von mises circular distribution. `https://www.mathworks.com/matlabcentral/fileexchange/37241-vmrand-fmu-fkappa-varargin`, 2012. [Online; accessed 2-January-2020].

[31] Averse. Radial velocity. `https://en.wikipedia.org/wiki/Radial_velocity#/media/File:Radialgeschwindigkeit.gif`, 2006. [Online; accessed 2-January-2020].

[32] C. Soares, J. Xavier, and J. Gomes. Simple and fast convex relaxation method for cooperative localization in sensor networks using range measurements. *IEEE Transactions on Signal Processing*, 63(17):4532–4543, 2015.

[33] C. Soares, F. Valdeira, and J. Gomes. Range and Bearing Data Fusion for Precise Convex Network Localization. *IEEE Signal Processing Letters*, 27(1):670–674, 2020. doi: 10.1109/LSP.2020.2988178.

[34] Y. T. Chan and F. L. Jardine. Target Localization and Tracking From Doppler-Shift Measurements. *IEEE Journal of Oceanic Engineering*, 15(3):251–257, 1990. ISSN 15581691. doi: 10.1109/48.107154.

[35] R. J. Webster. An Exact Trajectory Solution from Doppler-shift Measurements. *IEEE Transactions on Aerospace and Electronic Systems*, AES-18(2):249–252, 1982. ISSN 00189251. doi: 10.1109/TAES.1982.309235.

[36] Y. T. Chan and S. W. Rudnicki. Bearings-Only and Doppler-Bearing Tracking Using Instrumental Variables. *IEEE Transactions on Aerospace and Electronic Systems*, 28(4):1076–1083, 1992. ISSN 00189251. doi: 10.1109/7.165369.

[37] K. C. Ho and Y. T. Chan. Geometric-polar tracking from bearings-only and doppler-bearing measurements. *IEEE Transactions on Signal Processing*, 56(11):5540–5554, 2008. doi: 10.1109/TSP.2008.928701.

[38] J. S. Picard and A. J. Weiss. Time-delay and Doppler-shift based geolocation by Semi-Definite Programming. *European Signal Processing Conference*, (Eusipco):1189–1193, 2012. ISSN 22195491.

[39] Y. Du, P. Wei, W. Li, and H. Liao. Doppler-shift based target localization using semidefinite relaxation. *IEICE Transactions on Fundamentals of Electronics, Communications and Computer Sciences*, E97.A:397–400, 01 2014. doi: 10.1587/transfun.E97.A.397.

[40] N. Saeed, A. Elzanaty, H. Almorad, H. Dahrouj, T. Y. Al-Naffouri, and M. S. Alouini. CubeSat Communications: Recent Advances and Future Challenges. *IEEE Communications Surveys and Tutorials*, 22(3):1839–1862, 2020. ISSN 1553877X. doi: 10.1109/COMST.2020.2990499.

[41] I. Shames, A. N. Bishop, M. Smith, and B. D. Anderson. Doppler shift target localization. *IEEE Transactions on Aerospace and Electronic Systems*, 49(1):266–276, jan 2013. ISSN 00189251. doi: 10.1109/TAES.2013.6404102.

[42] S. C. Chapra and R. P. Canale. *Numerical methods for engineers*, volume 33. McGraw-Hill Science/Engineering/Math, 1991. ISBN 9780073397924. doi: 10.1016/0378-4754(91)90127-o.

[43] K. Yang, G. Wang, and Z. Q. Luo. Efficient convex relaxation methods for robust target localization by a sensor network using time differences of arrivals. *IEEE Transactions on Signal Processing*, 57 (7):2775–2784, 2009. ISSN 1053587X. doi: 10.1109/TSP.2009.2016891.

[44] S. Boyd and L. Vandenberghe. Semidefinite programming. *SIAM Review*, 38(1):49–95, 1996. ISSN 03772217. doi: 10.1016/S0377-2217(01)00143-6.

[45] Y. Shen Du, P. Wei, W. Chun Li, and H. Shu Liao. Doppler-shift based target localization using semidefinite relaxation. *IEICE Transactions on Fundamentals of Electronics, Communications and Computer Sciences*, E97-A(1):397–400, 2014. ISSN 17451337. doi: 10.1587/transfun.E97.A.397.

[46] Z. Q. Luo, W. K. Ma, A. So, Y. Ye, and S. Zhang. Semidefinite relaxation of quadratic optimization problems. *IEEE Signal Processing Magazine*, 27(3):20–34, 2010. ISSN 10535888. doi: 10.1109/MSP.2010.936019.

[47] R. Cabral, F. De la Torre, J. P. Costeira, and A. Bernardino. Unifying nuclear norm and bilinear factorization approaches for low-rank matrix decomposition. *Proceedings of the IEEE International Conference on Computer Vision*, pages 2488–2495, 2013.

[48] NASA. Orbit determination toolbox (ODTBX). `https://opensource.gsfc.nasa.gov/projects/ODTBX/`, October 24, 2019. [Online; accessed 10-April-2020].

Appendix A

Orbit propagation with Classical Elements

$$\cos(E_1) = \frac{e + \cos(\theta_1)}{1 + e\cos(\theta_1)} \tag{A.1}$$

$$\sin(E_1) = \frac{\sqrt{1 - e^2}\sin(\theta_1)}{1 + e\cos(\theta_1)} \tag{A.2}$$

$$E_1 = \arctan2\left(\sin(E_1), \cos(E_1)\right) \tag{A.3}$$

$$M_1 = E_1 - e\sin(E_1) \tag{A.4}$$

$$M_2 = M_1 + n(t_2 - t_1) \tag{A.5}$$

$$n = \sqrt{\frac{\mu}{a^3}} \tag{A.6}$$

$$M_2 = E_2 - e\sin(E_2) \tag{A.7}$$

$$\cos(\theta_2) = \frac{\cos E_2 - e}{1 - e\cos E} \tag{A.8}$$

$$\sin(\theta_2) = \frac{\sqrt{1 - e^2}\sin(\mathrm{E}_2)}{1 - e\cos(E_2)} \tag{A.9}$$

$$\theta_2 = \arctan2(\sin(\theta_2), \cos(\theta_2)) \tag{A.10}$$

Appendix B

Cartesian to Classical Elements

$$\xi = \frac{\|v_0\|^2}{2} - \frac{\mu}{\|r_0\|} \tag{B.1}$$

$$a = -\frac{\mu}{2\xi} \tag{B.2}$$

$$\boldsymbol{e} = \frac{1}{\mu}\left[\left(\|v_0\|^2 - \frac{\mu}{\|r_0\|}\right)\boldsymbol{r}_0 - (\boldsymbol{r}_0 \cdot \boldsymbol{v}_0)\,\boldsymbol{v}_0\right] \tag{B.3}$$

$$e = \|\boldsymbol{e}\| \tag{B.4}$$

$$\boldsymbol{k} = \boldsymbol{r}_0 \times \boldsymbol{v}_0 \tag{B.5}$$

$$i = \arccos\left(\frac{\boldsymbol{K} \cdot \boldsymbol{h}}{\|\boldsymbol{h}\|}\right) \tag{B.6}$$

$$\boldsymbol{n} = \boldsymbol{K} \times \boldsymbol{h} \tag{B.7}$$

$$\cos(\Omega) = \frac{\boldsymbol{I} \cdot \boldsymbol{n}}{\|\boldsymbol{n}\|} \tag{B.8}$$

$$\sin(\Omega) = \frac{\boldsymbol{J} \cdot \boldsymbol{n}}{\|\boldsymbol{n}\|} \tag{B.9}$$

$$\Omega = \arctan2(\sin(\Omega), \cos(\Omega)) \tag{B.10}$$

$$\begin{cases} \omega = \arccos(\frac{\boldsymbol{n}\cdot\boldsymbol{e}}{\|\boldsymbol{n}\|\,e}), & \boldsymbol{e}_z > 0 \\ \omega = 2\pi - \arccos(\frac{\boldsymbol{n}\cdot\boldsymbol{e}}{\|\boldsymbol{n}\|\,e}), & \boldsymbol{e}_z < 0 \end{cases} \tag{B.11}$$

$$\begin{cases} \theta = \arccos\left(\frac{\boldsymbol{e}\cdot\boldsymbol{r_0}}{e\,\|\boldsymbol{r_0}\|}\right), & \boldsymbol{r}_0 \cdot \boldsymbol{r}_0 > 0 \\ \theta = 2\pi - \arccos\left(\frac{\boldsymbol{e}\cdot\boldsymbol{r_0}}{e\,\|\boldsymbol{r_0}\|}\right), & \boldsymbol{r}_0 \cdot \boldsymbol{r}_0 < 0 \end{cases} \tag{B.12}$$

Appendix C

Classical Elements to Cartesian Coordinates

$$p = a(1 - e^2) \tag{C.1}$$

$$r = \frac{p}{1 + e\cos(\theta)} \tag{C.2}$$

$$\boldsymbol{P} = [1 \quad 0 \quad 0]^T \tag{C.3}$$

$$\boldsymbol{Q} = [0 \quad 1 \quad 0]^T \tag{C.4}$$

$$\boldsymbol{r}_{PQW} = r\cos(\theta)\boldsymbol{P} + r\sin(\theta)\boldsymbol{Q} \tag{C.5}$$

$$h = \sqrt{\mu\, p} \tag{C.6}$$

$$\boldsymbol{v}_{PQW} = -\frac{\mu}{h}\sin(\theta)\boldsymbol{P} + \frac{\mu}{h}\left(e + \cos(\theta)\right)\boldsymbol{Q} \tag{C.7}$$

$$R = \begin{bmatrix} c_\Omega c_\omega - s_\Omega s_\omega c_i & -c_\Omega s_\omega - s_\Omega c_\omega c_i & s_\Omega s_i \\ s_\Omega c_\omega + c_\Omega s_\omega c_i & -s_\Omega s_\omega + c_\Omega c_\omega c_i & -c_\Omega s_i \\ s_\omega s_i & c_\omega s_i & c_i \end{bmatrix} \tag{C.8}$$

$$\boldsymbol{r}_{ECI} = R\boldsymbol{r}_{PQW} \tag{C.9}$$

$$\boldsymbol{v}_{ECI} = R\boldsymbol{v}_{PQW} \tag{C.10}$$

Appendix D

Information-theoretical view of Doppler-shift measurements

D.1 General Formulation

The analysis of Cramér-Rao Lower Bound may quickly become cumbersome for a generic distribution since the calculations must be done directly according to the definitions in Sec. 2.4.2. However the result is well known for a multivariate random variable which follows a Normal distribution, $\boldsymbol{x} \sim \mathcal{N}(\boldsymbol{\mu}(\boldsymbol{\theta}), \boldsymbol{C}(\boldsymbol{\theta}))$, with unknown mean, $\boldsymbol{\mu} \in \mathbb{R}^{N\times 1}$, and measurement covariance matrix, $\boldsymbol{C}(\boldsymbol{\theta}) \in \mathbb{R}^{N\times N}$, with N the number of measurements.
These moments are dependent on a vector parameter $\boldsymbol{\theta} \in \mathbb{R}^{M}$, where M is the number of parameters to estimate such that the (i^{th},j^{th}) entry of the FIM may be written as

$$I_{i,j} = \frac{\partial \boldsymbol{\mu}(\boldsymbol{\theta})}{\partial \theta_i}^T \boldsymbol{C}(\boldsymbol{\theta})^{-1} \frac{\partial \boldsymbol{\mu}(\boldsymbol{\theta})}{\partial \theta_j} + \frac{1}{2} \operatorname{tr}\left(\boldsymbol{C}(\boldsymbol{\theta})^{-1} \frac{\partial \boldsymbol{C}(\boldsymbol{\theta})}{\partial \theta_i} \boldsymbol{C}(\boldsymbol{\theta})^{-1} \frac{\partial \boldsymbol{C}(\boldsymbol{\theta})}{\partial \theta_j} \right). \tag{D.1}$$

In the case where the covariance matrix is constant, $\frac{\partial \boldsymbol{C}(\boldsymbol{\theta})}{\partial \theta_i} = 0$, the computation is reduced to the first term such that each entry may be computed as

$$I_{i,j} = \frac{\partial \boldsymbol{\mu}(\boldsymbol{\theta})}{\partial \theta_i}^T \boldsymbol{C}^{-1} \frac{\partial \boldsymbol{\mu}(\boldsymbol{\theta})}{\partial \theta_j}. \tag{D.2}$$

In order to use this generic result, the directional von Mises-Fisher distribution that was used in Sec. 2.6 must be approximated by a Normal Distribution which essentially encodes the same information. To do this, one may observe that the angular information can also be obtained from Azimuth and Elevation angles introduced in Sec. 2.1.3, so that, the ML formulation that uses these angles is a good approximation of the VMF distribution for small angular dispersion.
An approximate correspondence between the concentration parameter, κ, and the variances for azimuth,

σ^2_{Az}, and elevation, σ^2_{Ez}, suitable for a preliminary error study, is given in [29]

$$\kappa \approx \frac{1}{\max\left(\sigma^2_{Az}, \sigma^2_{El}\right)}. \tag{D.3}$$

The *pdf's* for each one of the distance and Doppler-shift measurements are recalled from Sec. 2.6.1

$$p(\rho^k|\boldsymbol{r}^k) = \frac{\exp\left(-\frac{\left(\rho^k - \left\|\boldsymbol{r}^k - \boldsymbol{r}^k_{gs}\right\|\right)^2}{2\sigma^2_\rho}\right)}{\sqrt{2\pi}\sigma_\rho} \tag{D.4}$$

$$p\left(\Delta f^k|\boldsymbol{v}^k\right) = \frac{\exp\left(-\frac{\left(\Delta f^k + \frac{f_{emm}}{c}\frac{(\boldsymbol{r}^k - \boldsymbol{r}^k_{gs})^T(\boldsymbol{v}^k - \boldsymbol{v}^k_{gs})}{\left\|\boldsymbol{r}^k - \boldsymbol{r}^k_{gs}\right\|}\right)^2}{2\sigma^2_f}\right)}{\sqrt{2\pi}\sigma_f}. \tag{D.5}$$

$$\tag{D.6}$$

The new *pdf's* for elevation and azimuth are based on (2.1)

$$p(El^k|\boldsymbol{r}^k) = \frac{\exp\left(-\frac{\left(El^k - \arctan\frac{\boldsymbol{r}^k_z}{\sqrt{\boldsymbol{r}^{k\,2}_x + \boldsymbol{r}^{k\,2}_y}}\right)^2}{2\sigma^2_{El}}\right)}{\sqrt{2\pi}\,\sigma_{El}} \tag{D.7}$$

$$p(Az^k|\boldsymbol{r}^k) = \frac{\exp\left(-\frac{\left(Az^k - \left(\pi - \arctan\frac{\boldsymbol{r}^k_y}{\boldsymbol{r}^k_x}\right)\right)^2}{2\sigma^2_{Az}}\right)}{\sqrt{2\pi}\,\sigma_{Az}}. \tag{D.8}$$

$$\tag{D.9}$$

The mean values for each of the *pdf's* are, by construction,

$$\boldsymbol{\mu}^k_\rho(\boldsymbol{\theta}) = \left\|\boldsymbol{r}^k - \boldsymbol{r}^k_{gs}\right\| \tag{D.10}$$

$$\boldsymbol{\mu}^k_f(\boldsymbol{\theta}) = -\frac{f_{emm}}{c}\frac{(\boldsymbol{r}^k - \boldsymbol{r}^k_{gs})^T(\boldsymbol{v}^k - \boldsymbol{v}^k_{gs})}{\left\|\boldsymbol{r}^k - \boldsymbol{r}^k_{gs}\right\|} \tag{D.11}$$

$$\boldsymbol{\mu}^k_{El}(\boldsymbol{\theta}) = \arctan\frac{\boldsymbol{r}^k_z}{\sqrt{\boldsymbol{r}^{k\,2}_x + \boldsymbol{r}^{k\,2}_y}} \tag{D.12}$$

$$\boldsymbol{\mu}^k_{Az}(\boldsymbol{\theta}) = \pi - \arctan\frac{\boldsymbol{r}^k_y}{\boldsymbol{r}^k_x} \tag{D.13}$$

for the particular case when $\boldsymbol{\theta} = \boldsymbol{r}^T$.

The velocity term is assumed to be known or it is approximated by finite-divided-difference methods depending on the case depicted in the following sections.

The entries of the information matrix for range measurements during the full observation window are, according to (D.2),

$$I_{\rho_{i,j}} = \left[\frac{\partial \boldsymbol{\mu}_\rho^1(\boldsymbol{r})}{\partial \boldsymbol{r}_i} \cdots \frac{\partial \boldsymbol{\mu}_\rho^k(\boldsymbol{r})}{\partial \boldsymbol{r}_i} \cdots \frac{\partial \boldsymbol{\mu}_\rho^N(\boldsymbol{r})}{\partial \boldsymbol{r}_i} \right] \boldsymbol{C}_\rho^{-1} \begin{bmatrix} \frac{\partial \boldsymbol{\mu}_\rho^1(\boldsymbol{r})}{\partial \boldsymbol{r}_j} \\ \vdots \\ \frac{\partial \boldsymbol{\mu}_\rho^k(\boldsymbol{r})}{\partial \boldsymbol{r}_j} \\ \vdots \\ \frac{\partial \boldsymbol{\mu}_\rho^N(\boldsymbol{r})}{\partial \boldsymbol{r}_j} \end{bmatrix} \tag{D.14}$$

being the same representation valid for the remaining observation types.

If there is no statistical dependency (the measurements are uncorrelated), then, the total information of the FIM is the sum of the individual contributions of each measurement type

$$I_T = I_\rho + I_f + I_{El} + I_{Az}. \tag{D.15}$$

D.2 Compare relaxations

In order to evaluate the dependency of the best achievable standard deviation with the position of the satellite along the entire pass, the calculation of the CRLB was made for all the instants of the pass depicted in Fig. 4.1.

Three Doppler-shift measurement models were analyzed: the first, μ_{f-tv}^k, uses the original Doppler function with knowledge of the true satellite's velocity at each instant; the second model, μ_{f-rra}^k, uses the range-rate approximation in (3.2); the third model, μ_{f-va}^k, uses the velocity approximation as in (3.7).

These choices are translated in the following mean values

$$\boldsymbol{\mu}_{f-tv}^k(\boldsymbol{\theta}) = \left[-\frac{f_t}{c} \frac{(\boldsymbol{r}^1 - \boldsymbol{r}_{gs}^1)^T (\boldsymbol{v}^1 - \boldsymbol{v}_{gs}^1)}{\left\| \boldsymbol{r}^1 - \boldsymbol{r}_{gs}^1 \right\|} \quad \cdots \quad \cdots \quad -\frac{f_t}{c} \frac{(\boldsymbol{r}^N - \boldsymbol{r}_{gs}^N)^T (\boldsymbol{v}^N - \boldsymbol{v}_{gs}^N)}{\left\| \boldsymbol{r}^N - \boldsymbol{r}_{gs}^N \right\|} \right] \tag{D.16}$$

$$\boldsymbol{\mu}_{f-rra}^k(\boldsymbol{\theta}) = \left[0 \quad \cdots \quad -\frac{f_t}{c} \frac{\left\| \boldsymbol{r}^{k+1} - \boldsymbol{r}_{gs}^{k+1} \right\| - \left\| \boldsymbol{r}^{k-1} - \boldsymbol{r}_{gs}^{k-1} \right\|}{2\Delta_t} \quad \cdots \quad -\frac{f_t}{c} \frac{\left\| \boldsymbol{r}^N - \boldsymbol{r}_{gs}^N \right\| - \left\| \boldsymbol{r}^{N-2} - \boldsymbol{r}_{gs}^{N-2} \right\|}{2\Delta_t} \right]^T \tag{D.17}$$

$$\boldsymbol{\mu}_{f-va}^k(\boldsymbol{\theta}) = \left[0 \quad \cdots \quad -\frac{f_t}{c} \frac{\boldsymbol{r}^{k^T} \frac{\left(\boldsymbol{r}^{k+1} - \boldsymbol{r}^{k-1}\right)}{2\Delta_t}}{\left\| \boldsymbol{r}^k - \boldsymbol{r}_{gs}^k \right\|} \quad \cdots \quad -\frac{f_t}{c} \frac{\boldsymbol{r}^{N-1^T} \frac{\left(\boldsymbol{r}^N - \boldsymbol{r}^{N-2}\right)}{2\Delta_t}}{\left\| \boldsymbol{r}^{N-1} - \boldsymbol{r}_{gs}^{N-1} \right\|} \right]^T \tag{D.18}$$

The calculation of (D.14) was facilitated by the use of MATLAB® *Symbolic Math* Toolbox. After substituting the standard deviations corresponding to the small noise case (Tab. 4.3) and the true positions and velocities obtained for all instants of a simulated pass (Fig. 4.1), the results obtained are plotted in Figure D.1.

The original Doppler-Shift function (blue line in Fig.D.1) sets the ground truth to compare the performance of the developed approximations.

For every case, the improvement in information increases when the satellite is closer to the observing

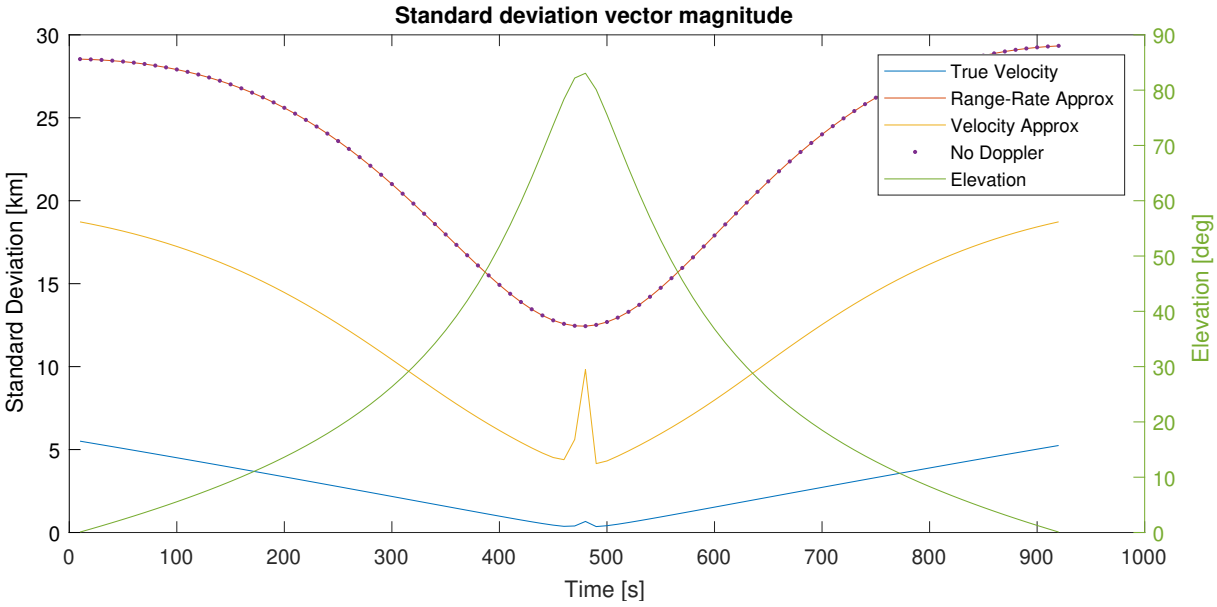

Figure D.1: Comparison of CRLB for several Doppler-shift measurement models: $\boldsymbol{\mu}^k_{f-tv}$, *a priori* knowledge of satellite's velocity (blue), $\boldsymbol{\mu}^k_{f-rra}$, range-rate approximation by difference of ranges (orange), $\boldsymbol{\mu}^k_{f-va}$, velocity approximation by difference of positions (yellow); over the entire pass depicted in Figure 4.1 with measurement standard deviations: $\sigma_\rho = 0.2\,\text{km}$, $\sigma_\alpha = 0.1°$, $\sigma_f = 0.01\,\text{Hz}$. The vertical axis corresponds to the norm of the position standard deviation vector at each instant.

station. The unexpected "spike" at the satellite's point of closest approximation in Fig. D.1 may be related to the large condition number (in the order of 10^{11}) associated with the FIM computed for the "Velocity Approximation" case.

The conclusion that may be taken from Fig. D.1 is that the Doppler-shift model with the bigger potential to improve the information quantity is the one that uses the velocity approximation by differences in positions since it is closer to the original function curve (blue line). On the other hand, in a case with noisier pseudo-range measurements, the CRLB analysis shows a theoretical advantage of including Doppler-shift measurements since now both approximations show a gain in information, as depicted in Fig. D.2.

Despite the promising results in Fig. D.2, this is only a best case study, i.e., the calculated values only corresponds to the best achievable standard deviation, and does not necessarily reflect the real-world performance of any given estimator.

It is also very important to note that none of the terms in (D.17) and (D.18) are convex, they are just closer models to the developed relaxations, but still, non-convex. This implies that the CRLB results will just capture the impact of the noise measurements in the estimation of the unknown parameters (satellite positions), but will not reflect the tightness of the relaxations.

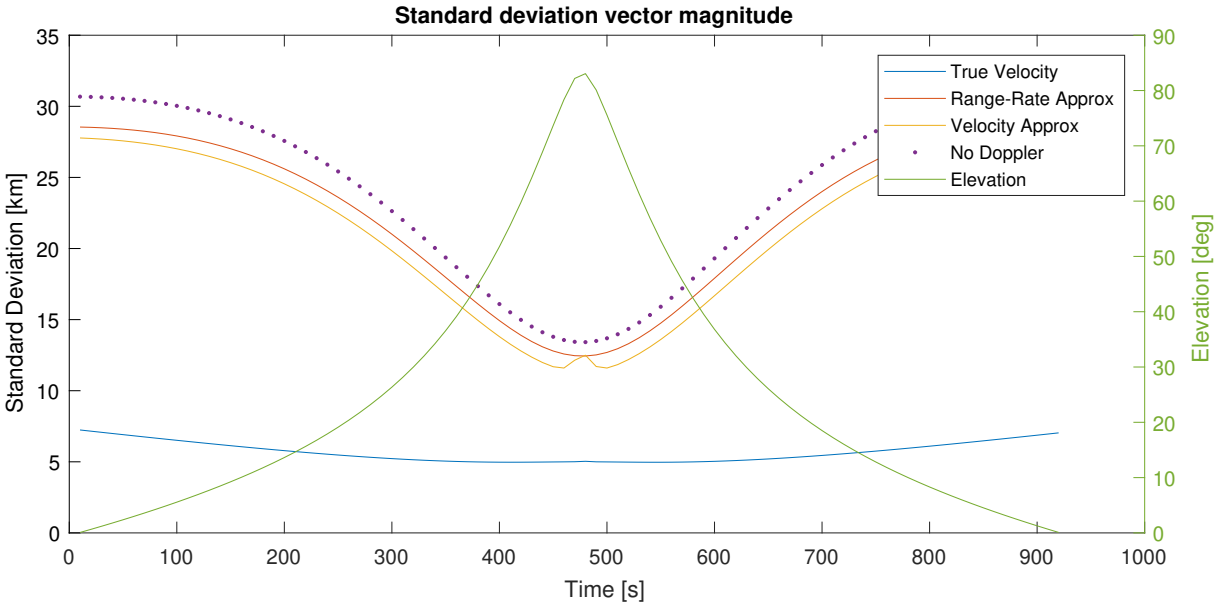

Figure D.2: Comparison of CRLB for several Doppler-shift measurement models: $\boldsymbol{\mu}^k_{f-tv}$, *a priori* knowledge of satellite's velocity (blue), $\boldsymbol{\mu}^k_{f-rra}$, range-rate approximation by difference of ranges (orange), $\boldsymbol{\mu}^k_{f-va}$, velocity approximation by difference of positions (yellow); over the entire pass depicted in Figure 4.1 with measurement standard deviations: $\sigma_\rho = 5\,\text{km}$, $\sigma_\alpha = 0.1°$, $\sigma_f = 0.01\,\text{Hz}$.

Appendix E

Empirical error study

E.1 Derivative finite-divided-difference approximation error

Order	Type	Δt = 1s	Δt = 10s	Δt = 60s	Δt = 120s	Δt = 180s	Δt = 240s
1^{st}	BW	6.18e-02	6.18e-01	3.71e+00	7.41e+00	1.11e+01	1.48e+01
	CT	2.80e-05	2.80e-03	1.01e-01	4.01e-01	8.96e-01	1.58e+00
	FW	6.18e-02	6.18e-01	3.71e+00	7.41e+00	1.11e+01	1.48e+01
2^{nd}	BW	5.60e-05	5.60e-03	2.01e-01	8.02e-01	1.79e+00	3.16e+00
	CT	2.64e-07	1.86e-07	2.29e-04	3.54e-03	1.69e-02	4.96e-02
	FW	5.60e-05	5.60e-03	2.01e-01	8.02e-01	1.79e+00	3.16e+00

Table E.1: Error comparison for different order approximations of satellite velocity for small eccentricity ($e = 0.1$)

Order	Type	Δt = 1s	Δt = 10s	Δt = 60s	Δt = 120s	Δt = 180s	Δt = 240s
1^{st}	BW	1.73e-01	1.73e+00	1.03e+01	1.99e+01	2.86e+01	3.63e+01
	CT	3.19e-04	3.18e-02	1.08e+00	3.76e+00	7.04e+00	1.03e+01
	FW	1.73e-01	1.73e+00	1.03e+01	2.00e+01	2.88e+01	3.66e+01
2^{nd}	BW	6.38e-04	6.37e-02	2.17e+00	7.49e+00	1.39e+01	2.02e+01
	CT	2.90e-06	7.72e-05	6.69e-02	4.71e-01	1.11e+00	1.83e+00
	FW	6.38e-04	6.37e-02	2.17e+00	7.57e+00	1.43e+01	2.13e+01

Table E.2: Error comparison for different order approximations of satellite velocity for large eccentricity ($e = 0.6$)

E.2 Angle approximation error study

Range Error [km]/ True Range [km]	400	600	800	1000	1200	1400	1600	1800	2000
5	1.25	0.83	0.62	0.50	0.42	0.36	0.31	0.28	0.25
10	2.50	1.67	1.25	1.00	0.83	0.71	0.62	0.56	0.50
15	3.75	2.50	1.88	1.50	1.25	1.07	0.94	0.83	0.75
20	5.00	3.33	2.50	2.00	1.67	1.43	1.25	1.11	1.00
25	6.25	4.17	3.12	2.50	2.08	1.79	1.56	1.39	1.25
30	7.50	5.00	3.75	3.00	2.50	2.14	1.88	1.67	1.50
35	8.75	5.83	4.38	3.50	2.92	2.50	2.19	1.94	1.75
40	10.00	6.67	5.00	4.00	3.33	2.86	2.50	2.22	2.00

Table E.3: Norm approximation for angular term. Errors in percentage.

Appendix F

SDP based problem - Matrix version

$$\underset{\boldsymbol{G},\boldsymbol{q}}{\text{minimize}} \quad \sum_{k=1}^{N-1} \frac{1}{2\sigma_f^2}\frac{1}{(\rho^k)^2}\left[\Delta f^k \boldsymbol{G}_{(3N+k,3N+k)} + \frac{f_t^k}{c}\left(\frac{\mathrm{Tr}\left(\boldsymbol{G}_{(k(1:3),3+k(1:3))}\right)}{\Delta t} - \frac{\mathrm{Tr}\left(\boldsymbol{G}_{(3(k-1)+(1:3),3(k-1)+(1:3))}\right)}{\Delta t} - \boldsymbol{G}_{(3k+(1:3),4N+1)}{}^T \boldsymbol{v}_{gs}^k - \frac{\boldsymbol{r}_{gs}^k{}^T \boldsymbol{G}_{(3k+(1:3),4N+1)}}{\Delta t} + \frac{\boldsymbol{r}_{gs}^k{}^T \boldsymbol{G}_{(3(k-1)+(1:3),4N+1)}}{\Delta t} + \boldsymbol{r}_{gs}^k{}^T \boldsymbol{v}_{gs}^k\right)\right]^2 \tag{F.1}$$

$$\text{subject to} \quad \boldsymbol{q} = \begin{bmatrix} \boldsymbol{G}_{(3+3k,2+3(k-1))} - \boldsymbol{G}_{(2+3k,3k)} \\ \boldsymbol{G}_{(1+3k,3k)} - \boldsymbol{G}_{(3+3k,1+3(k-1))} \\ \boldsymbol{G}_{(2+3k,1+3(k-1))} - \boldsymbol{G}_{(1+3k,2+3(k-1))} \end{bmatrix} \qquad k = 1,\dots,N-1 \tag{F.2}$$

$$\boldsymbol{G}_{(3N+k,3N+4)} = \mathrm{Tr}\left(\boldsymbol{G}_{(3(k-1)+(1:3),3(k-1)+(1:3))}\right) - 2\boldsymbol{r}_{gs}^k{}^T \boldsymbol{G}_{(3(k-1)+(1:3),4N+1)} + \left\|\boldsymbol{r}_{gs}^k\right\|^2 \qquad k = 1,\dots,N$$

$$\boldsymbol{G}(4N+1, 4N+1) = 1$$

$$\mathbf{G} \succeq 0$$